

Exclusive photon-fusion production of even-spin resonances and exotic QED atoms in high-energy hadron collisions

David d'Enterria^{1,*} and Karen Kang^{2,†}

¹*CERN, EP Department, CH-1211 Geneva, Switzerland*

²*Amherst College, Amherst, MA 01002, USA*

The cross sections for the single exclusive production of (pseudo)scalar and (pseudo)tensor hadrons, as well as of even-spin QED bound states formed by pairs of opposite-charge leptons or hadrons, are estimated for photon-fusion processes in ultraperipheral collisions (UPCs) of proton-proton, proton-nucleus, and nucleus-nucleus at the RHIC, LHC and FCC colliders, as well as in proton-air interactions at the highest energies reached by cosmic-rays impinging on earth. The UPC cross sections are computed in the equivalent photon approximation with realistic photon fluxes from the charged form factors of proton, lead, gold, and nitrogen ions. The production of four types of even-spin systems are considered: quarkonium (spin-0,2,4 meson bound states, from the lightest π^0 meson up to toponium), exotic hadrons (including candidate multiquark states), leptonium (positronium, dimuonium, and ditauonium), as well as mesonium (pionium, kaonium, D-onia, and B-onia) and baryonium (notably, protonium) QED atoms. The expected yields at the different colliders are presented for about 50 such even-spin composite resonances, for which the ALICE and LHCb experiments have potential reconstruction capabilities at the LHC. The impact of the diphoton decays of such even-spin states is also discussed as resonant backgrounds in the measurement of light-by-light scattering ($\gamma\gamma \rightarrow \gamma\gamma$) over $m_{\gamma\gamma} = 0.1\text{--}15$ GeV in Pb-Pb UPCs at the LHC.

Contents

1. Introduction	1
2. Theoretical ingredients	5
A. Effective photon-photon collision luminosities in UPCs	5
B. Basic properties of QED bound states	5
3. Photon-fusion production of even-spin hadron resonances	7
A. Production of light meson resonances	8
B. Production of heavy quarkonium resonances	15
C. Production of exotic hadrons	21
4. Photon-fusion production of leptonium states	24
5. Photon-fusion production of QED hadronium states	24
6. Total $\gamma\gamma$ even-spin resonance cross sections in UPCs	28
7. Two-photon even-spin backgrounds to LbL scattering in Pb-Pb UPCs at the LHC	31
8. Summary	32
References	33

1. INTRODUCTION

The electric field created by a charged particle accelerated to high energies can be interpreted, in the Weizsäcker–Williams (WW) equivalent photon approximation (EPA) [1, 2], as a flux of quasireal photons whose energies E_γ and number densities N_γ grow proportionally to the Lorentz relativistic factor ($E_\gamma \propto \gamma_L$) and squared charge ($N_\gamma \propto Z^2$) of the beam particles [3, 4]. Such quasireal photon beams have been exploited for decades to study high-energy

*Electronic address: david.d'enterria@cern.ch

†Electronic address: kkang25@amherst.edu

photon-photon ($\gamma\gamma$) interactions at particle colliders [5–9]. Research on $\gamma\gamma$ interactions at multi-GeV energies was first realized in the laboratory in e^+e^- collisions at DESY PETRA in the 1980s [5] and at CERN LEP in the 1990s [6], and has received a significant experimental and theoretical boost at hadron colliders in the last twenty years thanks to the large EPA γ energies and luminosities accessible at the BNL Relativistic Heavy-Ion Collider (RHIC) [7] and at the CERN Large Hadron Collider (LHC) [8, 9]. At hadron colliders, photon-photon processes can be studied in particularly clean conditions in the so-called ultraperipheral collisions (UPCs), where the colliding hadrons interact with transverse separations larger than their matter radii, i.e., without hadronic overlap, and thereby survive their purely electromagnetic interaction. Such UPCs provide the means to study the exclusive production of a single neutral object, or a pair of opposite-charge objects, at central rapidities in an otherwise empty detector [10].

The quantity of interest in a $\gamma\gamma$ collision of charges A and B is the effective two-photon luminosity, $\mathcal{L}_{\gamma\gamma}^{(AB)}$, obtained from the integral of the EPA photon fluxes of the colliding charges. By denoting as $f(x)dx$ the number of photons carrying a fraction between x and $x + dx$ of the energy of the charge Z, i.e., $x = E_\gamma/E_{\text{beam}}$, the two-photon luminosity as a function of the fractional center-of-mass (c.m.) energy $\tau = \hat{s}_{\gamma\gamma}/s$ (where s and $\hat{s}_{\gamma\gamma}$ are the squared c.m. energy of the colliding hadronic and $\gamma\gamma$ system, respectively) can be written¹ as [11, 12],

$$\frac{d\mathcal{L}_{\gamma\gamma}^{(AB)}}{d\tau} = \int_\tau^1 dx_1 dx_2 f(x_1) f(x_2) \delta(\tau - x_1 x_2) = \int_\tau^1 \frac{dx}{x} f(x) f(\tau/x), \quad (1)$$

where the last equality assumes that the colliding charges are identical (and of opposite momentum) and that their γ fluxes factorize² as a function of x . The inclusive photon-photon cross section for any final state X in a $AB \xrightarrow{\gamma\gamma} A X B$ collision can then be obtained from the corresponding elementary $\gamma\gamma$ cross section, $\hat{\sigma}_{\gamma\gamma \rightarrow X}(\hat{s}_{\gamma\gamma})$, via

$$\sigma(AB \xrightarrow{\gamma\gamma} A X B) = \int d\tau \frac{d\mathcal{L}_{\gamma\gamma}^{(AB)}}{d\tau} \hat{\sigma}_{\gamma\gamma \rightarrow X}(\hat{s}_{\gamma\gamma}). \quad (2)$$

Once the EPA flux of the colliding charges $f(x)$ is known, one can compute any arbitrary $\gamma\gamma$ cross section in high-energy collisions. If the γ source is an electron (with mass m_e), the EPA flux depends on the photon virtuality Q^2 , and reads

$$f_{\gamma/e}(x) = \frac{Z^2 \alpha}{\pi x} \int_{x^2 m_e^2}^\infty \frac{dQ^2}{Q^2} \approx \frac{\alpha}{\pi x} \ln(s/m_e^2), \quad (3)$$

where α is the fine structure constant, and the last approximation, obtained by setting $Z = 1$ and the upper limit of integration to s , agrees with the usual WW form: $f(x) = \frac{\alpha}{\pi x} \ln(s/(4m_e^2)) \frac{1}{2} [1 + (1-x)^2]$. The EPA photon flux for a hadronic beam A, with nucleon (proton) mass $m_N = 0.9315$ (0.9383) GeV, has much smaller virtualities, constrained by the form factor of the matter distribution $F_A(Q^2)$, and reads

$$f_{\gamma/A}(x) = \frac{Z^2 \alpha}{\pi x} \int_{x^2 m_N^2}^\infty \frac{dQ^2}{Q^2} F_A(Q^2)^2 \left(1 - \frac{x^2 m_N^2}{Q^2}\right) \approx \frac{Z^2 \alpha}{\pi x} \ln\left(\frac{Q_0^2}{(x m_N)^2}\right), \quad (4)$$

with $\alpha = 1/137.036$, and where the last approximation, valid for not too large x values, takes a maximum virtuality $Q_0 \approx 1/R_A$ given by the inverse of the transverse radius of the hadron R_A . Indeed, the coherent photon emission from the full hadron charge distribution forces the photons to be (quasi) real, i.e., (almost) on-mass shell, limiting their virtuality to very low values $Q^2 < 1/R_A^2$, namely $Q_0^2 \approx 0.08$ GeV² for protons (with $R_A \approx 0.7$ fm), and $Q_0^2 \approx 4 \cdot 10^{-3}$ GeV² for nuclei (with $R_A \approx 1.2 A^{1/3}$ fm, for mass number $A > 14$). The $f_{\gamma/A}(x) \propto 1/x$ behavior of Eq. (4) shows that the longitudinal photon energies have a typical E_γ^{-1} bremsstrahlung-like spectrum, up to energies of the order of $E_\gamma^{\text{max}} \approx \gamma_L/R_A$ (beyond which the photon flux is not zero, but decreases much more steeply) where $\gamma_L = \sqrt{s_{\text{NN}}}/2m_N$ is the Lorentz gamma factor of the beam. Plugging the photon flux (4) into Eq. (1) and integrating over photon fractional energies, one obtains a simple approximate parametrization for the effective two-photon luminosity in hadronic UPCs as a function of fractional $\gamma\gamma$ c.m. energy [11, 12],

$$\frac{d\mathcal{L}_{\gamma\gamma}^{(AB)}}{d\tau} \approx \left(\frac{Z^2 \alpha}{\pi}\right)^2 \frac{16}{3\tau} \ln^3\left(\frac{\gamma_L}{m_N R_A}\right), \quad (5)$$

¹ Natural units, $\hbar = c = 1$, are used throughout the paper.

² Simple factorization of photon fluxes is not fully realistic for quantitatively accurate estimates of $\gamma\gamma$ cross sections in UPCs, as discussed below, but it is a good approximation for illustrative purposes here.

which illustratively provides intuitive parametric dependencies of the c.m.-fractional photon-photon luminosities in UPCs: they scale as Z^4 and as $\ln^3(\sqrt{s_{\text{NN}}})$. The fourth power on the charge Z enhances the $\gamma\gamma$ cross sections by a factor of about $50 \cdot 10^6$ in Pb-Pb compared to e^+e^- or p-p collisions, although larger $\sqrt{s_{\gamma\gamma}}$ can be reached with charges with smaller radii given the $E_{\gamma}^{\text{max}} \propto 1/R_A$ dependence. Since the $\gamma\gamma$ luminosity increases as the cube of the logarithm of the beam energy, UPCs are anticipated to play an even bigger role at the upcoming Future Circular Collider (FCC), with c.m. energies about one order of magnitude larger than at the LHC, $\sqrt{s_{\text{NN}}} = 39\text{--}100$ TeV [13], and even more in proton-air (p-air, mostly p-nitrogen) collisions at the maximum energies observed in interactions of primary cosmic-ray protons with air nuclei in the upper atmosphere³, the so-called Greisen–Zatsepin–Kuzmin (GZK) cutoff [14, 15] corresponding to c.m. energies of $\sqrt{s_{\text{NN}}} \approx 400$ TeV [16]. Table 1 summarizes the typical parameters for p-p, p-A, and A-A UPCs at RHIC, LHC and FCC energies, as well as in p-air collisions at the GZK cutoff. For the latter fixed-target collisions, the Lorentz factor of the proton projectile and c.m. systems are related via $\gamma_L = \sqrt{(\gamma_p + 1)/2}$, and we consider a photon energy of the nitrogen nucleus at rest of $\mathcal{O}(10 \text{ MeV})$, typical of collective nuclear excitations.

TABLE 1: Summary of the generic characteristics of photon-photon collisions in ultraperipheral proton and nuclear collisions at RHIC, HL-LHC [17, 18] and FCC [13, 19] energies, and in fixed-target cosmic-ray collisions at GZK-cutoff energies [16]. For each colliding system, we quote its (i) nucleon-nucleon (NN) c.m. energy $\sqrt{s_{\text{NN}}}$, (ii) nominal total integrated luminosity per experiment \mathcal{L}_{int} (for p-p, we quote in parentheses the estimated values collected under low pileup conditions), (iii) beam energies E_{beam} , (iv) Lorentz factor $\gamma_L = E_{\text{beam}}/m_N$, (v) effective charge radius R_A , (vi) photon “maximum” energy $E_{\gamma}^{\text{max}} \approx \gamma_L/R_A$, and (vii) “maximum” photon-photon c.m. energy $\sqrt{s_{\gamma\gamma}^{\text{max}}} = \sqrt{4E_{\gamma,1}E_{\gamma,2}}$.

System	$\sqrt{s_{\text{NN}}}$	\mathcal{L}_{int}	$E_{\text{beam1}} + E_{\text{beam2}}$	γ_L	R_A	E_{γ}^{max}	$\sqrt{s_{\gamma\gamma}^{\text{max}}}$
Au-Au	200 GeV	10 nb ⁻¹	100 + 100 GeV	107	6.9 fm	3.1 GeV	6.2 GeV
Pb-Pb	5.52 TeV	10 nb ⁻¹	2.76 + 2.76 TeV	2960	7.1 fm	80 GeV	160 GeV
p-Pb	8.8 TeV	1 pb ⁻¹	7.0 + 2.76 TeV	7450, 2960	0.7, 7.1 fm	2.45 TeV, 130 GeV	1.1 TeV
p-p	14 TeV	3 ab ⁻¹ (1 fb ⁻¹)	7.0 + 7.0 TeV	7450	0.7 fm	2.45 TeV	4.5 TeV
Pb-Pb	39.4 TeV	110 nb ⁻¹	19.7 + 19.7 TeV	21 100	7.1 fm	600 GeV	1.2 TeV
p-Pb	62.8 TeV	29 pb ⁻¹	50. + 19.7 TeV	53 300, 21 100	0.7, 7.1 fm	15.2 TeV, 600 GeV	6.0 TeV
p-p	100 TeV	30 ab ⁻¹ (10 fb ⁻¹)	50. + 50. TeV	53 300	0.7 fm	15.2 TeV	30.5 TeV
p-air	400 TeV	–	$\approx 10^8$ TeV + ≈ 0	$\approx 225\,000$, 1	0.7, 2.9 fm	$\approx 3.2 \cdot 10^5$, ≈ 10 MeV	≈ 100 TeV

In photon-photon collisions, any singly produced particle $\gamma\gamma \rightarrow X$ must have J^{PC} quantum numbers (representing total angular momentum J , parity P , and charge conjugation C) that respect basic quantum conservation rules. In particular, the production of vector (spin-1) particles is forbidden in $\gamma\gamma$ collisions because real (massless) photons cannot combine to form a vector particle as per the Landau–Yang theorem [20, 21], and only even-spin resonance states with positive C -parity, such as $J^{\text{PC}} = 0^{-+}, 0^{++}, 2^{-+}, 2^{++}, \dots$, are allowed. Such a selection rule makes of photon-photon collisions a particularly clean environment for the study of $J = 0$ (pseudo)scalar and $J = 2$ (pseudo)tensor particles [5, 6, 22]. Higher even-spin $J = 4, \dots$ resonances can also be theoretically produced, but none of the few presently known spin-4 hadrons has a clearly established $\gamma\gamma$ decay width [23], and they remain unobserved in such a production mode. Interestingly, $\gamma\gamma$ processes can also produce a pair of opposite-charged particles that can subsequently form short-lived spin- and C -even bound states under their common quantum electrodynamics (QED) interaction. Photon-photon collisions provide thereby ideal conditions to produce and investigate exotic QED atoms such as leptonium ($\ell^+\ell^-$)₀, for $\ell^{\pm} = e^{\pm}, \mu^{\pm}, \tau^{\pm}$ leptons, and “hadronium” atoms of two sorts: “mesonium” (A_{2h}), for $h = \pi^{\pm}, K^{\pm}, D^{\pm}, B^{\pm}$ mesons) and “baryonium (hh)₀, for $h =$ baryons where the ‘0’ subindex indicates their spin-0 para-state).

³ Atmospheric nuclei are not fully stripped of their electrons, at variance with nuclei at colliders, and therefore their full charge (and associated “target” γ flux) is not visible to the “projectile” γ flux unless the p-air interaction happens at small impact parameters below the first electron shell, i.e., smaller than the Bohr radius $b < 53 \cdot 10^3 \text{ fm}/Z \approx 3800 \text{ fm}$ for nitrogen ($Z = 14$), which is the case for most of the systems produced in the $\gamma\gamma$ collisions considered here (except, maybe, for a fraction of the positronium yields).

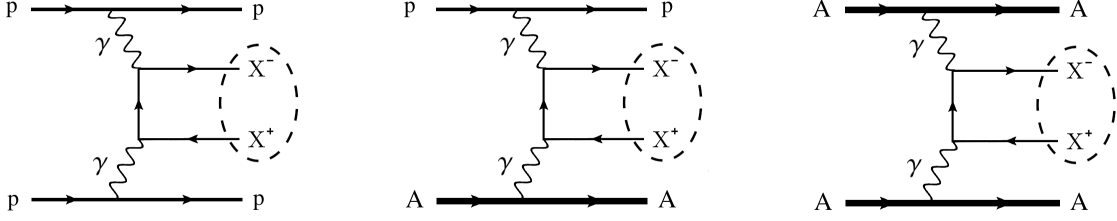


FIG. 1: Schematic diagrams of the photon-photon production of a pair of opposite-charge particles X^+X^- followed by the formation of an (X^+X^-) onium-like bound state in p-p (left), proton-nucleus (center), and nucleus-nucleus (right) collisions. The (X^+X^-) states considered in this work are even-spin states formed by pairs of quarks ($X = q$) bound by their QCD interaction, or of leptons ($X = e, \mu, \tau$) or hadrons ($X = \text{mesons, orbaryons}$) bound by their QED interaction.

The purpose of this paper is to study the two-photon production of even-spin systems in UPCs of protons and/or ions via the process shown in Fig. 1. The elementary cross-section for the production of a resonance X of mass m_X , even spin J , total width Γ_{tot} , and two-photon width $\Gamma_{\gamma\gamma}$, in photon-photon collisions at a center-of-mass energy $\sqrt{\hat{s}_{\gamma\gamma}} = \sqrt{4E_{\gamma 1}E_{\gamma 2}}$ is given by Low’s formula [24],

$$\hat{\sigma}_{\gamma\gamma \rightarrow X}(\hat{s}_{\gamma\gamma}) = 8\pi^2(2J+1) \frac{\Gamma_{\gamma\gamma}\Gamma_{\text{tot}}}{(\hat{s}_{\gamma\gamma} - m_X^2)^2 + (m_X\Gamma_{\text{tot}})^2} = 4\pi^2(2J+1) \frac{\Gamma_{\gamma\gamma}}{m_X^2} \delta(\hat{s}_{\gamma\gamma} - m_X^2), \quad (6)$$

where the second equality holds in the narrow-width approximation, $\Gamma_{\text{tot}} \ll m_X$, and the delta function ensures total 4-momentum conservation as physical particles can only be produced on their mass shell. Since the $\gamma\gamma$ decay and production modes use the same matrix elements, Eq. (6) provides a simple and useful expression that allows relating the diphoton width to the $\gamma\gamma$ -fusion cross section, with proper phase-space and polarization summation factors. From this last expression and Eq. (2), one can derive the “master formula” used in the remainder of this work to compute the production of any given C-even resonance X via photon-photon collisions in a generic UPC of charged hadrons A and B at nucleon-nucleon c.m. energy $\sqrt{s_{\text{NN}}}$ [4],

$$\sigma(AB \xrightarrow{\gamma\gamma} A X B) = 4\pi^2(2J+1) \frac{\Gamma_{\gamma\gamma}}{m_X^2} \left. \frac{d\mathcal{L}_{\gamma\gamma}^{(AB)}}{d\hat{s}_{\gamma\gamma}} \right|_{\hat{s}_{\gamma\gamma}=m_X^2}, \quad (7)$$

where $\left. \frac{d\mathcal{L}_{\gamma\gamma}^{(AB)}}{d\hat{s}_{\gamma\gamma}} \right|_{\hat{s}_{\gamma\gamma}=m_X^2}$ is the value of the photon-photon luminosity at the resonance mass m_X .

The $\gamma\gamma$ production of even-spin resonances, QED bound states, and other exotic atoms in UPCs (Fig. 1) has been first considered in Refs. [22, 25–30] as well as in more recent works [31–42]. In our paper, we extend these previous studies (i) to include multiple new hadronic resonances and exotic atoms not considered previously, (ii) using improved photon-photon luminosities for UPCs, (iii) with a proper propagation of theoretical uncertainties to their production cross sections, and also (iv) adding predictions for current and future colliders, such as the FCC-hh, as well for cosmic-rays interactions at GZK cutoff energies. According to Table 1, UPCs at RHIC can produce even-spin particles with masses $m_X \lesssim 6$ GeV, whereas UPCs at the LHC, FCC, and GZK-cutoff energies can produce any resonance with masses up to hundreds or thousands of GeV. In our study, we will present the production cross sections for all C-even states (with known diphoton width) between the lowest-mass (positronium) and the highest-mass (toponium) objects currently known.

The paper is organized as follows. In Section 2 the basic theoretical ingredients are presented, including realistic effective two-photon luminosity functions as a function of $\gamma\gamma$ invariant mass obtained with the gamma-UPC Monte Carlo code [36], which allow the determination of the production cross sections of any given C-even resonance in UPCs by means of the Low’s formula (Section 2A), as well as a concise overview of the generic properties of QED bound states that can be produced in two-photon collisions (Section 2B). In Sections 3, 4, and 5, we present, respectively, the theoretical UPC cross sections computed for quarkonium, leptonium, and hadronium final states for all colliding systems shown in the diagrams of Fig. 1. In Section 7, we assess the impact of the diphoton decays of such objects as resonant backgrounds for the measurement of light-by-light scattering ($\gamma\gamma \rightarrow \gamma\gamma$) over $m_{\gamma\gamma} = 0.1\text{--}10$ GeV in Pb-Pb UPCs at the LHC. The main findings are summarized in Section 8.

2. THEORETICAL INGREDIENTS

The effective $\gamma\gamma$ luminosities used in our cross section calculations, as well as a discussion of the basic formulas to obtain relevant properties (mass, Bohr radius, and diphoton width) of the exotic QED atoms studied in this work, are presented in this section.

A. Effective photon-photon collision luminosities in UPCs

Often in the literature, approximate expressions for the effective $\gamma\gamma$ luminosities such as Eq. (5) have been used to estimate cross sections for the production of even-spin resonances in UPCs. Those formulas are valid in the limit where the hadrons are described with a simplistic form factor, such e.g., as a “hard sphere” of radius R_A , and include interactions where their matter distributions overlap and produce final states that are not distinguishable from standard hadronic interactions. In this work, we employ more realistic expressions based on the effective two-photon luminosity implemented in gamma-UPC [36]:

$$\frac{d\mathcal{L}_{\gamma\gamma}^{(AB)}}{d\hat{s}_{\gamma\gamma}} = \frac{2\hat{s}_{\gamma\gamma}}{s_{\text{NN}}} \int \frac{dE_{\gamma_1}}{E_{\gamma_1}} \frac{dE_{\gamma_2}}{E_{\gamma_2}} \delta\left(\frac{\hat{s}_{\gamma\gamma}}{s_{\text{NN}}} - \frac{4E_{\gamma_1}E_{\gamma_2}}{s_{\text{NN}}}\right) \frac{d^2N_{\gamma_1/Z_1, \gamma_2/Z_2}^{(AB)}}{dE_{\gamma_1}dE_{\gamma_2}}, \quad (8)$$

where

$$\frac{d^2N_{\gamma_1/Z_1, \gamma_2/Z_2}^{(AB)}}{dE_{\gamma_1}dE_{\gamma_2}} = \int d^2\mathbf{b}_1 d^2\mathbf{b}_2 P_{\text{no inel}}(\mathbf{b}_1, \mathbf{b}_2) N_{\gamma_1/Z_1}(E_{\gamma_1}, \mathbf{b}_1) N_{\gamma_2/Z_2}(E_{\gamma_2}, \mathbf{b}_2), \quad (9)$$

is derived from the convolution of the two photon number densities $N_{\gamma_i/Z_i}(E_{\gamma_i}, \mathbf{b}_i)$ with energies $E_{\gamma_{1,2}}$ at impact parameters $\mathbf{b}_{1,2}$ from hadrons A and B, respectively (the vectors \mathbf{b}_1 and \mathbf{b}_2 have their origins at the center of each hadron, and, therefore, $|\mathbf{b}_1 - \mathbf{b}_2|$ is the impact parameter between them); and $P_{\text{no inel}}(\mathbf{b}_1, \mathbf{b}_2)$ encodes the probability of hadrons A and B to remain intact after their interaction, which depends on their relative impact parameters. For the $P_{\text{no inel}}(b)$ probability to have no inelastic hadronic interaction at impact parameter b , the standard opacity (optical density, also known as “eikonal Glauber” [43]) expressions are used:

$$P_{\text{no inel}}(b) = \begin{cases} e^{-\sigma_{\text{inel}}^{\text{NN}} T_{\text{AB}}(b)}, & \text{for nucleus-nucleus UPCs} \\ e^{-\sigma_{\text{inel}}^{\text{NN}} T_{\text{A}}(b)}, & \text{for proton-nucleus UPCs} \\ |1 - \Gamma(s_{\text{NN}}, b)|^2, & \text{with } \Gamma(s_{\text{NN}}, b) \propto e^{-b^2/(2b_0)} \text{ for p-p UPCs.} \end{cases} \quad (10)$$

Here $T_{\text{A}}(b)$ and $T_{\text{AB}}(b)$ are the nuclear thickness and overlap functions, respectively, commonly derived from the hadron transverse density profile via a Glauber MC model [44], $\sigma_{\text{inel}}^{\text{NN}} \equiv \sigma_{\text{inel}}^{\text{NN}}(\sqrt{s_{\text{NN}}})$ is the inelastic NN scattering cross section at the hadronic c.m. energy $\sqrt{s_{\text{NN}}}$, and $\Gamma(s_{\text{NN}}, b)$ is the Fourier transform of the p-p elastic scattering amplitude modelled by an exponential function [45] with inverse slope $b_0 \equiv b_0(\sqrt{s_{\text{NN}}})$ dependent on the NN c.m. energy. The $\sigma_{\text{inel}}^{\text{NN}}$ and b_0 parameters dependent on $\sqrt{s_{\text{NN}}}$ that are used in gamma-UPC are obtained from fits of experimental data [46].

In order to compute the $\gamma\gamma$ cross sections via Eq. (7) for a variety of final states and for multiple colliding systems at RHIC, LHC, FCC, and GZK-cutoff energies, we employ the effective photon-photon luminosities obtained through Eqs. (8)–(10) with the gamma-UPC code, using the photon fluxes $N_{\gamma_i/Z_i}(E_{\gamma_i}, \mathbf{b}_i)$ derived from the charged form-factors of protons and ions [36]. The ion charged form-factor is more realistic than the dipole form-factor commonly used in the literature, as it covers the full range of impact parameters and reproduces better the precision $\gamma\gamma \rightarrow \ell^+\ell^-$ measurements performed at the LHC, leading to theoretical uncertainties associated to the photon flux in the few percent (and neglected hereafter) [47]. The corresponding $\gamma\gamma$ luminosities $d\mathcal{L}_{\gamma\gamma}/dm_X$ as a function of m_X are plotted in Fig. 2 for Au-Au UPCs at RHIC as well as for Pb-Pb, p-Pb, and p-p UPCs at the LHC (left), and for Pb-Pb, p-Pb, and p-p UPCs at FCC and p-air collisions at the GZK cutoff (right). The plotted luminosities cover 12–14 orders-of-magnitude from $m_X = 0.1$ MeV up to the high-mass tails and they approximately follow, except in the tails, a power-law decrease with a dependence of the form $d\mathcal{L}_{\gamma\gamma}/dm_X \propto m_X^{-n}$, with exponent $n = 1.25$ – 1.8 depending on the system and c.m. energy. Employing such $\gamma\gamma$ luminosity curves and Eq. (7), we can compute the production cross section for any arbitrary C-even system existing between the lowest-mass (positronium) and the highest-mass (toponium) C-even particles currently known.

B. Basic properties of QED bound states

For the predictions of the production cross section of onium states and exotic atoms in photon-photon collisions, it is useful to review the basic properties of QED bound states such as their mass, Bohr radius, and diphoton width.

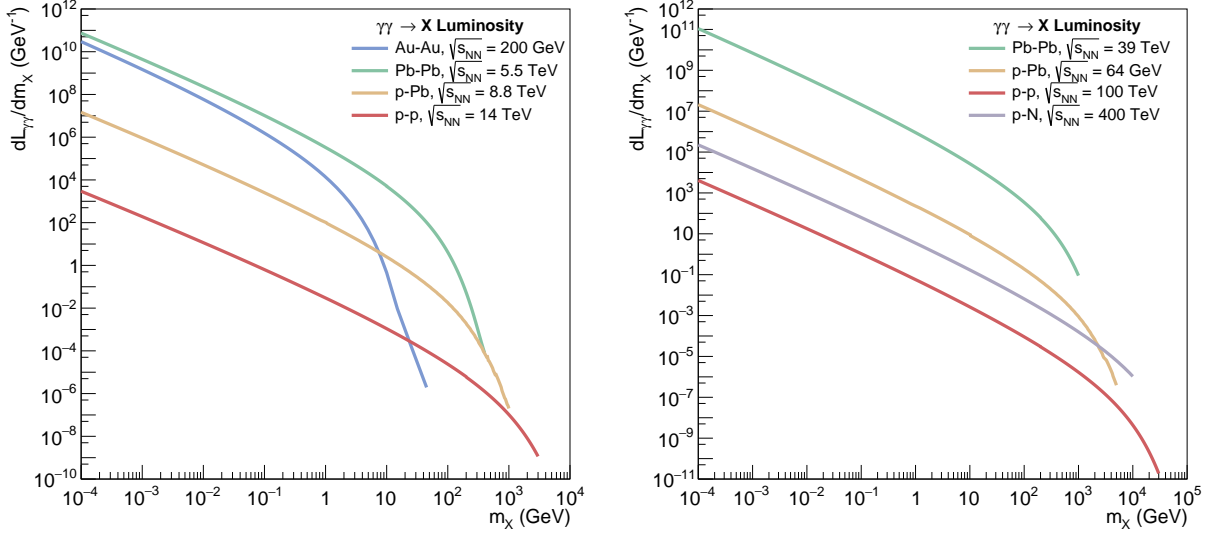


FIG. 2: Effective photon-photon luminosities as a function of m_X , $d\mathcal{L}_{\gamma\gamma}/dm_X$ given by Eqs. (8)–(10), for ultraperipheral Au-Au (200 GeV), Pb-Pb (5.5 TeV), p-Pb (8.8 TeV), and p-p (14 TeV) collisions at RHIC and LHC (left), and Pb-Pb (39 TeV), p-Pb (62.8 TeV), and p-p (100 TeV) at FCC, and p-air (400 TeV) for cosmic rays at the GZK cutoff (right), obtained with the gamma-UPC code with γ photon fluxes derived from the corresponding ion charged form factors.

An onium system formed by two identical opposite-charge particles X^\pm , of mass m_X and electric charge Z , bound by their common QED interaction, has nonrelativistic momenta and, at first approximation, can be described by the nonrelativistic Schrödinger equation for the wavefunction $\psi(\vec{r})$ of an atom,

$$\left(-\frac{\nabla^2}{2m_{\text{red}}} + V(r)\right)\psi(\vec{r}) = \left(-\frac{\nabla^2}{m_X} + V(r)\right)\psi(\vec{r}) = E_n\psi(\vec{r}), \quad (11)$$

where $m_{\text{red}} = \frac{m_1 m_2}{m_1 + m_2}$ is the reduced mass of the system, which simplifies (second equality) to $m_{\text{red}} = m_X/2$ in the symmetric case of two opposite-charge constituents of equal mass ($m_X = m_1 = m_2$), E_n is the energy of the state with principal quantum number n , and $V(r)$ is the one-photon-exchange Coulomb potential as a function of the radial distance r ,

$$V(r) = -\frac{Z\alpha}{r}, \quad (12)$$

with α the fine structure constant evaluated at m_X . The average distance between the constituents of such an onium system is given by their Bohr radius

$$r_{\text{Bohr}} = \frac{n^2}{Z\alpha m_{\text{red}}} = \frac{2n^2}{Z\alpha m_X}, \quad (13)$$

(where again the last equality assumes equal-mass constituents). Since, apart from meson resonances, we will be focusing on QED bound states, this formula is useful to check that the average distance between any pair of hadronic objects is much larger than the range of the strong interactions, $r_{\text{Bohr}} \gg 1$ fm, so that the pure QED formulas below are applicable.

For bound states in a central potential, it is convenient to decompose the Schrödinger wavefunction $\psi(\vec{r})$ of Eq. (11) into radial R_{nl} and angular Y_l^m parts (with l and m , the orbital angular momentum and its projection), as $\psi_{nlm}(r, \theta, \phi) = R_{nl}(r) \cdot Y_l^m(\theta, \phi)$. A simple Coulomb model for the binding force implies that for the S-wave level (i.e., $l = 0$) n state ($n = 1$ is the ground state, and $l = 0, m = 0$), the radial part $R_{n0}(r)$ depends on the principal quantum number n with probability at the origin $|R_{n0}(0)|^2 = 4n^3/r_{\text{Bohr}}^3 = (\alpha m)^3/n^3$, where the n^3 term comes from the Laguerre polynomial with $l = 0$, and the spherical harmonic is constant: $Y_0^0(\theta, \phi) = \frac{1}{\sqrt{4\pi}}$. Thus, all the nonperturbative information about the formation of a given bound state is contained in the amplitude of the radial wavefunction at the origin $|R_{n0}(0)|$ (and its derivatives, for non-zero angular momentum states). In the case of an onium resonance formed by two fermions, the ground state has two states with total angular momentum $J = 0$ and 1 , depending on the relative (opposite or parallel) orientation of its constituent particles, known as para- ($J^{\text{PC}} = 0^{-+}$) and ortho- ($J^{\text{PC}} = 1^{--}$) states. Since,

as aforementioned, only the para-state is producible in photon-photon collisions, we will focus on this state. The wavefunction at the origin of a QED para-onium bound state, $\psi_{\text{para}(X^+X^-)}(r=0)$, amounts to

$$|\psi_{\text{para}(X^+X^-)}(r=0)|^2 = |R_{n0}(0) \cdot Y_0^0(\theta, \phi)|^2 = \frac{1}{4\pi} |R_{n0}(0)|^2 = \frac{1}{\pi r_{\text{Bohr}}^3} = \frac{(Z\alpha m_X)^3}{8\pi n^3}, \quad (14)$$

where the binding energy of the ground ($n=1$) and excited states are given, respectively, by:

$$E_{\text{bind}, n=1} = -\frac{1}{4}m_X (Z\alpha)^2, \quad \text{and} \quad E_{\text{bind}, n} = \frac{E_{n=1}}{n^2}. \quad (15)$$

The first relativistic correction to the Coulomb potential can be computed in the so-called nonrelativistic QED framework. The main contribution can be determined in the Breit potential approach [48] taking into account scattering and annihilation channels. The leading $O(m_X(Z\alpha)^4)$ relativistic Breit correction to the binding energy is

$$\delta E_{\text{Breit}} = -\frac{1}{2m_X} (E^2 - 2E \langle V \rangle + \langle V^2 \rangle) = -\frac{5}{16}m_X (Z\alpha)^4 \frac{1}{n^3}. \quad (16)$$

Combining Eqs. (15) and (16), the mass of the QED para-onium ground state ($n=1$), $\psi_{\text{para}(X^+X^-)}$, is then given by⁴

$$m_{\psi_{\text{para}(X^+X^-)}} = 2m_X + E_{\text{bind}, n=1} + \delta E_{\text{Breit}} = m_X \left[2 - \frac{1}{4}(Z\alpha)^2 - \frac{5}{16}(Z\alpha)^4 \right], \quad (17)$$

As a last step, we lay out the general formula to compute the diphoton decay width of a even-spin QED-onium state. Fermi's Golden Rule provides the means to calculate the transition rate (decay width) from an initial quantum state $|i\rangle$ to a final state $|f\rangle$ under the influence of a perturbing Hamiltonian H_{int} :

$$\Gamma = 2\pi |\langle f | H_{\text{int}} | i \rangle|^2 \rho(E_f), \quad (18)$$

where $\langle f | H_{\text{int}} | i \rangle$ is the matrix element of the interaction Hamiltonian between the initial and final states, and $\rho(E_f)$ is the density of final states with energy E_f . The general form for the two-photon decay width involves the annihilation cross-section described by the matrix element $|\mathcal{M}|$, their relative velocity, and their probability density at the origin:

$$\Gamma = \int \frac{|\mathcal{M}|^2}{m_{\psi_{\text{para}}}^2} |\psi_{\text{para}}(0)|^2 \delta(E - |\vec{k}_1| - |\vec{k}_2|) d^3k_1 d^3k_2. \quad (19)$$

For a pair of bound charged fermions, such as positronium⁵ (see Section 4), the matrix elements and phase space integration gives:

$$\Gamma_{\psi_{\text{para}(X^+X^-)} \rightarrow \gamma\gamma} = \frac{(Z\alpha)^5 m_X}{2n^3}, \quad \text{for } X = \text{fermion}. \quad (20)$$

For a pair of bound charged bosons, such as a $(\pi^+\pi^-)$ ‘‘pionium’’ state⁶ (see Section 5), the symmetric wavefunction introduces an additional $1/2$ factor, resulting in:

$$\Gamma_{\psi_{\text{scalar}(X^+X^-)} \rightarrow \gamma\gamma} = \frac{(Z\alpha)^5 m_X}{4n^3}, \quad \text{for } X = \text{boson}. \quad (21)$$

3. PHOTON-FUSION PRODUCTION OF EVEN-SPIN HADRON RESONANCES

The cross section for the single exclusive production of a given C-even meson X through $\gamma\gamma$ fusion in an UPC can be computed through Eq. (7), and is completely determined from its spin $J = 0, 2, 4, \dots$, two-photon width $\Gamma_{\gamma\gamma}$, and the

⁴ At leading order, the wavefunction of the spin-1 and spin-0 bound states are equal, $\psi_{\text{ortho}(X^+X^-)}(0) = \psi_{\text{para}(X^+X^-)}(0)$, since they satisfy the same Schrödinger equation, but the ortho state is slightly more massive as [49]: $m_{\psi_{\text{ortho}(X^+X^-)}} \approx \left(1 + \frac{7}{12} \frac{(Z\alpha)^4}{(2 - \frac{1}{4}(Z\alpha)^2 - \frac{5}{16}(Z\alpha)^4)} \right) m_{\psi_{\text{para}(X^+X^-)}}$.

⁵ The two-photon annihilation of positronium is a standard result found in QED textbooks such as e.g., Sec. 89 of [50] or p. 282 of [51].

⁶ Hadronic systems bound by their QED interaction are treated perturbatively neglecting their strong interaction, which is justified as long as their Bohr radius is $r_{\text{Bohr}} \gg 1$ fm, which is the case for the scalar pionium bound state [52].

photon-photon effective luminosity of the colliding system at the particle mass (curves of Fig. 2). In the following, we collect the cross sections results for the UPC production of even-spin meson resonances formed by light (u, d, s) quarkonium in Section 3 A, and heavy (c, b, t) quarkonium in Section 3 B. We provide first the meson properties, and then the computed cross sections and expected yields in UPCs at current and future hadron colliders. In Section 3 C, we also compute the theoretical cross sections for the production of exotic hadron states (including multi-quark candidate states).

A. Production of light meson resonances

Table 2 lists the relevant properties of all experimentally known spin-0, 2, 4 mesons formed by light quarks (u, d, s) listed in the PDG review, with known diphoton width [23]. For each particle we list its mass, total and partial diphoton widths, and dominant decay mode (with branching fraction \mathcal{B}). We include only established particles, which is around 80% of the PDG catalog. Their quoted diphoton widths are either those experimentally measured (and quoted in the PDG) or, in some cases, theoretically computed as explained below and/or in the provided references.

Scalar mesons decay dominantly into pairs of pseudoscalar mesons ($\pi\pi$, $K\bar{K}$, $\pi\eta$, $\eta\eta$ or $\eta\eta'$) and, since broad overlapping states decaying into the same final state interfere, this complicates the determination of their masses and widths. The scalar resonances of light mesons are particularly difficult to resolve experimentally because they can have large decay widths [53]. Their mass (m) and width (Γ) can be theoretically estimated from the position of the nearest pole in the process amplitude (S- or T-matrix) at an unphysical sheet of the complex energy plane, traditionally labeled $\sqrt{s_{\text{pole}}} = m - i\Gamma/2$. One such case is the $f_0(500)$ particle, also known as the σ meson, the scalar partner of the SU(3) chiral meson nonet, which decays into $\pi\pi$ and $\gamma\gamma$ final states and for which the Breit–Wigner parameterization fails [54]. The quark/gluon/meson composition of such a broad state is subject of discussions since many years, and its measurement in UPCs would provide useful information. The same holds true for the $a_0(980)$, $f_0(980)$ scalars, which have been often considered as four-quark states. Furthermore, the 0^{++} ground-state glueball expected below 2 GeV, will mix with the isoscalar 0^{++} $q\bar{q}$ states. The study of all these states in UPCs would therefore provide additional discriminating information.

The two-photon width of the $f_0(500)$ cannot be easily extracted from data due to its large width but, in the narrow width approximation, it has been estimated as $\Gamma_{\gamma\gamma} \simeq \alpha^2 |g_\gamma|^2 / (4\text{Re} \sqrt{s_{\text{pole}}}) = \alpha^2 |g_\gamma|^2 / (4m)$, where g_γ is the residue at the pole to two photons, and α is the electromagnetic fine-structure constant [55]. Over the last decade, multiple calculations using dispersive techniques have been performed of the diphoton decay width of the $f_0(500)$ meson, but the interpretation of the results remains inconclusive, yielding $\mathcal{O}(1.2\text{--}3.1)$ keV values [56]. A more recent dispersive analysis of the $\gamma\gamma \rightarrow \pi\pi$ data [57] suggests $\Gamma_{\gamma\gamma} = 0.33 \pm 0.07$ keV (for a mass at $m = 471 \pm 23$ MeV), which we use in our narrow width approximation here. The diphoton widths of the $f_2(1565)$ and $a_2(1700)$ mesons are obtained from analyses of L3 data at LEP [58].

Table 3 lists sixteen even-spin hadrons with no precise value of their diphoton partial in the latest PDG review. There are two isoscalar 0^{++} mesons, $f_0(1370)$ and $f_0(1500)$, which are expected to mix with the $f_0(1710)$ meson. Both $f_0(1500)$ and $f_0(1710)$ have been proposed as glueball candidates. Among the signatures naively expected for glueballs is a reduced $\gamma\gamma$ coupling (although photon couplings of glueballs are sensitive to glue mixing with $q\bar{q}$ mesons). The observation of the production of any such resonance in UPCs (in any of their dominant decay modes listed in the last column of the table) would allow determining their partial diphoton decays, by simply inverting Eq. (7), namely, by using their measured cross section $\sigma_{\text{exp}}(AB \xrightarrow{\gamma\gamma} A X B)$ divided by the expected two-photon luminosity at their mass, via

$$\Gamma_{X \rightarrow \gamma\gamma} = \frac{\sigma_{\text{exp}}(AB \xrightarrow{\gamma\gamma} A X B)}{4\pi^2(2J+1)} m_X^2 \left[\frac{d\mathcal{L}_{\gamma\gamma}^{(AB)}}{d\hat{s}_{\gamma\gamma}} \Big|_{\hat{s}_{\gamma\gamma}=m_X} \right]^{-1}. \quad (22)$$

The two spin-4 resonances known ($a_4(1970)$, although this state has no established $\gamma\gamma$ decay mode yet, and $f_4(2050)$) have theoretical $\gamma\gamma$ cross sections enhanced by factors of $(2J+1) = 9$ compared to spin-0 mesons of similar mass, and therefore should be produced with an order-of-magnitude larger probability than any lower-spin counterpart with equal mass and diphoton width.

The photon-fusion production of pseudoscalar bosons in UPCs, shown in Fig. 1 (left), is just a realization of the well-known ‘‘Primakoff effect’’ [66]. Tables 4, 5, and 6 report the computed $\gamma\gamma$ cross sections for all the (pseudo) scalar/tensor resonances listed in Table 2 —grouped by mass ranges: $m_X \lesssim 1$ GeV, $m_X \approx 1\text{--}1.5$ GeV, and $m_X = 1.5\text{--}2$ GeV, respectively— produced in p-p, p-Pb, and Pb-Pb UPCs at LHC and FCC c.m. energies as well as p-air collisions at GZK-cutoff energies, derived using Eq. (7). We have propagated into the final cross sections the parametric uncertainties from the m_X and $\Gamma_{\gamma\gamma}$ values of each resonance. Uncertainties due to the photon luminosities are subpercent in this mass range [47] and are neglected. Whenever available, we also quote the cross sections results from previous studies. Our results agree in general with older calculations (which did not quote theoretical

TABLE 2: Properties of C-even light quark (u,d,s) resonances (spin-0, 2, 4 mesons). For each particle, we quote its J^{PC} quantum numbers, mass m_X , full width Γ , diphoton partial width $\Gamma_{\gamma\gamma}$ and branching fraction $\mathcal{B}(X \rightarrow \gamma\gamma)$, from measurements [23] or theoretical predictions (with the indicated reference), and dominant decay modes (and their branching fraction \mathcal{B}).

Resonance	J^{PC}	m_X (MeV)	Γ_{tot} (MeV)	$\Gamma_{\gamma\gamma}$ (keV)	$\mathcal{B}(X \rightarrow \gamma\gamma)$	Dominant decay (\mathcal{B})
π^0	0^{-+}	134.9768 ± 0.0005	$(7.808 \pm 0.120) \cdot 10^{-6}$	$(7.716 \pm 0.119) \cdot 10^{-3}$	$(98.823 \pm 0.034)\%$	$\gamma\gamma$
η	0^{-+}	547.862 ± 0.017	$(1.31 \pm 0.05) \cdot 10^{-3}$	0.515 ± 0.018	$(39.36 \pm 0.18)\%$	$\gamma\gamma; 3\pi^0$ (32.57 \pm 0.21%)
$\sigma/f_0(500)$	0^{++}	449^{+22}_{-16}	550 ± 24	0.33 ± 0.07 [57]	$(6.0 \pm 1.3) \cdot 10^{-7}$	$\pi\pi, \gamma\gamma$ seen
η'	0^{-+}	957.78 ± 0.06	0.188 ± 0.006	4.34 ± 0.14	$(2.307 \pm 0.033)\%$	$\pi^+\pi^-\eta$ (42.5 \pm 0.5%)
$f_0(980)$	0^{++}	990 ± 20	10–100	$0.29^{+0.11}_{-0.06}$	$(2.9 \pm 0.6) \cdot 10^{-6}$	$\pi\pi, K\bar{K}, \gamma\gamma$ seen
$a_0(980)$	0^{++}	980 ± 20	50–100	0.30 ± 0.10 ^a	$(3.0 \pm 1.0) \cdot 10^{-6}$	$\eta\pi, K\bar{K}, \eta'\pi, \gamma\gamma$ seen
$f_2(1270)$	2^{++}	1275.4 ± 0.8	186.6 ± 2.3	2.6 ± 0.5	$(1.42 \pm 0.24) \cdot 10^{-5}$	$\pi\pi$ (84.3 ^{+2.9} _{-0.9} %)
$a_2(1320)$	2^{++}	1318.2 ± 0.6	107 ± 5	1.00 ± 0.06	$(9.4 \pm 0.7) \cdot 10^{-6}$	3π (70.1 \pm 2.7%)
$a_0(1450)$	0^{++}	1439 ± 34	258 ± 14	$(4.65 \pm 0.12) \cdot 10^{-3}$ ^b	$(1.8 \pm 0.2) \cdot 10^{-5}$	$\pi\eta$ (9.3 \pm 2.0%)
$f_2'(1525)$	2^{++}	1517.4 ± 2.5	86 ± 5	0.082 ± 0.009	$(1.12 \pm 0.15) \cdot 10^{-6}$	$K\bar{K}$ (87.6 \pm 2.2%)
$f_2(1565)$	2^{++}	1571 ± 13	132 ± 23	0.70 ± 0.14	$(5.3 \pm 1.7) \cdot 10^{-6}$	$K\bar{K}$ (87.6 \pm 2.2%)
$a_2(1700)$	2^{++}	1706 ± 14	380^{+60}_{-50}	0.30 ± 0.05	$(7.9 \pm 1.7) \cdot 10^{-7}$	$\eta\pi$ (2.5 \pm 0.6%)
$f_0(1710)$	0^{++}	1733^{+8}_{-7}	150^{+12}_{-10}	$(3.33 \pm 0.68) \cdot 10^{-5}$ ^c	$(2.2 \pm 0.5) \cdot 10^{-7}$	$K\bar{K}$ (36 \pm 12%)
$\eta_2(1870)$	2^{-+}	1842 ± 8	225 ± 14	$4.53 \pm 0.29 \pm 0.51$ [62]	$(2.0 \pm 0.3) \cdot 10^{-5}$	$\eta\pi\pi, a_2(1320)\pi, f_2(1270)\eta, a_0(980)\pi$
$f_4(2050)$	4^{++}	2018 ± 11	237 ± 18	$(1.36 \pm 0.02) \cdot 10^{-4}$ ^d	$(5.7 \pm 0.6) \cdot 10^{-7}$	$\pi\pi$ (17.0 \pm 1.5%)

^aUsing $\Gamma_{\gamma\gamma}\mathcal{B}(\eta\pi) = (0.24 \pm 0.08)$ keV [59].

^bUsing $\Gamma_{\gamma\gamma}\mathcal{B}(\pi\eta) = (432 \pm 6^{+1073}_{-256})$ keV [60].

^cUsing $\Gamma_{\gamma\gamma}\mathcal{B}(K\bar{K}) = (12^{+3+227}_{-2-8})$ keV [61].

^dUsing $\Gamma_{\gamma\gamma}\mathcal{B}(\pi\pi) = (23.1^{+3.6+70.5}_{-3.3-15.6})$ keV [63].

TABLE 3: Properties of C-even light quark (u,d,s) resonances (spin-0, -2, -4 mesons) without known diphoton decay width. For each particle, we quote its J^{PC} quantum numbers, mass m_X , full width Γ , upper limit (if known) of the diphoton partial width $\Gamma_{\gamma\gamma}$, and dominant decay modes from measurements [23].

Resonance	J^{PC}	m_X (MeV)	Γ_{tot} (MeV)	$\Gamma_{\gamma\gamma}$ (keV)	Dominant decay
$\eta(1295)$	0^{-+}	1294 ± 4	55 ± 5	< 0.066	$\eta\pi^+\pi^-, a_0(980)\pi, \eta\pi^0\pi^0, \eta(\pi\pi)_{S\text{-wave}}, \sigma\eta, K\bar{K}\pi$ seen
$\pi(1300)$	0^{-+}	1300 ± 100	200–600	$< 0.8 \cdot 10^3$ [58]	$\rho\pi, \pi(\pi\pi)_{S\text{-wave}}$ seen
$f_0(1370)$	0^{++}	1370 ± 170	200–500	seen	$\pi\pi, 4\pi, \eta\eta, K\bar{K}$
$\eta(1405)$	0^{-+}	1408.8 ± 2.0	50.3 ± 2.5	< 1.78	$K\bar{K}\pi, \eta\pi\pi, a_0(980)\pi, \eta(\pi\pi), f_0(980)\eta, 4\pi, \rho^0\gamma, K^*K$ seen
$\eta(1475)$	0^{-+}	1475 ± 4	90 ± 9	$\Gamma_{\gamma\gamma}\mathcal{B}(K\bar{K}\pi) < (0.23 \pm 0.07)$ [64]	$K\bar{K}\pi, K\bar{K}^* + \text{c.c.}, a_0(980)\pi, \gamma\gamma$
$f_0(1500)$	0^{++}	1522 ± 25	108 ± 33	no obs. $\gamma\gamma$ decay	$\pi\pi$ (34.5 \pm 2.2%)
$\eta_2(1645)$	2^{-+}	1617 ± 5	181 ± 11	no obs. $\gamma\gamma$ decay	$a_2(1320)\pi, K\bar{K}\pi, K^*\bar{K}, \eta\pi^+\pi^-, a_0(980)\pi$
$\pi_2(1670)$	2^{-+}	$1670.6^{+2.9}_{-1.2}$	258^{+8}_{-9}	< 0.072	3π (95.8 \pm 1.4%)
$\pi(1800)$	0^{-+}	1810^{+9}_{-11}	215^{+7}_{-8}	no obs. $\gamma\gamma$ decay	$\pi^+\pi^-\pi^-, f_0(500, 980, 1370)\pi^-, \eta\eta\pi^-, a_0(980)\eta,$ $f_0(1500)\pi^-, \eta\eta'(958)\pi^-, K_0^*(1430)K^-$
$\pi_2(1880)$	2^{-+}	1874^{+26}_{-5}	237^{+33}_{-30}	no obs. $\gamma\gamma$ decay	$\eta\eta\pi^-, a_0(980)\eta, a_2(1320)\eta, f_0(1500)\eta, f_1(1285)\pi, \omega\pi^-\pi^0$
$f_2(1950)$	2^{++}	1936 ± 12	464 ± 24	$\Gamma_{\gamma\gamma}\mathcal{B}(K\bar{K}) = (122 \pm 4 \pm 26) \cdot 10^{-3}$ [65]	$K^*\bar{K}^*, \pi^+\pi^-, \pi^0\pi^0, 4\pi, \eta\eta, \bar{K}, \gamma\gamma, p\bar{p}$
$a_4(1970)$	4^{++}	1967 ± 16	324^{+15}_{-18}	no obs. $\gamma\gamma$ decay	$K\bar{K}, \pi^+\pi^-\pi^0, \rho\pi, f_2(1270)\pi, \omega\pi^-\pi^0,$ $\omega\rho, \eta\pi, \eta'(958)\pi$
$f_2(2010)$	2^{++}	2011^{+60}_{-80}	202 ± 60	no obs. $\gamma\gamma$ decay	$\phi\phi, K\bar{K}$ seen
$f_0(2020)$	0^{++}	$1982^{+54.1}_{-3}$	436 ± 50	no obs. $\gamma\gamma$ decay	$\rho\pi\pi, \pi^0\pi^0, \rho\rho, \omega\omega, \eta\eta, \eta'\eta'$ seen
$f_2(2300)$	2^{++}	2297 ± 28	149 ± 40	seen	$\phi\phi, K\bar{K}, \gamma\gamma, \Lambda\bar{\Lambda}$ seen
$f_2(2340)$	2^{++}	2346^{+21}_{-10}	331^{+27}_{-18}	no obs. $\gamma\gamma$ decay	$\phi\phi, K\bar{K}$ seen

uncertainties) with differences appearing due to the previous use of simplified photon fluxes, absence of survival probability corrections, and/or outdated diphoton widths, although there are also some inconsistencies likely due to typos and/or errors in past results. One can see, as expected from Eq. (7), that for the same particle spin, all cross sections decrease with resonance mass following the $\propto m_X^{-2}$ dependence of the photon-fusion cross section as well as the m_X^{-n} power-law decrease (with exponents $n = 1.25\text{--}1.8$ depending on the system and c.m. energy) of the two-photon effective luminosities (Figs. 2). Although, in some cases, such a generic trend is partially compensated by comparatively larger diphoton partial widths for concrete heavier resonances. The UPC cross sections results at colliders of Tables 4, 5, and 6 are plotted as a function of collision energy in Figs. 3, 4, and 5, respectively, showing their dependence on $\ln^3(s_{NN})$.

Tables 4, 5, and 6 list also the total yields $N_{\text{evts}}(\gamma\gamma \rightarrow X) = \sigma(\gamma\gamma \rightarrow X) \times \mathcal{L}_{\text{int}}$, as well as the yields in their diphoton

TABLE 4: Photon-fusion cross sections $\sigma(\gamma\gamma \rightarrow X)$, total yields $N_{\text{evts}}(\gamma\gamma \rightarrow X)$, and yields $N_{\text{evts}}(\gamma\gamma \rightarrow X(\gamma\gamma))$ in the diphoton decay mode, for the production of light-quark spin-0,-2 resonances with masses $m_X \lesssim 1$ GeV and known $\gamma\gamma$ decay widths (Table 2) in UPCs for various colliding systems at RHIC, LHC, and FCC c.m. energies. Previously derived cross sections (if available) are also listed for reference. The last row gives the corresponding cross sections in proton-air collisions at GZK-cutoff energies.

System, $\sqrt{s_{\text{NN}}}$, \mathcal{L}_{int}	Ref.	π^0	η	$f_0(500)$	η'
Au-Au, 0.2 TeV, 10 nb^{-1} :					
$\sigma(\gamma\gamma \rightarrow X)$	Eq. (7)	$6.1 \pm 0.1 \text{ mb}$	$1.6 \pm 0.06 \text{ mb}$	$2.3 \pm 0.5 \text{ mb}$	$1.1 \pm 0.04 \text{ mb}$
	[22, 27, 28]	5.72, 5.0, 4.94 mb	1.29, 0.85, 1.00 mb	—	0.99, 0.59, 0.75 mb
$N_{\text{evts}}(\gamma\gamma \rightarrow X)$		6.1×10^7	1.6×10^7	2.3×10^7	1.1×10^7
$N_{\text{evts}}(\gamma\gamma \rightarrow X(\gamma\gamma))$		6.1×10^7	6.2×10^6	15	2.6×10^5
Pb-Pb, 5.5 TeV, 10 nb^{-1} :					
$\sigma(\gamma\gamma \rightarrow X)$	Eq. (7)	$45 \pm 1 \text{ mb}$	$23 \pm 1 \text{ mb}$	$29 \pm 6 \text{ mb}$	$26 \pm 1 \text{ mb}$
	[22, 27, 28, 41]	43, 46, 28, 38 ^a mb	19.9, 20, 16, 17.3 ^a mb	—	24.8, 25, 21, 21.8 ^a mb
$N_{\text{evts}}(\gamma\gamma \rightarrow X)$		4.5×10^8	2.3×10^8	2.9×10^8	2.6×10^8
$N_{\text{evts}}(\gamma\gamma \rightarrow X(\gamma\gamma))$		4.4×10^8	8.9×10^7	180	6.0×10^6
p-Pb, 8.8 TeV, 1 pb^{-1} :					
$\sigma(\gamma\gamma \rightarrow X)$	Eq. (7)	$11.1 \pm 0.2 \mu\text{b}$	$6.4 \pm 0.2 \mu\text{b}$	$8.1 \pm 1.8 \mu\text{b}$	$7.9 \pm 0.3 \mu\text{b}$
$N_{\text{evts}}(\gamma\gamma \rightarrow X)$		1.1×10^7	6.4×10^6	8.1×10^6	7.9×10^6
$N_{\text{evts}}(\gamma\gamma \rightarrow X(\gamma\gamma))$		1.1×10^7	2.5×10^6	5	1.8×10^5
p-p, 14 TeV, 1 fb^{-1} :					
$\sigma(\gamma\gamma \rightarrow X)$	Eq. (7)	$2.8 \pm 0.1 \text{ nb}$	$1.8 \pm 0.1 \text{ nb}$	$2.2 \pm 0.5 \text{ nb}$	$2.3 \pm 0.1 \text{ nb}$
$N_{\text{evts}}(\gamma\gamma \rightarrow X)$		2.8×10^6	1.8×10^6	2.2×10^6	2.3×10^6
$N_{\text{evts}}(\gamma\gamma \rightarrow X(\gamma\gamma))$		2.8×10^6	7.1×10^5	1.3	5.4×10^4
Pb-Pb, 39.4 TeV, 110 nb^{-1} :					
$\sigma(\gamma\gamma \rightarrow X)$	Eq. (7)	$93 \pm 1.4 \text{ mb}$	$56 \pm 2 \text{ mb}$	$70 \pm 15 \text{ mb}$	$70 \pm 2 \text{ mb}$
$N_{\text{evts}}(\gamma\gamma \rightarrow X)$		1.0×10^{10}	6.1×10^9	7.7×10^9	7.7×10^9
$N_{\text{evts}}(\gamma\gamma \rightarrow X(\gamma\gamma))$		1.0×10^{10}	2.4×10^9	4.6×10^3	1.8×10^8
p-Pb, 62.8 TeV, 29 pb^{-1} :					
$\sigma(\gamma\gamma \rightarrow X)$	Eq. (7)	$21.0 \pm 0.3 \mu\text{b}$	$13 \pm 0.5 \mu\text{b}$	$17 \pm 3.6 \mu\text{b}$	$18 \pm 0.6 \mu\text{b}$
$N_{\text{evts}}(\gamma\gamma \rightarrow X)$		6.1×10^8	3.9×10^8	4.9×10^8	5.1×10^8
$N_{\text{evts}}(\gamma\gamma \rightarrow X(\gamma\gamma))$		6.0×10^8	1.5×10^8	290	1.2×10^7
p-p, 100 TeV, 10 fb^{-1} :					
$\sigma(\gamma\gamma \rightarrow X)$	Eq. (7)	$4.8 \pm 0.1 \text{ nb}$	$3.3 \pm 0.12 \text{ nb}$	$4.1 \pm 0.9 \text{ nb}$	$4.5 \pm 0.14 \text{ nb}$
$N_{\text{evts}}(\gamma\gamma \rightarrow X)$		4.8×10^7	3.3×10^7	4.1×10^7	4.5×10^7
$N_{\text{evts}}(\gamma\gamma \rightarrow X(\gamma\gamma))$		4.8×10^7	1.3×10^7	25	1.0×10^6
p-air, 400 TeV:					
$\sigma(\gamma\gamma \rightarrow X)$	Eq. (7)	$280 \pm 4 \text{ nb}$	$200 \pm 7 \text{ nb}$	$246_{-54}^{+55} \text{ nb}$	$270 \pm 9 \text{ nb}$

^aResult for Pb-Pb(5.02 TeV) UPCs.

decay mode $N_{\text{evts}}(\gamma\gamma \rightarrow X(\gamma\gamma))$ (obtained by multiplying the former by their $\mathcal{B}(X \rightarrow \gamma\gamma)$ value), expected in UPCs at the various colliders. To obtain such numbers, we use the nominal integrated luminosities for the p-A and A-A running modes (Table 1), but only a small fraction of the p-p data (1 fb^{-1} at the LHC, and 10 fb^{-1} at the FCC-hh) that is assumed to be recorded under the low-pileup conditions needed to properly identify exclusive processes in UPCs and reconstruct such low-mass objects. Given the inherent uncertainty on the actual luminosity integrated by the experiments, we provide the values of $N_{\text{evts}}(\gamma\gamma \rightarrow X)$ and $N_{\text{evts}}(\gamma\gamma \rightarrow X) \rightarrow \gamma\gamma$ without uncertainties, as an indication of the order-of-magnitude events expected (here, and in all other tables of the paper).

The number of UPC collisions expected to exclusively produce light-quark even-spin resonances over 0.14–2.3 GeV masses is very large, amounting to millions to hundred-millions events at the LHC, and about factors of 10 to 1000 smaller for Au-Au(200 GeV) UPCs at RHIC. The number of those resonances that “decay back” to a pair of photons is several orders-of-magnitude smaller (except for the two lightest, π^0 and η , mesons), but some of them will have enough number of events to be also observed in such a clean decay mode. However, their small masses and the fact that photon-fusion leads to negligible transverse momentum (p_T) boosts, implies decays into very soft hadronic or diphoton final states that make their observation very difficult in the large-acceptance ATLAS [67] and CMS [68] experiments,

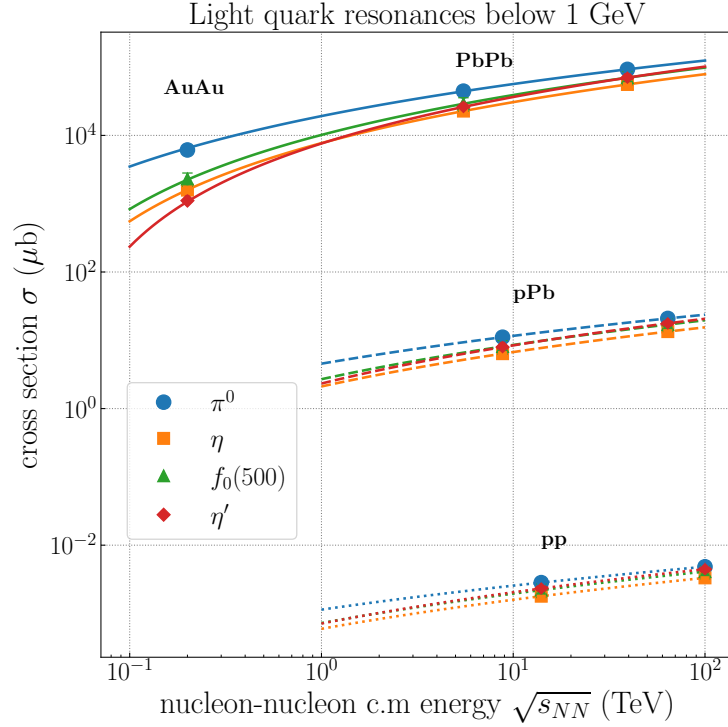


FIG. 3: Cross sections for the $\gamma\gamma$ production of even-spin light mesons (with $m_X \lesssim 1$ GeV and known $\gamma\gamma$ widths) as a function of nucleon-nucleon c.m. energy $\sqrt{s_{NN}}$, in Pb-Pb or Au-Au (solid curves), p-Pb (dashed curves), and p-p (dotted curves) UPCs. The curves are $\ln^3(s_{NN})$ fits to guide the eye.

which are optimized for the reconstruction of particles with much larger p_T values. Despite smaller acceptances (as well as, comparatively reduced integrated luminosities in some cases), the ALICE [69] (in particular, the proposed ALICE-3 [70]) as well as the LHCb [71] (in particular, the proposed LHCb upgrade II [72, 73]) experiments have much better adapted detectors to reconstruct such soft decays. In the hadronic decays modes there will be potentially larger backgrounds from other processes –such as exclusive photoproduction for UPCs with ions (photon-pomeron interactions) and central-exclusive (pomeron-pomeron) processes for p-p collisions– but the diphoton decays (despite being comparatively suppressed) offer a cleaner final state to attempt their observation on top of the light-by-light continuum (Section 7). Of course, experimental acceptance and efficiency losses will further reduce the yields (a determination of them goes beyond the scope of this paper), but the measurement of the cross sections for such light mesons in UPCs at the LHC, and the subsequent determination of their diphoton widths (which are badly known in most cases) via Eq. (22), provides additional interesting physics cases for the future ALICE 3 and LHCb-upgrade-II experiments.

TABLE 5: Photon-fusion cross sections $\sigma(\gamma\gamma \rightarrow X)$, total yields $N_{\text{evts}}(\gamma\gamma \rightarrow X)$, and yields $N_{\text{evts}}(\gamma\gamma \rightarrow X(\gamma\gamma))$ in the diphoton decay mode, for the production of light-quark spin-0,-2 resonances with masses $m_X \approx 1\text{--}1.5$ GeV and known $\gamma\gamma$ decay widths (Table 2) in UPCs for various colliding systems at RHIC, LHC, and FCC c.m. energies. Previously derived cross sections (if available) are also listed for reference. The last row gives the corresponding cross sections in proton-air collisions at GZK-cutoff energies.

System, $\sqrt{s_{\text{NN}}}$, \mathcal{L}_{int}	Ref.	$f_0(980)$	$a_0(980)$	$f_2(1270)$	$a_2(1320)$	$a_0(1450)$
Au-Au, 0.2 TeV, 10 nb ⁻¹ :						
$\sigma(\gamma\gamma \rightarrow X)$	Eq. (7)	$66^{+25}_{-14} \mu\text{b}$	$71 \pm 24 \mu\text{b}$	$920 \pm 180 \mu\text{b}$	$310 \pm 20 \mu\text{b}$	$190 \pm 10 \mu\text{b}$
	[22, 27, 28]	$91 \mu\text{b}, -, -$	—	$680, 410, 545 \mu\text{b}$	$250, 140, 195 \mu\text{b}$	—
$N_{\text{evts}}(\gamma\gamma \rightarrow X)$		6.6×10^5	7.1×10^5	9.2×10^6	3.1×10^6	1.9×10^6
$N_{\text{evts}}(\gamma\gamma \rightarrow X(\gamma\gamma))$		2	2	130	30	35
Pb-Pb, 5.5 TeV, 10 nb ⁻¹ :						
$\sigma(\gamma\gamma \rightarrow X)$	Eq. (7)	$1.5^{+0.6}_{-0.3} \text{mb}$	$1.7 \pm 0.6 \text{mb}$	$28 \pm 5.3 \text{mb}$	$9.5 \pm 0.6 \text{mb}$	$6.4 \pm 0.3 \text{mb}$
	[22, 27, 28, 41]	$2.50 \text{mb}, -, -, -$	—	$24.7, 25, 22, 22.4^a \text{mb}$	$9.54, 7.7, 8.2, 8.3^a \text{mb}$	—
$N_{\text{evts}}(\gamma\gamma \rightarrow X)$		1.5×10^7	1.7×10^7	2.8×10^8	9.5×10^7	6.4×10^7
$N_{\text{evts}}(\gamma\gamma \rightarrow X(\gamma\gamma))$		45	50	3900	890	1100
p-Pb, 8.8 TeV, 1 pb ⁻¹ :						
$\sigma(\gamma\gamma \rightarrow X)$	Eq. (7)	$470^{+180}_{-100} \text{nb}$	$510 \pm 170 \text{nb}$	$9.3 \pm 1.8 \mu\text{b}$	$3.2 \pm 0.2 \mu\text{b}$	$2.2 \pm 0.1 \mu\text{b}$
$N_{\text{evts}}(\gamma\gamma \rightarrow X)$		4.7×10^5	5.1×10^5	9.3×10^6	3.2×10^6	2.2×10^6
$N_{\text{evts}}(\gamma\gamma \rightarrow X(\gamma\gamma))$		1.5	1.5	130	30	40
p-p, 14 TeV, 1 fb ⁻¹ :						
$\sigma(\gamma\gamma \rightarrow X)$	Eq. (7)	$140^{+50}_{-30} \text{pb}$	$150 \pm 50 \text{pb}$	$2.6 \pm 0.5 \text{nb}$	$910 \pm 55 \text{pb}$	$630 \pm 26 \text{pb}$
$N_{\text{evts}}(\gamma\gamma \rightarrow X)$		1.4×10^5	1.5×10^5	2.6×10^6	9.1×10^5	6.3×10^5
$N_{\text{evts}}(\gamma\gamma \rightarrow X(\gamma\gamma))$		0.5	0.5	40	10	10
Pb-Pb, 39.4 TeV, 110 nb ⁻¹ :						
$\sigma(\gamma\gamma \rightarrow X)$	Eq. (7)	$4.1^{+1.6}_{-0.9} \text{mb}$	$4.5 \pm 1.5 \text{mb}$	$78 \pm 15 \text{mb}$	$27 \pm 2 \text{mb}$	$18 \pm 1 \text{mb}$
$N_{\text{evts}}(\gamma\gamma \rightarrow X)$		4.6×10^8	4.9×10^8	8.6×10^9	3.0×10^9	2.0×10^9
$N_{\text{evts}}(\gamma\gamma \rightarrow X(\gamma\gamma))$		1300	1500	1.2×10^5	2.8×10^4	3.6×10^4
p-Pb, 62.8 TeV, 29 pb ⁻¹ :						
$\sigma(\gamma\gamma \rightarrow X)$	Eq. (7)	$1.1^{+0.4}_{-0.2} \mu\text{b}$	$1.1 \pm 0.4 \mu\text{b}$	$21 \pm 4 \mu\text{b}$	$7.2 \pm 0.4 \mu\text{b}$	$5.0 \pm 0.2 \mu\text{b}$
$N_{\text{evts}}(\gamma\gamma \rightarrow X)$		3.1×10^7	3.3×10^7	6.1×10^8	2.1×10^8	1.4×10^8
$N_{\text{evts}}(\gamma\gamma \rightarrow X(\gamma\gamma))$		100	100	85×10^3	2000	2600
p-p, 100 TeV, 10 fb ⁻¹ :						
$\sigma(\gamma\gamma \rightarrow X)$	Eq. (7)	$265^{+100}_{-55} \text{pb}$	$280 \pm 95 \text{pb}$	$5.2 \pm 1.0 \text{nb}$	$1.8 \pm 0.1 \text{nb}$	$1.24 \pm 0.05 \text{nb}$
$N_{\text{evts}}(\gamma\gamma \rightarrow X)$		2.6×10^6	2.8×10^6	5.2×10^7	1.8×10^7	1.2×10^7
$N_{\text{evts}}(\gamma\gamma \rightarrow X(\gamma\gamma))$		10	10	720	170	220
p-air, 400 TeV:						
$\sigma(\gamma\gamma \rightarrow X)$	Eq. (7)	16^{+6}_{-3}nb	$17 \pm 6 \text{nb}$	$320 \pm 60 \text{nb}$	$110 \pm 7 \text{nb}$	$76 \pm 3 \text{nb}$

^aResult for Pb-Pb(5.02 TeV) UPCs.

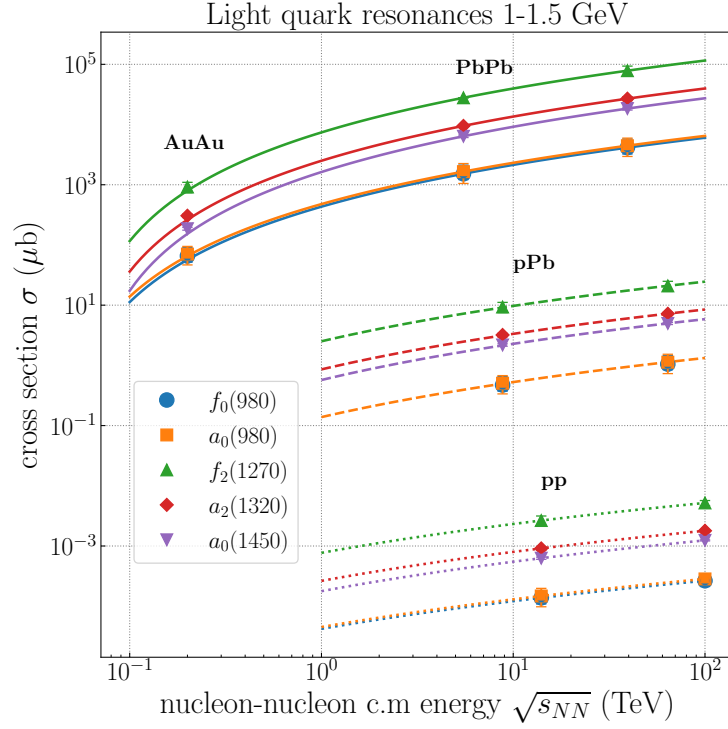


FIG. 4: Cross sections for the $\gamma\gamma$ production of even-spin light mesons (with $m_X = 1-1.5$ GeV and known $\gamma\gamma$ widths) as a function of nucleon-nucleon c.m. energy $\sqrt{s_{NN}}$, in Pb-Pb or Au-Au (solid curves), p-Pb (dashed curves), and p-p (dotted curves) UPCs. The curves are $\ln^3(s_{NN})$ fits to guide the eye.

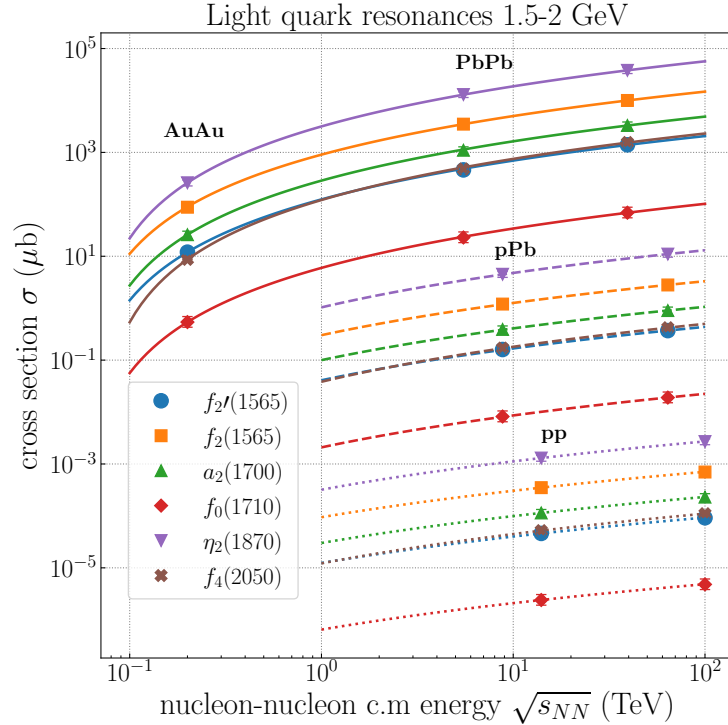


FIG. 5: Cross sections for the $\gamma\gamma$ production of light mesons (with $m_X = 1.5-2.0$ GeV and known $\gamma\gamma$ widths) as a function of nucleon-nucleon c.m. energy $\sqrt{s_{NN}}$, in Pb-Pb or Au-Au (solid curves), p-Pb (dashed curves), and p-p (dotted curves) UPCs. The curves are $\ln^3(s_{NN})$ fits to guide the eye.

TABLE 6: Photon-fusion cross sections $\sigma(\gamma\gamma \rightarrow X)$, total yields $N_{\text{evts}}(\gamma\gamma \rightarrow X)$, and yields $N_{\text{evts}}(\gamma\gamma \rightarrow X(\gamma\gamma))$ in the diphoton decay mode, for the production of light-quark spin-0,-2 resonances with masses $m_X \approx 1.5\text{--}2$ GeV and known $\gamma\gamma$ decay widths (Table 2) in UPCs for various colliding systems at RHIC, LHC, and FCC c.m. energies. Previously derived cross sections (if available) are also listed for reference. The last row gives the corresponding cross sections in proton-air collisions at GZK-cutoff energies.

System, $\sqrt{s_{\text{NN}}}$, \mathcal{L}_{int}	Ref.	$f'_2(1525)$	$f_2(1565)$	$a_2(1700)$	$f_0(1710)$	$\eta_2(1870)$	$f_4(2050)$
Au-Au, 0.2 TeV, 10 nb ⁻¹ :							
$\sigma(\gamma\gamma \rightarrow X)$	Eq. (7) [22, 27]	$12 \pm 1.3 \mu\text{b}$ -, $6.6 \mu\text{b}$	$88 \pm 18 \mu\text{b}$ —	$26 \pm 4.4 \mu\text{b}$ —	$540^{+150}_{-110} \text{ nb}$ —	$264 \pm 34 \mu\text{b}$ —	$8.7 \pm 0.17 \mu\text{b}$ $22.1^a \mu\text{b}$, —
$N_{\text{evts}}(\gamma\gamma \rightarrow X)$		1.2×10^5	8.8×10^5	2.6×10^5	5.4×10^3	2.6×10^6	8.7×10^3
$N_{\text{evts}}(\gamma\gamma \rightarrow X(\gamma\gamma))$		0.1	5	0.2	10^{-3}	50	0.05
Pb-Pb, 5.5 TeV, 10 nb ⁻¹ :							
$\sigma(\gamma\gamma \rightarrow X)$	Eq. (7) [22, 27]	$465 \pm 50 \mu\text{b}$ -, $450 \mu\text{b}$	$3.5 \pm 0.7 \text{ mb}$ —	$1.1 \pm 0.2 \text{ mb}$ —	$23^{+6.4}_{-4.7} \mu\text{b}$ —	$13 \pm 1.6 \text{ mb}$ —	$480 \pm 10 \mu\text{b}$ 1.6^a mb , —
$N_{\text{evts}}(\gamma\gamma \rightarrow X)$		4.6×10^6	3.5×10^7	1.1×10^7	2.3×10^5	1.3×10^8	4.8×10^6
$N_{\text{evts}}(\gamma\gamma \rightarrow X(\gamma\gamma))$		5	180	10	0.05	2500	3
p-Pb, 8.8 TeV, 1 pb ⁻¹ :							
$\sigma(\gamma\gamma \rightarrow X)$	Eq. (7)	$0.16 \pm 0.02 \mu\text{b}$	$1.2 \pm 0.2 \mu\text{b}$	$390 \pm 65 \text{ nb}$	$8.2^{+2.3}_{-1.7} \text{ nb}$	$4.5 \pm 0.58 \mu\text{b}$	$175 \pm 3 \text{ nb}$
$N_{\text{evts}}(\gamma\gamma \rightarrow X)$		1.6×10^5	1.2×10^6	3.9×10^5	8200	4.5×10^6	1.8×10^5
$N_{\text{evts}}(\gamma\gamma \rightarrow X(\gamma\gamma))$		0.2	6	0.3	10^{-3}	90	0.1
p-p, 14 TeV, 1 fb ⁻¹ :							
$\sigma(\gamma\gamma \rightarrow X)$	Eq. (7)	$46 \pm 5 \text{ pb}$	$350 \pm 70 \text{ pb}$	$110 \pm 20 \text{ pb}$	$2.4^{+0.7}_{-0.5} \text{ pb}$	$1.3 \pm 0.17 \text{ nb}$	$52 \pm 1 \text{ pb}$
$N_{\text{evts}}(\gamma\gamma \rightarrow X)$		4.6×10^4	3.5×10^5	1.1×10^5	2400	1.3×10^6	5.2×10^4
$N_{\text{evts}}(\gamma\gamma \rightarrow X(\gamma\gamma))$		0.05	2	0.1	5×10^{-4}	30	0.03
Pb-Pb, 39.4 TeV, 110 nb ⁻¹ :							
$\sigma(\gamma\gamma \rightarrow X)$	Eq. (7)	$1.4 \pm 0.1 \text{ mb}$	$10 \pm 2 \text{ mb}$	$3.3 \pm 0.5 \text{ mb}$	$69.3^{+19}_{-14} \mu\text{b}$	$38 \pm 5 \text{ mb}$	$1.6 \pm 0.03 \text{ mb}$
$N_{\text{evts}}(\gamma\gamma \rightarrow X)$		1.5×10^8	1.1×10^9	3.6×10^8	7.6×10^6	4.2×10^9	1.7×10^8
$N_{\text{evts}}(\gamma\gamma \rightarrow X(\gamma\gamma))$		140	6000	290	2	8×10^4	100
p-Pb, 62.8 TeV, 29 pb ⁻¹ :							
$\sigma(\gamma\gamma \rightarrow X)$	Eq. (7)	$370 \pm 40 \text{ nb}$	$2.8 \pm 0.6 \mu\text{b}$	$900 \pm 150 \text{ nb}$	$19^{+5.3}_{-3.9} \text{ nb}$	$11 \pm 1.4 \mu\text{b}$	$420 \pm 8 \text{ nb}$
$N_{\text{evts}}(\gamma\gamma \rightarrow X)$		1.1×10^7	8.1×10^7	2.6×10^7	5.5×10^5	3.1×10^8	1.2×10^7
$N_{\text{evts}}(\gamma\gamma \rightarrow X(\gamma\gamma))$		10	430	20	0.1	6100	7
p-p, 100 TeV, 10 fb ⁻¹ :							
$\sigma(\gamma\gamma \rightarrow X)$	Eq. (7)	$92 \pm 10 \text{ pb}$	$700 \pm 140 \text{ pb}$	$280 \pm 47 \text{ pb}$	$4.8^{+1.3}_{-1.0} \text{ pb}$	$2.7 \pm 0.4 \text{ nb}$	$110 \pm 2 \text{ pb}$
$N_{\text{evts}}(\gamma\gamma \rightarrow X)$		9.2×10^5	7.0×10^6	2.3×10^6	4.8×10^4	2.7×10^7	1.1×10^6
$N_{\text{evts}}(\gamma\gamma \rightarrow X(\gamma\gamma))$		1	40	0.2	0.01	540	0.6
p-air, 400 TeV:							
$\sigma(\gamma\gamma \rightarrow X)$	Eq. (7)	$5.7 \pm 0.6 \text{ nb}$	$43 \pm 8.6 \text{ nb}$	$14 \pm 2.4 \text{ nb}$	$300^{+82}_{-61} \text{ pb}$	$164 \pm 21 \text{ nb}$	$6.9 \pm 0.1 \text{ nb}$

^aUsing $\Gamma_{\gamma\gamma} = 1.4 \text{ keV}$, which is about 10 times larger than the value we used.

B. Production of heavy quarkonium resonances

Table 7 lists the relevant properties of all presently known (pseudo) scalar and tensor resonances formed by charmonium and bottomonium bound states with masses over $m_X \approx 3\text{--}10$ GeV. Moreover, we also list the para-toponium $\eta_t \equiv (\bar{t}t)_0$ state, a theoretical quasibound object formed by a top-antitop quark pair interacting via the QCD interaction for ultrashort time scales [74], that has been hinted at in the LHC data recently [75]. Masses are measured precisely for all the particles, but not all their two-photon widths have been (properly) experimentally determined [23]. On the one hand, starting with the lightest heavy-quarkonium state ($\eta_c(1S)$), a recent direct measurement by BES-III finds $\Gamma(\eta_c(1S) \rightarrow \gamma\gamma) = 11.30 \pm 1.43$ keV [76], which is more than twice larger than the current PDG world-average for this decay, $\Gamma(\eta_c(1S) \rightarrow \gamma\gamma) = 5.06 \pm 0.40$ keV. Similarly, the diphoton width of the $\eta_c(2S)$ state is also badly known, and has presently a $\pm 60\%$ experimental uncertainty. On the other hand, the $\gamma\gamma$ decays of the four $b\bar{b}$ resonances ($\eta_b(1S)$, $\eta_b(2S)$, χ_{b0} , χ_{b2}) remain unobserved so far. All these results highlight the issues affecting many heavy-quarkonium diphoton widths for which we use theoretical predictions as explained below. For the $\eta_c(1S) \rightarrow \gamma\gamma$ partial width, to avoid the aforementioned contradictory experimental results, we use the recent lattice QCD calculations of Ref. [77]. For the $\eta_b(1S)$ and $\eta_b(2S)$ cases, predictions exist for their two-photon partial widths in nonrelativistic QCD (NRQCD) [78, 79]. Exploiting heavy-quark spin symmetry, the two-photon $\eta_b(nS) \rightarrow \gamma\gamma$ and leptonic $\Upsilon(nS) \rightarrow \ell^+\ell^-$ decay widths are proportional to the same wavefunction at the origin, and the NRQCD calculations use the theoretical ratio between them, $\Gamma(n^3S_1 \rightarrow e^+e^-)/\Gamma(n^1S_0 \rightarrow \gamma\gamma)$, taking into cancellations between higher-order relativistic and radiative corrections, together with the (latest) experimental values of $\Gamma(\Upsilon(1S, 2S) \rightarrow e^+e^-) = 1.291 \pm 0.030$, 0.611 ± 0.050 keV [23], to obtain $\Gamma(\eta_b(1S), \eta_b(2S) \rightarrow \gamma\gamma) = 0.493 \pm 0.092$, 0.24 ± 0.04 keV, respectively. We quote this latter $\Gamma(\eta_b(2S) \rightarrow \gamma\gamma)$ value in Table 7, whereas for the $\eta_b(1S) \rightarrow \gamma\gamma$ partial width we use the more recent lattice QCD calculations that have a 6% precision [80]. The diphoton widths of χ_{b0}, χ_{b2} are based on the range of model predictions given in Ref. [81].

We also consider the ephemeral spin-singlet para-toponium bound state, η_t , formed by a top and anti-top quark [74], which can be perturbatively described in NRQCD with a single-gluon exchange potential of the form $V(r) = -C_F\alpha_s/r$, where $C_F = 4/3$ is the quark-antiquark color factor. Such a state has a mass of $m_{\eta_t} \approx 2m_t + E_{\text{bind}} = 343.1 \pm 0.9$ GeV, obtained using the current PDG mass value of $m_t = 172.5 \pm 0.45$ GeV [23] and $E_{\text{bind}} = -\frac{1}{4}m_t(C_F\bar{\alpha}_s)^2 \approx -1.9$ GeV, where $\bar{\alpha}_s \approx 0.16$ is the strong coupling evaluated⁷ at the typical scale given by the toponium radius, i.e., $\bar{\alpha}_s = \alpha_s(r_{\text{Bohr}}^{-1})$, whose numerical value can be obtained iteratively by finding the scale μ that satisfies $\mu = C_F m_t \alpha_s(\mu)$ [82–84]. Such a state has thus a Bohr radius of order $r_{\text{Bohr}} = (C_F/2\bar{\alpha}_s m_t)^{-1} \approx 0.01$ fm. Toponium is extremely short-lived and its revolution time of $t \approx r_{\text{Bohr}} \approx 0.01$ fm [85] is of the same order of magnitude as its lifetime driven by the electroweak decay of any of its constituent quarks $t, \bar{t} \rightarrow W^+b, W^-\bar{b}$. The η_t decay width is thus very large, of order $\Gamma(\eta_t) \approx 2\Gamma_t = 2.66$ GeV, using the NNLO value of the top-quark width $\Gamma_t = 1.33$ GeV [86]. The $\eta_t(1S)$ diphoton width can be obtained from the standard analytic expressions for heavy-quarkonium diphoton decays [87], which at NLO accuracy reads:

$$\Gamma(\eta_t(1S) \rightarrow \gamma\gamma) = \frac{12q_t^4\alpha^2}{m_{\eta_t}^2}|R_0(0)|^2 \left[1 + \frac{\alpha_s}{\pi} \left(\frac{\pi^2}{3} - \frac{20}{3} \right) \right], \quad (23)$$

where $|R_0(0)|^2 = 4n^3/r_{\text{Bohr}}^3 = 4(C_F/2\bar{\alpha}_s m_t)^3$ is the wavefunction at the origin, $q_t = 2/3$ the top quark electric charge, and $\alpha_s = \alpha_s(m_t) = 0.096$, yielding: $\Gamma(\eta_t(1S) \rightarrow \gamma\gamma) = 22.6$ keV. The diphoton widths of higher $\eta_t(nS)$ states amount to $\Gamma(\eta_t(nS) \rightarrow \gamma\gamma) = \Gamma(\eta_t(1S) \rightarrow \gamma\gamma)/n^3$, which implies $\Gamma(\eta_t(2S) \rightarrow \gamma\gamma) = 2.82$ keV for the 2S state. Since toponium is a very broad pseudoresonance, it is unlikely that one can experimentally separate the different nS para-states, and it is more realistic to consider the photon-photon production for the sum of all of them combined, which amounts to

$$\Gamma(\eta_t(nS) \rightarrow \gamma\gamma) = \zeta(3) \frac{12q_t^4\alpha^2}{m_{\eta_t}^2}|R_0(0)|^2 \left[1 + \frac{\alpha_s}{\pi} \left(\frac{\pi^2}{3} - \frac{20}{3} \right) \right], \quad \text{with } \zeta(3) = \sum_{n=1}^{\infty} \frac{1}{n^3} = 1.20205 \text{ (Apéry's constant)}. \quad (24)$$

Based on the diphoton widths of Table 7 and on Eq. (7), we provide the theoretical predictions for the photon-fusion cross sections for even-spin charmonium, bottomonium, and toponium resonances produced in UPCs at various c.m. energies in Tables 8 and 9, respectively. Uncertainties in the cross sections are dominated by the propagated uncertainty of the corresponding $\Gamma_{\gamma\gamma}$ widths and vary between 5% and 100%. The cross sections are compared to previous estimates, with differences appearing mostly due to updated values of a few heavy-quarkonium diphoton widths. The photon-fusion cross sections for the different charmonium, bottomonium, and toponium states produced

⁷ Equivalently, one can also find the expressions for the toponium properties written as a function of the typical velocity of the top quarks in the bound state: $v_t = C_F\bar{\alpha}_s = 0.21$.

TABLE 7: List of C-even heavy-quarkonium resonances that can be produced via two-photon fusion. For each particle, we quote its J^{PC} quantum numbers, mass m_X , total width Γ_{tot} , and diphoton partial width $\Gamma_{\gamma\gamma}$ and branching fraction $\mathcal{B}(X \rightarrow \gamma\gamma)$, from measurements [23] or theoretical predictions (for $\eta_c(1S)$, $\eta_b(1S)$, $\eta_b(2S)$, χ_{b0}, χ_{b2} , and $\eta_t(nS)$, see text for details), and dominant decay channels.

Resonance	J^{PC}	m_X (GeV)	Γ_{tot} (MeV)	$\Gamma_{\gamma\gamma}$ (keV)	$\mathcal{B}(X \rightarrow \gamma\gamma)$	Dominant decay (\mathcal{B})
$\eta_c(1S)$	0^{-+}	2.9841 ± 0.0004	30.5 ± 0.5	6.788 ± 0.061 [77]	$(2.23 \pm 0.06) \cdot 10^{-4}$	$2(\pi^+\pi^-\pi^0)$ ($15.9 \pm 2.0\%$)
$\eta_c(2S)$	0^{-+}	3.6377 ± 0.0009	11.8 ± 1.6	2.12 ± 1.45	$(1.8 \pm 1.2) \cdot 10^{-4}$	$K\bar{K}\pi$ ($1.9 \pm 1.2\%$)
χ_{c0}	0^{++}	3.41471 ± 0.00030	10.7 ± 0.6	2.18 ± 0.16	$(2.04 \pm 0.10) \cdot 10^{-4}$	$\pi^+\pi^-\pi^0\pi^0$ ($3.3 \pm 0.4\%$)
χ_{c2}	2^{++}	3.55617 ± 0.0007	1.98 ± 0.09	0.578 ± 0.035	$(2.92 \pm 0.12) \cdot 10^{-4}$	$J/\psi\gamma$ ($19.0 \pm 0.5\%$)
$\eta_b(1S)$	0^{-+}	9.3987 ± 0.0020	10^{+5}_{-4}	0.557 ± 0.032 [80]	$(5.6^{+4.0}_{-3.2}) \cdot 10^{-5}$	gg ($\approx 100\%$)
$\eta_b(2S)$	0^{-+}	9.999 ± 0.004	5^{+3}_{-2}	0.24 ± 0.04^a	$(4.8^{+4.7}_{-3.7}) \cdot 10^{-5}$	gg ($\approx 100\%$)
χ_{b0}	0^{++}	9.85944 ± 0.00052	$2.60^{+0.79}_{-0.57}$	$0.15^{+0.05}_{-0.03}$ [81]	$(5.8^{+3.1}_{-2.1}) \cdot 10^{-5}$	$\Upsilon(2S)\gamma$ ($1.94 \pm 0.27\%$)
χ_{b2}	2^{++}	9.91221 ± 0.00040	$0.180^{+0.016}_{-0.057}$	$(9.3^{+1.3}_{-6.2}) \cdot 10^{-3}$ [81]	$(5.2^{+1.0}_{-4.2}) \cdot 10^{-5}$	$\Upsilon(1S)\gamma$ ($18.0 \pm 1.0\%$)
$\eta_t(nS)$	0^{-+}	≈ 344	≈ 2660	27.2	$1.022 \cdot 10^{-5}$	$W^+W^-\bar{b}\bar{b}$ ($\approx 100\%$)

^aResult based on NRQCD calculations [79] and the latest experimental data (see text).

in UPCs at RHIC, LHC, and FCC-hh are plotted as a function of $\sqrt{s_{NN}}$ in Figs. 6–8, respectively. The tables provide also the number of heavy-quarkonium events expected for the considered integrated luminosities at each facility, so as to assess the feasibility of their potential experimental measurement. In Pb-Pb UPCs at the LHC, we expect hundreds to thousands events with even-spin charmonium resonances produced exclusively that decay back into a pair of photons. The measurement of exclusive charmonia in this decay mode (or in their much more abundant hadronic decays) appears therefore feasible for the ALICE and LHCb detectors (on top of the light-by-light continuum, see Section 7)). The perspectives for bottomonium appear more challenging, though. First, one can see that the exclusive bottomonium production cross sections are negligible at RHIC, because the effective two-photon luminosities are too low above $m_X \approx 4$ GeV at this collider (Fig. 2). The number of exclusive bottomonia produced in UPCs at the LHC are in the hundreds to thousands events (depending on the system and concrete particle) and their potential measurement would only be feasible in their dominant hadronic decays (although no concrete exclusive hadronic final states have been measured for $\eta_b(1S), \eta_b(2S) \rightarrow gg$, yet) or in their quarkonium + photon decays (for $\chi_{b0}, \chi_{b2} \rightarrow \Upsilon + \gamma$), as their diphoton branching fractions are too small.

Last but not least, the rightmost row of Table 9 gives the photon-fusion cross sections for $\eta_t(nS)$ para-toponium, which is the smallest ones considered in this study given the very high mass of this object. The cross section for such a system has large uncertainties at the LHC (see Fig. 8), because at such high energies the charged-form-factor photon fluxes are highly oscillating [36] and their integration is not fully reliable. Although the largest $\gamma\gamma \rightarrow \eta_t(nS)$ cross sections (tens of pb) are reached in Pb-Pb UPCs at the FCC-hh, the beam luminosities are too low for any meaningful number of events to be produced. The only system where the para-toponium measurement can be attempted is in p-p collisions at the LHC (with about 40 events expected) and FCC-hh (about 1300 events to be produced) by exploiting the whole data set of 6 and 30 ab^{-1} integrated luminosities to be collected under high pileup conditions. An observation of the $\gamma\gamma$ production of toponium could be realized in p-p collisions by searching for a back-to-back $t\bar{t}$ pair produced at rest (i.e., with zero pair p_T) in coincidence with two intact protons reconstructed in very forward proton spectrometers, such as those from the CMS-TOTEM PPS system [88], whose acceptance for photon-fusion systems is optimal in the toponium mass range, $m_{\gamma\gamma} \gtrsim 350$ GeV [89–91]. In this case, one will have to deal with a background from the $\gamma\gamma \rightarrow t\bar{t}$ continuum at around threshold $m_{t\bar{t}} = 2m_{\text{top}}$, which has a cross section larger than the toponium one by about a factor of 50, $\sigma(\gamma\gamma \rightarrow t\bar{t}) \approx 300$ ab at the LHC [36, 92] (but over all $t\bar{t}$ pair masses).

TABLE 8: Photon-fusion cross sections $\sigma(\gamma\gamma \rightarrow X)$, total yields $N_{\text{evts}}(\gamma\gamma \rightarrow X)$, and yields $N_{\text{evts}}(\gamma\gamma \rightarrow X(\gamma\gamma))$ in the diphoton decay mode, for the production of all known even-spin charmonium resonances (Table 7) in UPCs for various colliding systems at RHIC, LHC, and FCC c.m. energies. Previously derived cross sections (if available) are also listed for reference. The last row gives the corresponding cross sections in proton-air collisions at GZK-cutoff energies.

System, $\sqrt{s_{\text{NN}}}$, \mathcal{L}_{int}	Ref.	$\eta_c(1S)$	$\eta_c(2S)$	χ_{c0}	χ_{c2}
Au-Au, 0.2 TeV, 10 nb^{-1} :					
$\sigma(\gamma\gamma \rightarrow X)$	Eq. (7)	$5.7 \pm 0.05 \mu\text{b}$	$0.56 \pm 0.38 \mu\text{b}$	$0.85 \pm 0.04 \mu\text{b}$	$0.88 \pm 0.05 \mu\text{b}$
	[22, 27, 28]	3.66, 1.8, $3.3 \mu\text{b}$	—	1.36, 0.38, $0.63 \mu\text{b}$	—, 0.17, $0.59 \mu\text{b}$
$N_{\text{evts}}(\gamma\gamma \rightarrow X)$		5.6×10^4	5600	8500	8800
$N_{\text{evts}}(\gamma\gamma \rightarrow X(\gamma\gamma))$		10	1	2	2.5
Pb-Pb, 5.5 TeV, 10 nb^{-1} :					
$\sigma(\gamma\gamma \rightarrow X)$	Eq. (7)	$0.62 \pm 0.01 \text{ mb}$	$91 \pm 63 \mu\text{b}$	$0.12 \pm 0.01 \text{ mb}$	$0.14 \pm 0.01 \text{ mb}$
	[22, 27, 28]	0.56, 0.54, 0.61 mb	—	0.29, 0.17, 0.16 mb	—, 0.085, 0.15 mb
	[36, 39, 41]	0.46, 0.39, 0.43^a mb	95, 80, $90^a \mu\text{b}$	0.12, 0.10, 0.11^a mb	0.13, 0.11, 0.12^a mb
$N_{\text{evts}}(\gamma\gamma \rightarrow X)$		6.2×10^6	9.1×10^5	1.2×10^6	1.4×10^6
$N_{\text{evts}}(\gamma\gamma \rightarrow X(\gamma\gamma))$		1400	160	240	400
p-Pb, 8.8 TeV, 1 pb^{-1} :					
$\sigma(\gamma\gamma \rightarrow X)$	Eq. (7)	$220 \pm 2 \text{ nb}$	$33.6 \pm 23.0 \text{ nb}$	$44 \pm 3.2 \text{ nb}$	$50 \pm 3.1 \text{ nb}$
	[36, 39]	180, 160 nb	38, 33.2 nb	49, 43 nb	53, 46 nb
$N_{\text{evts}}(\gamma\gamma \rightarrow X)$		2.2×10^5	3.4×10^4	4.4×10^4	5.0×10^4
$N_{\text{evts}}(\gamma\gamma \rightarrow X(\gamma\gamma))$		50	5	10	15
p-p, 14 TeV, 1 fb^{-1} :					
$\sigma(\gamma\gamma \rightarrow X)$	Eq. (7)	$75.8 \pm 6.8 \text{ pb}$	$12.0 \pm 8.2 \text{ pb}$	$15.3 \pm 1.1 \text{ pb}$	$17.7 \pm 1.1 \text{ pb}$
	[36, 39]	56, 50 pb	12, 10.5 pb	15, 13.7 pb	17, 15 pb
$N_{\text{evts}}(\gamma\gamma \rightarrow X)$		7.6×10^4	1.2×10^4	1.5×10^4	1.8×10^4
$N_{\text{evts}}(\gamma\gamma \rightarrow X(\gamma\gamma))$		20	2	3	5
Pb-Pb, 39.4 TeV, 110 nb^{-1} :					
$\sigma(\gamma\gamma \rightarrow X)$	Eq. (7)	$2.1 \pm 0.02 \text{ mb}$	$0.33 \pm 0.22 \text{ mb}$	$0.42 \pm 0.03 \text{ mb}$	$0.49 \pm 0.03 \text{ mb}$
	[36]	1.6 mb	0.33 mb	0.43 mb	0.47 mb
$N_{\text{evts}}(\gamma\gamma \rightarrow X)$		2.3×10^8	3.6×10^7	4.6×10^7	5.3×10^7
$N_{\text{evts}}(\gamma\gamma \rightarrow X(\gamma\gamma))$		5.2×10^4	6500	9500	1.6×10^4
p-Pb, 62.8 TeV, 29 pb^{-1} :					
$\sigma(\gamma\gamma \rightarrow X)$	Eq. (7)	$610 \pm 60 \text{ nb}$	$98 \pm 67 \text{ nb}$	$130 \pm 1 \text{ nb}$	$144 \pm 5 \text{ nb}$
	[36]	460 nb	100 nb	130 nb	140 nb
$N_{\text{evts}}(\gamma\gamma \rightarrow X)$		1.8×10^7	2.8×10^6	3.6×10^6	4.2×10^6
$N_{\text{evts}}(\gamma\gamma \rightarrow X(\gamma\gamma))$		4000	510	740	1200
p-p, 100 TeV, 10 fb^{-1} :					
$\sigma(\gamma\gamma \rightarrow X)$	Eq. (7)	$160 \pm 1.4 \text{ pb}$	$26 \pm 18 \text{ pb}$	$33.0 \pm 2.4 \text{ pb}$	$37.9 \pm 2.3 \text{ pb}$
	[36]	120 nb	26 pb	33 pb	37 pb
$N_{\text{evts}}(\gamma\gamma \rightarrow X)$		1.6×10^6	2.58×10^5	3.28×10^5	3.79×10^5
$N_{\text{evts}}(\gamma\gamma \rightarrow X(\gamma\gamma))$		360	45	70	10
p-air, 400 TeV:					
$\sigma(\gamma\gamma \rightarrow X)$	Eq. (7)	$8.01 \pm 0.59 \text{ nb}$	$1.71 \pm 1.12 \text{ nb}$	$2.09 \pm 0.09 \text{ nb}$	$2.33 \pm 0.08 \text{ nb}$

^aResult for Pb-Pb(5.02 TeV) UPCs.

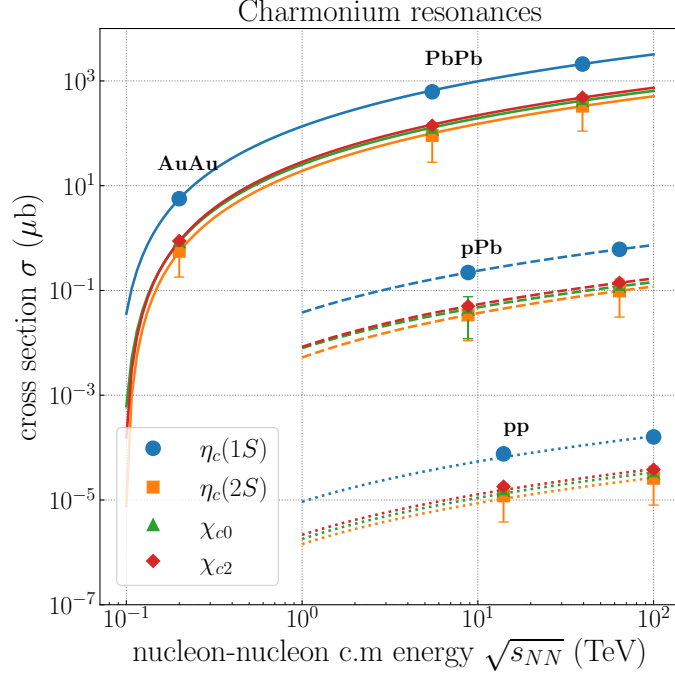


FIG. 6: Cross sections for the $\gamma\gamma$ production of even-spin charmonium mesons as a function of nucleon-nucleon c.m. energy $\sqrt{s_{NN}}$, in Pb-Pb or Au-Au (solid curves), p-Pb (dashed curves), and p-p (dotted curves) UPCs. The curves are $\ln^3(s_{NN})$ fits to guide the eye.

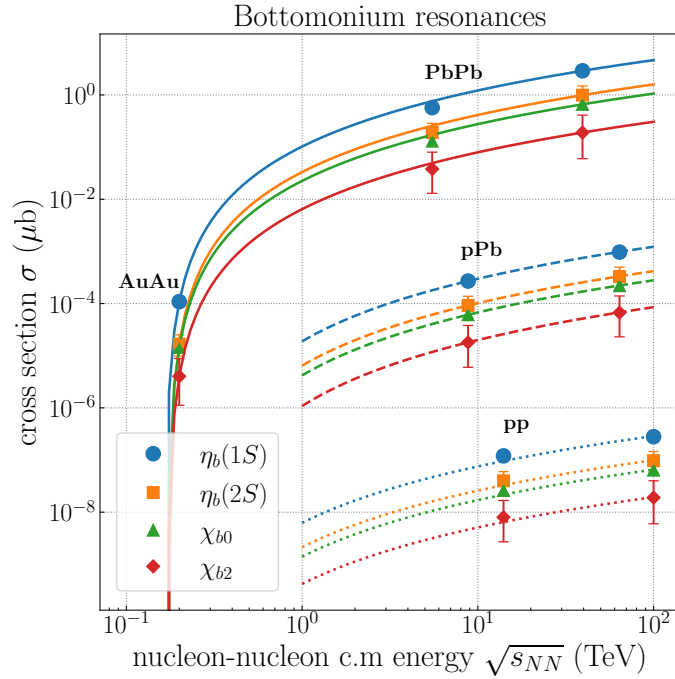


FIG. 7: Cross sections for the $\gamma\gamma$ production of even-spin bottomonium mesons as a function of nucleon-nucleon c.m. energy $\sqrt{s_{NN}}$, in Pb-Pb or Au-Au (solid curves), p-Pb (dashed curves), and p-p (dotted curves) UPCs. The curves are $\ln^3(s_{NN})$ fits to guide the eye.

TABLE 9: Photon-fusion cross sections $\sigma(\gamma\gamma \rightarrow X)$, total yields $N_{\text{evts}}(\gamma\gamma \rightarrow X)$, and yields $N_{\text{evts}}(\gamma\gamma \rightarrow X(\gamma\gamma))$ in the diphoton decay mode, for the production of all known even-spin bottomonium and toponium resonances (Table 7) in UPCs for various colliding systems at RHIC, LHC, and FCC c.m. energies. Previously derived cross sections (if available) are also listed for reference. The last row gives the corresponding cross sections in proton-air collisions at GZK-cutoff energies.

System, $\sqrt{s_{\text{NN}}}$, \mathcal{L}_{int}	Ref.	$\eta_b(1S)$	$\eta_b(2S)$	χ_{b0}	χ_{b2}	$\eta_t(\text{nS})$
Au-Au, 0.2 TeV, 10 nb ⁻¹ :						
$\sigma(\gamma\gamma \rightarrow X)$	Eq. (7) [22]	110 ± 10 pb 20 pb	16.8 ± 2.8 pb —	14.5 ^{+4.8} _{-2.9} pb —	4.0 ^{+0.6} _{-2.7} pb —	— —
$N_{\text{evts}}(\gamma\gamma \rightarrow X)$		1	0.2	0.15	0.05	—
$N_{\text{evts}}(\gamma\gamma \rightarrow X(\gamma\gamma))$		—	—	—	—	—
Pb-Pb, 5.5 TeV, 10 nb ⁻¹ :						
$\sigma(\gamma\gamma \rightarrow X)$	Eq. (7) [22, 27, 36]	570 ± 30 nb -, 410, 500 nb	190 ± 30 nb -, 320, 190 nb	130 ⁺⁴⁰ ₋₃₀ nb -, 15, 130 nb	38 ⁺⁵ ₋₂₅ nb -, 20, 38 nb	1.2 ^{+1.2} _{-0.96} fb —
$N_{\text{evts}}(\gamma\gamma \rightarrow X)$		5700	1900	1300	380	1 × 10 ⁻⁵
$N_{\text{evts}}(\gamma\gamma \rightarrow X(\gamma\gamma))$		0.3	0.1	0.1	0.02	—
p-Pb, 8.8 TeV, 1 pb ⁻¹ :						
$\sigma(\gamma\gamma \rightarrow X)$	Eq. (7) [36]	270 ± 20 pb 270 pb	92 ± 15 pb 106 pb	61 ⁺²⁰ ₋₁₂ pb 70 pb	18 ⁺³ ₋₁₂ pb 21 pb	0.63 ± 0.32 fb —
$N_{\text{evts}}(\gamma\gamma \rightarrow X)$		270	90	60	20	6 × 10 ⁻⁴
$N_{\text{evts}}(\gamma\gamma \rightarrow X(\gamma\gamma))$		0.01	5 × 10 ⁻³	3 × 10 ⁻³	10 ⁻³	—
p-p, 14 TeV, 1 fb ⁻¹ (6 ab ⁻¹ for $\eta_t(\text{nS})$):						
$\sigma(\gamma\gamma \rightarrow X)$	Eq. (7) [36]	116 ± 7 fb 100 fb	40 ± 7 fb 40 fb	26 ⁺⁹ ₋₃ fb 26 fb	8.0 ^{+1.1} _{-5.4} fb 8.0 fb	6.4 ± 2.0 ab —
$N_{\text{evts}}(\gamma\gamma \rightarrow X)$		120	40	25	10	40
$N_{\text{evts}}(\gamma\gamma \rightarrow X(\gamma\gamma))$		6 × 10 ⁻³	2 × 10 ⁻³	2 × 10 ⁻³	4 × 10 ⁻⁴	—
Pb-Pb, 39.4 TeV, 110 nb ⁻¹ :						
$\sigma(\gamma\gamma \rightarrow X)$	Eq. (7) [36]	2.88 ± 0.17 μb 2.5 μb	1.0 ± 0.2 μb 1.0 μb	0.66 ^{+0.22} _{-0.13} μb 0.66 μb	0.20 ^{+0.03} _{-0.13} μb 0.19 μb	40 pb —
$N_{\text{evts}}(\gamma\gamma \rightarrow X)$		3.2 × 10 ⁵	1.1 × 10 ⁵	7.2 × 10 ⁴	2.2 × 10 ⁴	4.5
$N_{\text{evts}}(\gamma\gamma \rightarrow X(\gamma\gamma))$		20	5	4	1	—
p-Pb, 62.8 TeV, 29 pb ⁻¹ :						
$\sigma(\gamma\gamma \rightarrow X)$	Eq. (7) [36]	0.97 ± 0.56 nb 0.83 nb	0.33 ± 0.06 nb 0.33 nb	0.22 ^{+0.07} _{-0.04} nb 0.22 nb	67 ⁺⁹ ₋₄₅ pb 67 pb	55 fb —
$N_{\text{evts}}(\gamma\gamma \rightarrow X)$		2.8 × 10 ⁴	9700	6400	1900	1.6
$N_{\text{evts}}(\gamma\gamma \rightarrow X(\gamma\gamma))$		2	50	0.4	0.1	—
p-p, 100 TeV, 10 fb ⁻¹ (30 ab ⁻¹ for $\eta_t(\text{nS})$):						
$\sigma(\gamma\gamma \rightarrow X)$	Eq. (7) [36]	0.28 ± 0.16 pb 0.24 pb	97 ± 16 fb 96 fb	64 ⁺²¹ ₋₁₃ fb 63 fb	19 ⁺³ ₋₁₃ fb 19 fb	40 ab —
$N_{\text{evts}}(\gamma\gamma \rightarrow X)$		2800	970	640	190	1300
$N_{\text{evts}}(\gamma\gamma \rightarrow X(\gamma\gamma))$		0.15	0.05	0.05	0.01	0.01
p-air, 400 TeV:						
$\sigma(\gamma\gamma \rightarrow X)$	Eq. (7)	18.0 ± 1.0 pb	6.3 ± 1.0 pb	4.2 ^{+1.4} _{-0.8} pb	1.3 ^{+0.2} _{-0.8} pb	3.4 fb

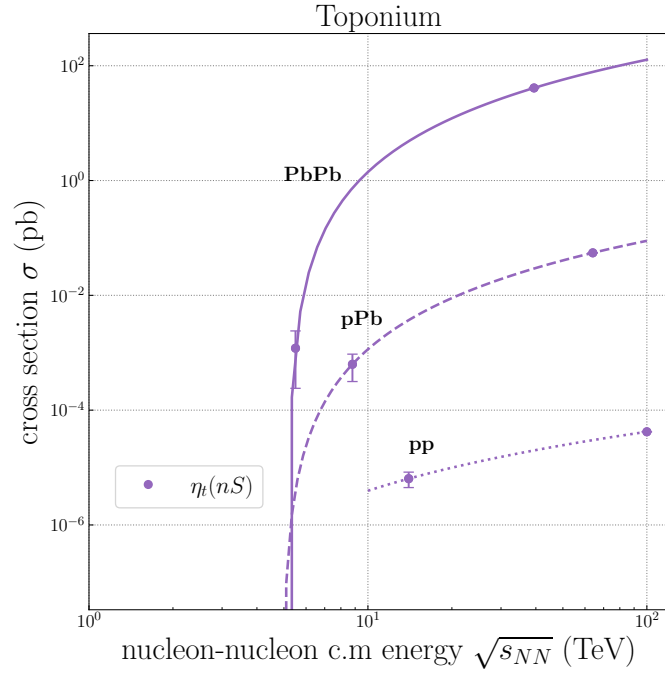


FIG. 8: Cross sections for the $\gamma\gamma$ production of toponium $\eta_t(nS)$ as a function of nucleon-nucleon c.m. energy $\sqrt{s_{NN}}$, in Pb-Pb (solid curves), p-Pb (dashed curves), and p-p (dotted curves) UPCs. The curves are $\ln^3(s_{NN})$ fits to guide the eye.

C. Production of exotic hadrons

In principle, QCD permits the existence of exotic types of hadrons — such as multiquark (tetra-, penta-, hexa-quarks), glueballs, hybrids (q \bar{q} states with “valence” gluons) states — that are beyond the conventional meson and baryon structure in the constituent quark model [93, 94]. The discovery of the first tetraquark candidate, $\chi_{c1}(3872)$, in 2003 [95] triggered a renewed interest in hadronic spectroscopy, and multiple types of new exotic hadronic states have been observed in the last years at the LHC and B-factories [96–98]. Any new exotic multiquark hadron with even spin can be produced via photon fusion provided its diphoton width is not too small. Since the actual existence of many of such states (with the PDG often omitting them from the summary tables unless they are confirmed by more than one experiment), as well as their exact nature (compact multiquark system, or hadronic molecule made of charge conjugated pairs of mesons) and spectroscopic properties are often not precisely known, the study of their production via photon-photon fusion in UPCs can help confirm their quantum numbers and/or determine their diphotons widths, among others. In this section, we extend previous studies [31, 32, 34, 35, 37, 38, 41] to consider all presently known even-spin exotic hadron states (Table 10), and compute their cross sections for a large variety of colliding systems (Table 11). In most of the cases, their exact spin (0 or 2) state, as well as their diphoton decays, remain experimentally unsettled. For their diphoton partial widths, we use the theoretical results of [31] or [34] and, given their large model dependencies, we only quote an approximate value for them.

TABLE 10: List of even-spin exotic hadrons producible via two-photon fusion. For each particle, we quote its J^{PC} quantum numbers, mass m_X , total width Γ_{tot} , and diphoton partial width $\Gamma_{\gamma\gamma}$ from measurements or theoretical predictions. The middle line separates light- from heavy-quark states.

Resonance	J^{PC}	m_X (MeV)	Γ_{tot} (MeV)	$\Gamma_{\gamma\gamma}$ (eV)	Decay(s); comment
X(2370)	0^{-+}	2377 ± 9	148^{+80}_{-28}	unknown	$K\bar{K}\eta', \pi\pi\eta'$; glueball candidate [99]
T_{cs0}^* (2900)	2^{++}	$2892 \pm 14 \pm 15$	$119 \pm 26 \pm 13$	unknown	$D_s\pi$; tetraquark candidate [100, 101]
$\chi_{c0}(3860)$	0^{++}	≈ 3862	≈ 200	unknown	$D^+D^-, D^0\bar{D}^0$
$\chi_{c0}(3915)$	$0^{++}/2^{++}$	3922.1 ± 1.8	20 ± 4	≈ 200	$D^+D^-, J/\psi\omega$
$\chi_{c2}(3930)$	2^{++}	3922.5 ± 1.0	35.2 ± 2.2	≈ 80	$D^+D^-, J/\psi\omega$
X(3940)	$0^{++}/2^{++}$	$3942^{+7}_{-6} \pm 6$	$37^{+26}_{-15} \pm 8$	≈ 300	$\mathcal{B}(D\bar{D}^* + \text{c.c.}) > 0.45$
$X_0(4140)$	0^{++} 2^{++}	4146.8 ± 2.5	19^{+8}_{-7}	≈ 630 ≈ 500	$c\bar{s}\bar{c}s$ tetraquark candidate
X(4350)	$0^{++}/2^{++}$	$4350.6^{+4.6}_{-5.1} \pm 0.7$	$13^{+18}_{-9} \pm 4$	unknown	$J/\psi\phi, \gamma\gamma$
$\chi_{c0}(4500)$	0^{++}	$4474 \pm 3 \pm 3$	$77 \pm 6^{+10}_{-8}$	unknown	$J/\psi\phi$
$\chi_{c0}(4700)$	0^{++}	$4694 \pm 4^{+16}_{-3}$	$87 \pm 8^{+16}_{-6}$	unknown	$J/\psi\phi$
$T_{ccc}(6900)$	$0^{++}/2^{++}$	6899 ± 12	153 ± 29	≈ 100 [34]	$J/\psi J/\psi$, tetra-charm candidate

The calculated photon-fusion cross-sections of exotic hadrons are listed in Table 11, and shown in graphical form as a function of collision energy in Fig. 9. The expected inclusive yields for such exotic states are relatively large, assuming that their estimated diphoton widths are correct, but their observation via diphoton decays appears unfeasible and experimental searches should be carried out in hadronic final states instead (D^+D^- ,). By searching for their $\gamma\gamma$ production in UPCs, their production yields can help ascertain whether their spin is 0 or 2, as in the latter case they are comparatively enhanced by a factor of five as per Eq. (7). Our cross section predictions are in general consistent with those of previous works, if available, except for the $T_{ccc}(6900)$ results of Ref. [41] that use $\Gamma_{\gamma\gamma} = 67/45$ keV (with/without interference), which is 500 times larger than the diphoton decay width that we have adopted. It is also worth noting that all cross sections quoted for [32] and [35] are total cross sections for the $\gamma\gamma \rightarrow \chi_{c0}(3915) \rightarrow J/\psi\omega$ and $\gamma\gamma \rightarrow X(6900) \rightarrow J/\psi J/\psi$ production, respectively.

TABLE 11: Photon-fusion cross sections $\sigma(\gamma\gamma \rightarrow X)$, total yields $N_{\text{evts}}(\gamma\gamma \rightarrow X)$, and yields $N_{\text{evts}}(\gamma\gamma \rightarrow X(\gamma\gamma))$ in the diphoton decay mode, for the production of spin-0,-2 exotic hadronic states (Table 10) in UPCs for various colliding systems at RHIC, LHC, and FCC c.m. energies. Previously derived cross sections (if available) are also listed for reference. The last row gives the corresponding cross sections in proton-air collisions at GZK-cutoff energies.

System, $\sqrt{s_{\text{NN}}}$, \mathcal{L}_{int}	Ref.	$\chi_{c0}(3915)$		$\chi_{c2}(3930)$	X(3940)		$X_0(4140)$		$T_{\text{ccc}}(6900)$	
		0 ⁺⁺	2 ⁺⁺		0 ⁺⁺	2 ⁺⁺	0 ⁺⁺	2 ⁺⁺	0 ⁺⁺	2 ⁺⁺
Au-Au, 0.2 TeV, 10 nb ⁻¹ :										
$\sigma(\gamma\gamma \rightarrow X)$	Eq. (7)	28.8 nb	144 nb	57.6 nb	42.2 nb	211 nb	69.2 nb	275 nb	290 pb	1.43 nb
$N_{\text{evts}}(\gamma\gamma \rightarrow X)$		290	1400	580	420	2100	690	2700	2.9	14
$N_{\text{evts}}(\gamma\gamma \rightarrow X(\gamma\gamma))$		10 ⁻³	0.01	10 ⁻³	10 ⁻³	0.02	0.02	0.1	–	–
Pb-Pb, 5.5 TeV, 10 nb ⁻¹ :										
$\sigma(\gamma\gamma \rightarrow X)$	Eq. (7)	6.5 μb	32 μb	13 μb	9.5 μb	48 μb	16 μb	65 μb	360 nb	1.8 μb
	[31]	6.7 μb	–	13.9 μb	10.8 μb	44.2 μb	–	–	–	–
	[32] ^a	1.5–2.8 μb	2.2–4.0 μb	–	–	–	–	–	–	–
	[35] ^a	–	–	–	–	–	–	–	171 nb	206 nb
	[41] ^a	6.0 μb	–	12.4 μb	9.7 μb	39.6 μb	–	–	238/160 μb	–
$N_{\text{evts}}(\gamma\gamma \rightarrow X)$		6.5 $\times 10^4$	3.2 $\times 10^5$	1.3 $\times 10^5$	9.5 $\times 10^4$	4.8 $\times 10^5$	1.6 $\times 10^5$	6.5 $\times 10^5$	3.6 $\times 10^3$	1.8 $\times 10^4$
$N_{\text{evts}}(\gamma\gamma \rightarrow X(\gamma\gamma))$		1	3	0.3	1	4	5	20	–	0.01
p-Pb, 8.8 TeV, 1 pb ⁻¹ :										
$\sigma(\gamma\gamma \rightarrow X)$	Eq. (7)	2.4 nb	12 nb	4.8 nb	3.5 nb	18 nb	6.2 nb	25 nb	0.15 nb	0.76 nb
	[31]	2.8 nb	–	5.7 nb	4.5 nb	18.3 nb	–	–	–	–
	[32] ^b	0.56–1.1 nb	0.84–1.6 nb	–	–	–	–	–	–	–
	[35] ^b	–	–	–	–	–	–	–	76.3 pb	92.4 pb
$N_{\text{evts}}(\gamma\gamma \rightarrow X)$		2.4 $\times 10^3$	1.2 $\times 10^4$	4.8 $\times 10^3$	3.5 $\times 10^3$	1.8 $\times 10^4$	6.2 $\times 10^3$	2.5 $\times 10^4$	150	760
$N_{\text{evts}}(\gamma\gamma \rightarrow X(\gamma\gamma))$		0.02	0.1	0.01	0.03	0.1	0.2	1	–	–
p-p, 14 TeV, 1 fb ⁻¹ :										
$\sigma(\gamma\gamma \rightarrow X)$	Eq. (7)	0.87 pb	4.4 pb	1.7 pb	1.3 pb	6.4 pb	2.3 pb	9.0 pb	62 fb	310 fb
	[31]	0.86 pb	–	1.8 pb	1.5 pb	5.7 pb	–	–	–	–
	[32] ^c	0.18–0.33 fb	0.27–0.49 fb	–	–	–	–	–	–	–
	[35] ^c	–	–	–	–	–	–	–	26.3 fb	31.9 fb
$N_{\text{evts}}(\gamma\gamma \rightarrow X)$		870	4.4 $\times 10^3$	1.7 $\times 10^3$	1.3 $\times 10^3$	6.4 $\times 10^3$	2.3 $\times 10^3$	9 $\times 10^3$	62	310
$N_{\text{evts}}(\gamma\gamma \rightarrow X(\gamma\gamma))$		0.01	0.05	10 ⁻³	0.01	0.05	0.1	0.2	–	–
Pb-Pb, 39.4 TeV, 110 nb ⁻¹ :										
$\sigma(\gamma\gamma \rightarrow X)$	Eq. (7)	24 μb	120 μb	47 μb	35 μb	170 μb	61 μb	240 μb	1.6 μb	7.9 μb
	[31]	24.5 μb	–	50.5 μb	39.6 μb	162 μb	–	–	–	–
	[41]	20.1 μb	–	41.7 μb	32.5 μb	133 μb	–	–	912/612 μb	–
$N_{\text{evts}}(\gamma\gamma \rightarrow X)$		2.6 $\times 10^6$	1.3 $\times 10^7$	5.2 $\times 10^6$	3.8 $\times 10^6$	1.9 $\times 10^7$	6.8 $\times 10^6$	2.7 $\times 10^7$	1.7 $\times 10^5$	8.7 $\times 10^5$
$N_{\text{evts}}(\gamma\gamma \rightarrow X(\gamma\gamma))$		26	130	10	30	160	220	710	0.1	1
p-Pb, 62.8 TeV, 29 pb ⁻¹ :										
$\sigma(\gamma\gamma \rightarrow X)$	Eq. (7)	7.1 nb	36 nb	14 nb	11 nb	53 nb	19 nb	75 nb	0.5 nb	2.6 nb
	[31]	7.0 nb	–	14.5 nb	11.3 nb	46.3 nb	–	–	–	–
$N_{\text{evts}}(\gamma\gamma \rightarrow X)$		2.1 $\times 10^5$	10 ⁶	4.1 $\times 10^5$	3 $\times 10^5$	1.5 $\times 10^6$	5.4 $\times 10^5$	2.1 $\times 10^6$	1.5 $\times 10^4$	7.4 $\times 10^4$
$N_{\text{evts}}(\gamma\gamma \rightarrow X(\gamma\gamma))$		2	10	1	2.5	10	20	50	0.01	0.05
p-p, 100 TeV, 10 fb ⁻¹ :										
$\sigma(\gamma\gamma \rightarrow X)$	Eq. (7)	1.9 pb	9.5 pb	3.8 pb	2.8 pb	14 pb	4.9 pb	20 pb	0.14 pb	0.7 pb
	[31]	1.8 pb	–	3.6 pb	2.8 pb	11.6 pb	–	–	–	–
$N_{\text{evts}}(\gamma\gamma \rightarrow X)$		1.9 $\times 10^4$	9.5 $\times 10^4$	3.8 $\times 10^4$	2.8 $\times 10^4$	1.4 $\times 10^5$	4.9 $\times 10^4$	2 $\times 10^5$	1400	7100
$N_{\text{evts}}(\gamma\gamma \rightarrow X(\gamma\gamma))$		0.2	1	0.1	0.2	1	2	5	–	–
p-air, 400 TeV:										
$\sigma(\gamma\gamma \rightarrow X)$	Eq. (7)	120 pb	600 pb	240 pb	180 pb	880 pb	310 pb	1.2 nb	9.1 pb	45 pb

^aResults for Pb-Pb(5.02 TeV) UPCs.

^bResults for p-Pb(8.1 TeV) UPCs.

^cResults for p-p(13 TeV) UPCs.

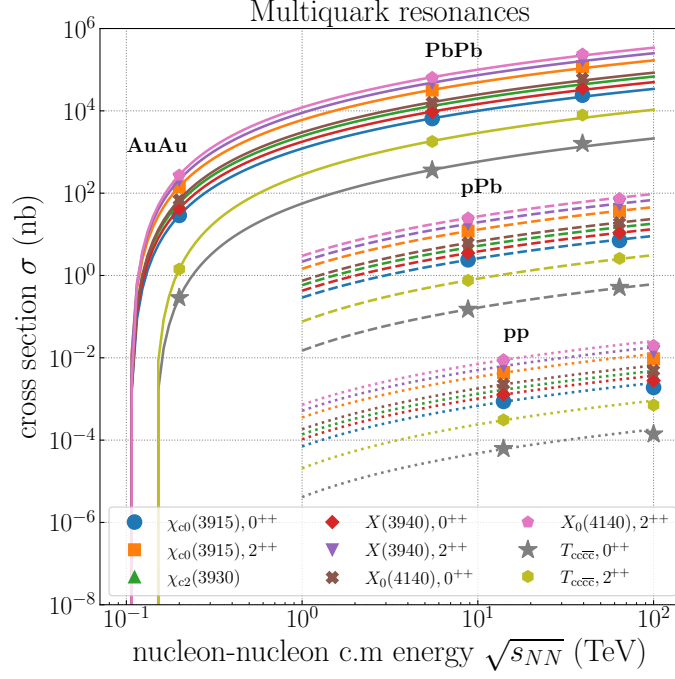


FIG. 9: Cross sections for the $\gamma\gamma$ production of even-spin exotic hadrons as a function of nucleon-nucleon c.m. energy $\sqrt{s_{NN}}$, in Pb-Pb or Au-Au (solid curves), p-Pb (dashed curves), and p-p (dotted curves) UPCs. The curves are $\ln^3(s_{NN})$ fits to guide the eye.

4. PHOTON-FUSION PRODUCTION OF LEPTONIUM STATES

Leptons with opposite charges ($\ell^+\ell^-$), such as electrons and positrons (e^\pm), muons (μ^\pm), and tau particles (τ^\pm), can temporarily pair up to form onium states under their QED interaction. The smallest of these pairs, known as positronium (a bound state of an electron and a positron), was first identified over 75 years ago [102], but its heavier siblings involving muon and tau particles (often called, respectively, dimuonium and ditauonium) have not yet been observed. The photon-photon production of leptonium states in UPCs has been considered several times in the literature [27, 29, 30, 33, 36, 39, 40, 42]. Here, we recall the basic properties of leptonium states, and present results for the production of all three species in UPCs at current and future hadron colliders.

The properties of the pure-QED leptonium systems can be straightforwardly derived from the expressions of Section 2 B. Here, we are interested in the para-leptonium systems, spin-singlet configurations where the lepton pairs have their spins aligned oppositely and are characterized by the quantum numbers $J^{PC} = 0^{-+}$, which can thus be produced in two-photon collisions. At leading order, the diphoton width of the para-leptonia ground state 1^1S_0 can be obtained from Eq. (20) and amounts to:

$$\Gamma_{(\ell^+\ell^-)_0 \rightarrow \gamma\gamma} = \frac{\alpha^5 m_\ell}{2}. \quad (25)$$

The formula for the corresponding photon-photon cross section in UPCs of hadrons A and B can be obtained by plugging this expression into Eq. (7). Neglecting the tiny binding and Breit mass corrections, Eq. (16), the para-leptonium production cross sections in UPCs read,

$$\sigma(\text{A B} \xrightarrow{\gamma\gamma} \text{A} (\ell^+\ell^-)_0 \text{B}) = \pi^2 (2J+1) \frac{\alpha^5}{m_\ell} \left. \frac{d\mathcal{L}_{\gamma\gamma}^{(\text{AB})}}{d\hat{s}_{\gamma\gamma}} \right|_{\hat{s}_{\gamma\gamma}=m_{(\ell^+\ell^-)_0}}, \quad (26)$$

which depend only on the ratio of fifth-power of the QED coupling over the lepton mass. For the determination of UPC cross sections, we will not use the LO expressions above, presented here for illustration purposes, but Eq. (7) with the leptonium masses and diphoton widths computed with the highest theoretical accuracy known today.

In Table 12, the basic properties of the para states of positronium [103–106], dimuonium [107, 108], and ditauonium [109, 110] are collected. Based on the diphoton widths of each object, the corresponding $\gamma\gamma$ cross sections are listed in Table 13. The results computed here are in general in agreement with previous estimates, if existing, except for the Au-Au at $\sqrt{s} = 0.2$ GeV case, where our calculated value for para-ditauonium, $(\tau^+\tau^-)_0$, falls between the values computed in Refs. [40, 42]. The production cross sections, and associated yields, are very large for positronium and dimuonium, whereas they are very small for the heaviest true-tauonium system. However, the observation of the production of any of the three para-leptonium ground states in UPCs appears unfortunately unfeasible. On the one hand, the fact that positronium is extremely light (leading to a pair of ultrasoft, 0.5 MeV, decay photons) and that the $(\tau^+\tau^-)_0 \rightarrow \gamma\gamma$ decay fully overlaps with the much more probable $\chi_{c2} \rightarrow \gamma\gamma$ final state [39], precludes the experimental observation of both leptonium states. On the other hand, dimuonium could only be observed if the experimental detectors are able to reconstruct two soft decay photons with $\mathcal{O}(100)$ MeV transverse momentum, given that the $(\mu^+\mu^-)_0$ production via quasireal photon-fusion leads to very small transverse boosts.

TABLE 12: Main properties of para-leptonium ground states $(\ell^+\ell^-)_0$: quantum numbers J^{PC} , mass $m_{(\ell^+\ell^-)_0}$, ground state binding energy $E_{n=1}$, Bohr radius r_{Bohr} , lifetime (τ), total width Γ_{tot} , diphoton width $\Gamma_{\gamma\gamma}$ from Eq. (20), and dominant decay branching ratio.

$(\ell^+\ell^-)_0$ state	J^{PC}	m_X (MeV)	$E_{n=1}$ (keV)	r_{Bohr} (fm)	τ (fs)	Γ_{tot} (meV)	$\Gamma_{\gamma\gamma}$ (meV)	Dominant decay (\mathcal{B})
$(e^+e^-)_0$	0^{-+}	1.02991	$-6.859 \cdot 10^{-3}$	$106 \cdot 10^3$	$125.2 \cdot 10^3$	$5.257 \cdot 10^{-3}$	$5.257 \cdot 10^{-3}$	$\gamma\gamma$ ($\approx 100\%$)
$(\mu^+\mu^-)_0$	0^{-+}	211.316	-1.407	512	595.4	1.105	1.105	$\gamma\gamma$ ($\approx 100\%$)
$(\tau^+\tau^-)_0$	0^{-+}	3553.6962 ± 0.240	-23.655	30.4	27.60	23.84	18.533	$\gamma\gamma$ (77.72%)

5. PHOTON-FUSION PRODUCTION OF QED HADRONIUM STATES

In this section, we discuss the photon-fusion production of even-spin systems formed by two identical hadrons of opposite charge, bound by their Coulomb interaction, which we refer to as QED ‘‘hadronium’’. The hadrons must be charged and long-lived enough so as to be able to form a bound state before decaying individually via the weak interaction. These implies the following list of six charged pseudoscalar mesons: $\pi^\pm, K^\pm, D^\pm, D_s^\pm, B^\pm, B_c^\pm$, (whose

TABLE 13: Photon-fusion cross sections $\sigma(\gamma\gamma \rightarrow X)$, total yields $N_{\text{evts}}(\gamma\gamma \rightarrow X)$, and yields $N_{\text{evts}}(\gamma\gamma \rightarrow X(\gamma\gamma))$ in the diphoton decay mode, for the production of paraleptonium states (Table 12) in UPCs for various colliding systems at RHIC, LHC, and FCC c.m. energies. The last row lists the corresponding cross sections in proton-air collisions at GZK-cutoff energies.

System, $\sqrt{s_{\text{NN}}}$, \mathcal{L}_{int}	Ref.	$(e^+e^-)_0$	$(\mu^+\mu^-)_0$	$(\tau^+\tau^-)_0$
Au-Au, 0.2 TeV, 10 nb ⁻¹ :				
$\sigma(\gamma\gamma \rightarrow X)$	Eq. (7) [27, 29] [33, 40, 42]	109 mb — -, 112.1, 136 mb	159 nb 150, 150 nb 160 ^a , 150, 200 nb	5.69 pb — -, 3.8, 9.68 pb
$N_{\text{evts}}(\gamma\gamma \rightarrow X)$		1.1×10^9	1600	0.06
$N_{\text{evts}}(\gamma\gamma \rightarrow X(\gamma\gamma))$		1.1×10^9	1600	0.04
Pb-Pb, 5.5 TeV, 10 nb ⁻¹ :				
$\sigma(\gamma\gamma \rightarrow X)$	Eq. (7) [27, 29, 30, 33] [36, 39, 40, 42]	328 mb -, -, 110 mb, - -, -, 333 ^b , 4010 ^c mb	1.36 μb 1.35, 1.35, -, 1.24 ^b μb -, -, 1.30 ^b , 1.59 μb	0.873 nb - 0.86, 0.74, 0.833 ^b , 1.08 nb
$N_{\text{evts}}(\gamma\gamma \rightarrow X)$		3.3×10^9	1.4×10^4	9
$N_{\text{evts}}(\gamma\gamma \rightarrow X(\gamma\gamma))$		3.3×10^9	1.4×10^4	7
p-Pb, 8.8 TeV, 1 pb ⁻¹ :				
$\sigma(\gamma\gamma \rightarrow X)$	Eq. (7) [36, 39]	67.5 μb —	351 pb —	0.356 pb 0.35, 0.31 pb
$N_{\text{evts}}(\gamma\gamma \rightarrow X)$		6.8×10^7	350	0.3
$N_{\text{evts}}(\gamma\gamma \rightarrow X(\gamma\gamma))$		6.8×10^7	350	0.2
p-p, 14 TeV, 1 fb ⁻¹ :				
$\sigma(\gamma\gamma \rightarrow X)$	Eq. (7) [36, 39]	14.3 nb —	92.0 fb —	0.113 fb 0.11, 0.11 fb
$N_{\text{evts}}(\gamma\gamma \rightarrow X)$		1.4×10^7	92	0.1
$N_{\text{evts}}(\gamma\gamma \rightarrow X(\gamma\gamma))$		1.4×10^7	92	0.1
Pb-Pb, 39.4 TeV, 110 nb ⁻¹ :				
$\sigma(\gamma\gamma \rightarrow X)$	Eq. (7) [33, 36, 40]	516 mb -, 538, - mb	2.97 μb -, 2.95, 2.74 μb	3.11 nb 3.1, 3.14 nb
$N_{\text{evts}}(\gamma\gamma \rightarrow X)$		5.7×10^{10}	3.3×10^5	340
$N_{\text{evts}}(\gamma\gamma \rightarrow X(\gamma\gamma))$		5.7×10^{10}	3.3×10^5	270
p-Pb, 62.8 TeV, 29 pb ⁻¹ :				
$\sigma(\gamma\gamma \rightarrow X)$	Eq. (7) [36]	102 μb —	682 pb —	0.924 pb 0.91 pb
$N_{\text{evts}}(\gamma\gamma \rightarrow X)$		3.0×10^9	2.0×10^4	27
$N_{\text{evts}}(\gamma\gamma \rightarrow X(\gamma\gamma))$		3.0×10^9	2.0×10^4	20
p-p, 100 TeV, 10 fb ⁻¹ :				
$\sigma(\gamma\gamma \rightarrow X)$	Eq. (7) [36]	20.6 nb —	0.16 pb —	0.24 fb 0.24 fb
$N_{\text{evts}}(\gamma\gamma \rightarrow X)$		2.1×10^8	1600	2.5
$N_{\text{evts}}(\gamma\gamma \rightarrow X \rightarrow \gamma\gamma)$		2.1×10^8	1600	2
p-air, 400 TeV:				
$\sigma(\gamma\gamma \rightarrow X)$	Eq. (7)	1.15 μb	9.52 pb	15.4 fb

^aResult for Pb-Pb(0.2 TeV) UPCs.

^bResult for Pb-Pb(5.02 TeV) UPCs.

^cThis value an order-of-magnitude larger than other estimates, and it is likely a typo of the paper.

shortest lifetimes among them are $\tau \approx 500$ fs for the D_s^\pm and B_c^\pm mesons, and $\tau \approx 1000, 1600$ fs for the D^\pm and B^\pm mesons), plus the following list of eight charged baryons: p, Σ^\pm , Ξ^\pm , Ω^\pm , Λ_c^\pm , Ξ_c^\pm , Ξ_b^\pm , Ω_b^\pm (where the proton is stable, and the rest of baryons have lifetimes $\tau \approx 10^{-10}$ – 10^{-13} s). The ‘‘mesonium’’ atoms are constituted by pairs of bosons and, therefore, are scalars with $J^{\text{PC}} = 0^{++}$ quantum numbers (as the pair parity P and C-parity combine as $(-1)^l$), whereas QED-baryonium, formed by opposite-charge identical fermions, can be in ortho- or para-states like leptonium, and we consider only the latter $J^{\text{PC}} = 0^{-+}$ pseudoscalar cases, which we denote as $(\text{hh})_0$, that are producible

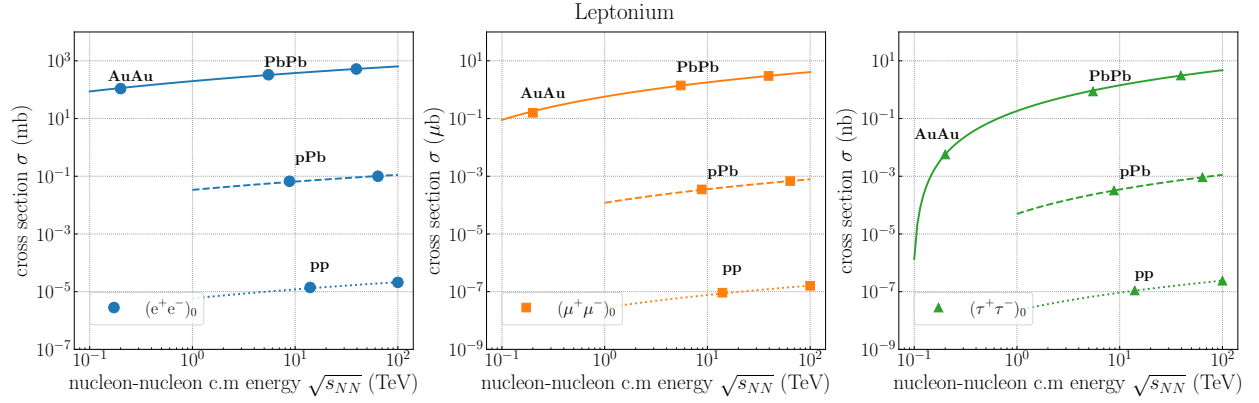


FIG. 10: Cross sections of positronium (left), dimuonium (center), and ditauonium (right) para-states in photon-photon fusion for various UPCs calculated in this work as a function of nucleon-nucleon c.m. energy.

in photon-photon collisions. We discuss here the following six QED-mesonium systems: pionium, kaonium, $D_{(s)}^{\pm}$ -onium, and $B_{(s)}^{\pm}$ -onium, which we denote by $A_{2h} \equiv (h^+h^-)$, where ‘A’ stands for an (exotic) atom and ‘h’ is the hadronic constituent. To our knowledge, the $A_{2D_s} = (D_s^+D_s^-)$ and $A_{2B_c} = (B_c^+B_c^-)$ onium states have not been considered before in the literature, whereas the other systems have been previously studied theoretically and/or experimentally. Among the QED-baryonium atoms, only protonium (also known as antiprotonic hydrogen) has been thoroughly investigated [111–115], whereas the rest of heavier systems have not been experimentally or theoretically studied to our knowledge.

The QED hadronium states are bound predominately by their Coulomb force (photon exchange) and have relatively large Bohr radii, of the order of 10–400 fm (Tables 14 and 15), that are (much) larger than the range of the strong interaction $O(1 \text{ fm})$ [116–120]. They should not be confused with hadronic molecules⁸, such as some of the objects discussed in Section 3 C, which are bound primarily by the strong interaction (gluon or pion exchanges), have much smaller radii, and much shorter lifetimes [121]. While their binding is electromagnetic, hadronium states decay mostly through the strong interaction, and their two-photon partial decay width is very small, i.e., their lifetimes are fully dominated by QCD effects. The production of such systems provides an interesting testbed for the study of low-energy hadron-hadron interactions, as modeled by chiral perturbation theory (ChPT), nonperturbative lattice QCD (LQCD) and dispersion relation analysis [122, 123]. In addition, the understanding of such A_{2h} atoms can also provide valuable information on loosely bound (molecular-like) tetraquark states [124]. Dimeson $A_{2\pi}$ and A_{2K} [125–127] atoms can be produced by colliding oppositely charged meson pairs with low relative momentum [128], and dedicated experiments, such as the CERN Proton Synchrotron Dimeson Relativistic Atom Complex (DIRAC) [129], have produced the lightest $A_{2\pi}$ atom. Similarly, experiments at the CERN Low Energy Antiproton Ring (LEAR) over the 1982–1996 period studied antiprotonic atoms via nucleon-antinucleon scattering at low energies, and in particular protonium (in states of high angular momenta l) via antiproton stopping in liquid hydrogen [111, 113].

Tables 14 and 15 list the properties of the even-spin mesonium and baryonium QED atoms, respectively, determined from the expressions of Section 2 B. Hadron masses are from the latest PDG values [23]. The diphoton widths $\Gamma_{\gamma\gamma}$ are obtained from Eqs. (21) and (20) for mesonium and baryonium systems, respectively. The dominant strong-interaction decays of the QED hadronium atoms (listed in the last column) are estimated by simple inspection of the valence quarks content of each annihilating pair and requiring the conservation of C and P quantum numbers, although their total width (or, equivalently, lifetime) has not been explicitly computed for about half of the systems⁹.

The first key observation is that the hadronium Bohr radii, derived using Eq. (13) with reduced $\mu = m_X/2$ mass

⁸ In particular, the term “baryonium” is used most often to refer to a baryon-antibaryon (not necessarily charged) system bound by pion exchange.

⁹ For those cases, we give an order-of-magnitude for Γ_{had} determined as follows. Since the dominant decay occurs via the strong interaction when the hadrons annihilate, the hadronic decay width is proportional to their squared wavefunction at the origin multiplied by the annihilation cross section times the relative velocity of the bound hadrons $v \propto \alpha$, i.e.,

$$\Gamma_{\text{had}} \approx |\psi(0)|^2 \cdot \langle \sigma_{\text{ann}} v \rangle \propto \frac{(am_h)^3}{m_h^2} \alpha \propto \alpha^4 m_h, \quad (27)$$

where the approximate scaling is derived using Eq. (14), and knowing that $\sigma_{\text{ann}} \propto 1/m_h^2$ (because annihilation happens at short distances comparable to the hadron Compton wavelength $\lambda \approx 1/m_h$). Since the hadronic decay width scales as m_h , we can approximate the total widths of heavy baryonia from the Γ_{had} values already determined for lighter hadronium systems.

TABLE 14: Main properties of QED mesonium states A_{2h} , with $h = \pi^\pm, K^\pm, D_{(s)}^\pm, B_{(c)}^\pm$. For each ground state ($n = 1$), we list its J^{PC} quantum numbers, constituent hadron mass m_{h^\pm} , atom mass m_X from Eq. (17), QED binding energy (from $E_{n=1} = 2m_h - m_X$), Bohr radius r_{Bohr} from Eq. (13), lifetime τ and total width Γ_{tot} (if known), diphoton width $\Gamma_{\gamma\gamma}$ from Eq. (21), and typical hadronic decays (and branching fraction for the pionium case).

Mesonium	J^{PC}	m_{h^\pm} (MeV)	m_X (MeV)	$E_{n=1}$ (keV)	r_{Bohr} (fm)	τ (fs)	Γ_{tot} (eV)	$\Gamma_{\gamma\gamma}$ (meV)	Typical decays (\mathcal{B})
$A_{2\pi}$	0^{++}	139.57039 ± 0.00018	279.140 ± 0.00036	-1.858	387	$3.15^{+0.28}_{-0.26}$	$(208.6^{+18.5}_{-17.2}) \cdot 10^{-3}$	0.873^a	$\pi^0\pi^0$ (99.6%)
A_{2K}	0^{++}	493.677 ± 0.013	987.347 ± 0.026	-6.576	110	$(2.2 \pm 0.9) \cdot 10^{-3}$	300 ± 120	2.56	$\pi\pi, \pi^0\eta$
A_{2D}	0^{++}	1869.66 ± 0.05	3739.32 ± 0.10	-24.90	28.88	$(0.36^{+0.28}_{-0.12}) \cdot 10^{-3}$	1800^{+1400}_{-600}	9.67	$D^0\bar{D}^0$
A_{2D_s}	0^{++}	1968.35 ± 0.14	3936.70 ± 0.28	-26.20	27.43	$\mathcal{O}(10^{-4})$	$\mathcal{O}(2000)$	10.18	$\eta\eta$
A_{2B}	0^{++}	5279.34 ± 0.12	10558.68 ± 0.24	-70.28	10.23	$\mathcal{O}(10^{-4})$	$\mathcal{O}(5000)$	27.31	$\pi\pi, \eta\eta$
A_{2B_c}	0^{++}	6274.47 ± 0.32	12548.94 ± 0.64	-83.53	8.60	$\mathcal{O}(10^{-5})$	$\mathcal{O}(6000)$	32.46	$D\bar{D}$

^aIncluding higher-order QED and QCD corrections.

for symmetric states, is (much) larger than the strong interaction range. For this reason, QCD effects do not change drastically the structure of the lightest hadronium bound-state spectra although they shift and broaden the purely QED energy levels. Both effects can be related to the S-wave hadron-hadron scattering length a_0 , a quantity of fundamental importance in studies of low-energy QCD interactions. The binding energies and diphoton widths quoted in Tables 14 and 15 are derived from the QED expressions alone (unless otherwise stated, as for the pionium case). Modifications of the binding energy of 1S hadronium atoms due to QCD effects can be estimated with the formula [130]

$$\Delta E_{n=1}^{\text{QCD}} \approx -4 \frac{|a_0|}{r_{\text{Bohr}}} E_{n=1}, \quad (28)$$

which is approximately valid for $|a_0| \ll r_{\text{Bohr}}$. Estimates of the QCD-induced modifications of the hadronium binding energies amount to a few percent for pionium and kaonium [131, 132], protonium [111, 113, 114] and D-onium [133], although they should arguably be larger for the heaviest charm and bottom hadronium atoms considered here.

The lightest system of Table 14 is pionium, discovered in 1993 at the 70-GeV Serpukhov proton-synchrotron in proton collisions on a Ta target [134], and further studied at the CERN DIRAC experiment [129, 135, 136]. Its lifetime, predicted to be $\tau = (2.90 \pm 0.10)$ fs by ChPT [137], has been experimentally determined with an 8%-precision ($\tau = 3.15^{+0.28}_{-0.26}$ fs) through a measurement of the S-wave $\pi\pi$ scattering length difference [136]. Pionium decays mostly into a pair of its lighter neutral counterparts via the $\pi^+\pi^- \rightarrow \pi^0\pi^0$ charge-exchange process [52, 116, 138, 139] and, to a much lesser extent, into two photons with a 0.36% branching ratio. For the latter partial decay width, the pure Coulomb width of $\Gamma_{\gamma\gamma} = 0.722$ meV from Eq. (21), is increased by about 21% to $0.722 \cdot [1 + 0.174 + 0.033] = 0.873$ meV by including higher-order QED (vacuum polarization) [118] and chiral expansion [122] corrections that are of $\mathcal{O}(1 + 0.132 + 0.004)$ and $\mathcal{O}(1 + 0.042 + 0.029)$ sizes, respectively. For the kaonium atom, contrary to the pionium case where charge exchange dominates, the $A_{2K} \rightarrow K^0\bar{K}^0$ decay is forbidden because the neutral kaon is heavier than the charged one. Thus, the principal strong decay modes are $A_{2K} \rightarrow \pi^+\pi^-, \pi^0\eta$ that proceed via strange quark annihilation. The kaonium lifetime has been calculated under different assumptions [126, 131, 140, 141] and found to be three orders of magnitude smaller than the pionium one. In Table 14, we use the value $\tau = (2.2 \pm 0.9) \cdot 10^{-3}$ fs (and associated total width $\Gamma = 1/\tau \approx 300$ eV) from Ref. [141].

The lightest heavy-quark QED mesonium system is the A_{2D} bound state, which decays dominantly via $A_{2D} \rightarrow D^0\bar{D}^0$ charge exchange thanks to the neutral D being slightly lighter than its charged counterparts. Searches for such an exotic atom have been proposed in the $D^0\bar{D}^0$ invariant mass distribution in high energy interactions [133] (where this exotic atom is dubbed ‘‘dionium’’). For its total decay width, we adopt the $\Gamma_{\text{tot}} = \Gamma_{D^0\bar{D}^0}$ estimate derived in Ref. [133] using lattice inputs for the $D\bar{D}$ strong interactions [142]. Its heavier sibling, the A_{2D_s} system, decays predominantly into $\eta\eta$ with charm-anticharm quark annihilation. The A_{2D_s} total width could be theoretically derived following the same approach used by Ref. [133] plus the LQCD calculations of Ref. [142], but such an exercise goes beyond the scope of this work. At variance with the A_{2D} case, the A_{2B} mesonium atom cannot decay via charge exchange as the B^0 mesons are slightly heavier than the charged ones. Its dominant decays are $A_{2B} \rightarrow \pi\pi, \eta\eta$ following bottom-antibottom annihilation. The heaviest QED mesonium system is A_{2B_c} , which decays more dominantly into $D\bar{D}$ pairs also after bottom-antibottom quark annihilation.

We now turn to the QED baryonium systems listed in Table 15, of which only protonium has been studied in detail, starting in the 1990s at the CERN LEAR through antiproton stopping in hydrogen, followed by atomic cascade of the highly excited states via X-rays emission, and final $p\bar{p}$ annihilation and production of mesons. More recently¹⁰,

¹⁰ Also, the BES III Collaboration has observed a pseudoscalar meson X(1880) in the mass spectrum of the decay of charmonium into a photon

highly-excited ($n \approx 68$) protonium has been measured by the ATHENA experiment via cold antiprotons interactions with molecular hydrogen ions in vacuum, $\bar{p} + \text{H}_2^+$, in a Penning trap at the CERN antiproton decelerator [144]. The 1S ground state of protonium decays mostly into a pair of neutral pions and η mesons. The total width of the 1S₀ ground state was found to be: $\Gamma_{\text{tot}} = 1096.7 \pm 42.3$ eV [113], which is 10^5 times larger than its partial diphoton decay width obtained via Eq. (20). The heavier even-spin QED baryonium systems considered here include those formed by pairs of light-quark (u, d, s) baryons — such as the $(\Sigma^+\Sigma^-)_0$, $(\Xi^-\Xi^+)_0$, and $(\Omega^-\Omega^+)_0$ — as well as by pairs of charmed and/or bottom baryons: $(\Lambda_c^+\Lambda_c^-)_0$, $(\Xi_c^+\Xi_c^-)_0$, $(\Xi_b^-\Xi_b^+)_0$, and $(\Omega_b^-\Omega_b^+)_0$, with generic properties listed in Table 15. We indicatively list some possible two-body decays from baryon-antibaryon annihilation at rest, but their large mass allows for multimeson decays too. None of these theoretical systems (which have increasing mass and decreasing Bohr radii) has been explicitly investigated previously, as far as we can tell.

TABLE 15: Main properties of QED baryonium para-states $(hh)_0$, with $h = p, \Sigma^\pm, \Xi^\pm, \Omega^\pm, \Lambda_c^\pm, \Xi_c^\pm, \Xi_b^\pm, \Omega_b^\pm$. For each ground state ($n = 1$), we list its J^{PC} quantum numbers, constituent hadron mass m_{h^\pm} , atom mass m_X from Eq. (17), QED binding energy (from $E_{n=1} = 2m_h - m_X$), Bohr radius r_{Bohr} from Eq. (13), lifetime τ and total width Γ_{tot} (assessed as explained in the text), diphoton width $\Gamma_{\gamma\gamma}$ from Eq. (20), and typical hadronic decays.

Baryonium	J^{PC}	m_{h^\pm} (MeV)	m_X (MeV)	$E_{n=1}$ (keV)	r_{Bohr} (fm)	τ (fs)	Γ_{tot} (eV)	$\Gamma_{\gamma\gamma}$ (meV)	Typical decays
$(p\bar{p})_0$	0^{++}	938.272088	1876.5317	-12.49	57.54	$(0.60 \pm 0.02) \cdot 10^{-3}$	1096.7 ± 42.3	9.71	$\pi^0\pi^0, \eta\eta$
$(\Sigma^+\Sigma^-)_0$	0^{++}	1189.37 ± 0.07	2378.72 ± 0.14	-15.84	45.40	$O(10^{-3})$	$O(1000)$	12.31	$\pi^0\pi^0, \eta\eta, \Sigma^0\Sigma^0$
$(\Xi^-\Xi^+)_0$	0^{++}	1321.71 ± 0.07	2643.40 ± 0.14	-17.60	40.85	$O(10^{-3})$	$O(1000)$	13.68	$\pi\pi, \eta\eta, \text{KK}$
$(\Omega^-\Omega^+)_0$	0^{++}	1672.45 ± 0.29	3344.88 ± 0.58	-22.3	32.3	$O(10^{-4})$	$O(2000)$	17.3	$\eta\eta, \eta'\eta'$
$(\Lambda_c^+\Lambda_c^-)_0$	0^{++}	2286.46 ± 0.14	4572.89 ± 0.28	-30.4	23.6	$O(10^{-4})$	$O(2000)$	23.7	$D^0\bar{D}^0, \dots$
$(\Xi_c^+\Xi_c^-)_0$	0^{++}	2467.71 ± 0.23	4935.39 ± 0.46	-32.8	21.9	$O(10^{-4})$	$O(2000)$	25.5	$\pi\pi, \eta\eta, \text{KK}, \dots$
$(\Xi_b^-\Xi_b^+)_0$	0^{++}	5797.0 ± 0.6	11593.9 ± 1.2	-77.2	9.3	$O(10^{-4})$	$O(6000)$	60.0	mult. mesons
$(\Omega_b^-\Omega_b^+)_0$	0^{++}	6045.8 ± 0.8	12091.5 ± 1.6	-80.5	8.9	$O(10^{-4})$	$O(6000)$	62.5	mult. mesons

To our knowledge, the photon-fusion production of QED hadronium states has never been considered before in the literature, although such exotic systems should be theoretically producible through this channel given their nonzero diphoton widths. We estimate here their cross sections in UPCs through our “master formula” Eq. (7). The QED mesonium cross sections and expected yields in UPCs at different colliders are listed in Table 16, and the cross sections as a function of c.m. energy are plotted in Fig. 11. Whereas the cross sections appear too low to be visible above backgrounds in p-p and p-Pb UPCs, they are not that small in Pb-Pb UPCs for the case of light-quark dimeson systems, where a few thousands pionium and hundreds kaonium events are expected with the nominal LHC integrated luminosity. The ALICE (or ALICE-3) and LHCb experiments could have a chance to measure the lightest of such exotic QED atoms in their dominant hadronic decay modes. However, the $\gamma\gamma$ production of heavy-quark QED mesonium systems ($A_{2D}, A_{2D_s}, A_{2B}, A_{2B_c}$) features much smaller cross sections and is only potentially visible in UPCs at the FCC-hh.

The QED baryonium cross sections and expected yields in UPCs at the various colliders are listed in Table 17, and shown graphically in Fig. 11 as a function of c.m. energy. Cross sections appear too low to be visible above backgrounds in p-p and p-Pb UPCs, but light-quark baryonium systems appear producible in Pb-Pb UPCs, where a few tens of $(p\bar{p})_0$, $(\Sigma^+\Sigma^-)_0$, $(\Xi^-\Xi^+)_0$, $(\Omega^-\Omega^+)_0$ events are expected with the nominal LHC integrated luminosity. The ALICE (or ALICE-3) and LHCb experiments could attempt a measurement of such exotic QED atoms in their dominant hadronic decay modes. The $\gamma\gamma$ production of QED baryonium systems with charm or bottom quarks features much smaller cross sections and would be potentially visible only in PbPb UPCs at the FCC-hh energies.

6. TOTAL $\gamma\gamma$ EVEN-SPIN RESONANCE CROSS SECTIONS IN UPCs

In Table 18 we collect the sum of all photon-photon resonance cross sections computed in this work (Tables 4–17) for UPCs at RHIC/LHC/FCC/GZK-cutoff energies, and compare their values to the total hadronic cross section for each system. The latter have been computed with the Glauber model of Ref. [44] using the parametrization of the inelastic nucleon-nucleon cross section $\sigma_{\text{inel,had}}(\text{NN} \rightarrow \text{X})$ vs. \sqrt{s} of Ref. [46]. The photon-fusion cross sections are dominated by the sum of the lightest even-spin systems that have the largest individual cross sections. In general, the photon-fusion cross sections represent a very small fraction of the p-p (about 1 part in 1 million) and proton-nucleus (1

plus three pairs of charged pions $J/\psi \rightarrow \gamma 3(\pi^+\pi^-)$ [143], which appears consistent with protonium, although being much broader than the QED state discussed here, it is rather a molecular $(p\bar{p})_0$ state bound by the QCD interaction.

TABLE 16: Photon-fusion cross sections $\sigma(\gamma\gamma \rightarrow X)$, total yields $N_{\text{evts}}(\gamma\gamma \rightarrow X)$, and yields $N_{\text{evts}}(\gamma\gamma \rightarrow X(\gamma\gamma))$ in the diphoton decay mode, for the production of QED mesonium states (Table 14) in UPCs for various colliding systems at RHIC, LHC, and FCC c.m. energies. The last row lists the corresponding cross sections in proton-air collisions at GZK-cutoff energies.

System, $\sqrt{s_{\text{NN}}}$, \mathcal{L}_{int}	Ref.	$A_{2\pi}$	A_{2K}	A_{2D}	A_{2D_s}	A_{2B}	A_{2B_c}
Au-Au, 0.2 TeV, 10 nb^{-1} :							
$\sigma(\gamma\gamma \rightarrow X)$	Eq. (7)	42 nb	0.6 nb	2.1 pb	1.5 pb	1.5 ab	0.7 ab
$N_{\text{evts}}(\gamma\gamma \rightarrow X)$		420	5.9	0.02	0.01	–	–
Pb-Pb, 5.5 TeV, 10 nb^{-1} :							
$\sigma(\gamma\gamma \rightarrow X)$	Eq. (7)	410 nb	14 nb	0.38 nb	0.33 nb	17 pb	10 pb
$N_{\text{evts}}(\gamma\gamma \rightarrow X)$		4100	100	4	3	0.2	0.1
p-Pb, 8.8 TeV, 1 pb^{-1} :							
$\sigma(\gamma\gamma \rightarrow X)$	Eq. (7)	110 pb	4.3 pb	140 fb	120 fb	8.5 fb	5.3 fb
$N_{\text{evts}}(\gamma\gamma \rightarrow X)$		100	4	0.1	0.1	–	–
p-p, 14 TeV, 1 fb^{-1} :							
$\sigma(\gamma\gamma \rightarrow X)$	Eq. (7)	28.8 fb	1.2 fb	50 ab	44 ab	3.8 ab	2.4 ab
$N_{\text{evts}}(\gamma\gamma \rightarrow X)$		30	1	–	–	–	–
Pb-Pb, 39.4 TeV, 110 nb^{-1} :							
$\sigma(\gamma\gamma \rightarrow X)$	Eq. (7)	920 nb	37 nb	1.36 nb	1.2 nb	92 pb	58 pb
$N_{\text{evts}}(\gamma\gamma \rightarrow X)$		1.0×10^5	4100	100	100	10	6
p-Pb, 62.8 TeV, 29 pb^{-1} :							
$\sigma(\gamma\gamma \rightarrow X)$	Eq. (7)	215 nb	9.4 pb	0.4 pb	0.36 pb	29 fb	19 fb
$N_{\text{evts}}(\gamma\gamma \rightarrow X)$		6200	270	10	10	1	0.5
p-p, 100 TeV, 10 fb^{-1} :							
$\sigma(\gamma\gamma \rightarrow X)$	Eq. (7)	50 fb	2.4 fb	0.1 fb	95 ab	9 ab	6 ab
$N_{\text{evts}}(\gamma\gamma \rightarrow X)$		500	25	1	1	0.1	0.05
p-air, 400 TeV:							
$\sigma(\gamma\gamma \rightarrow X)$	Eq. (7)	3.0 pb	0.14 pb	6.8 ab	6.0 ab	0.6 ab	0.4 ab

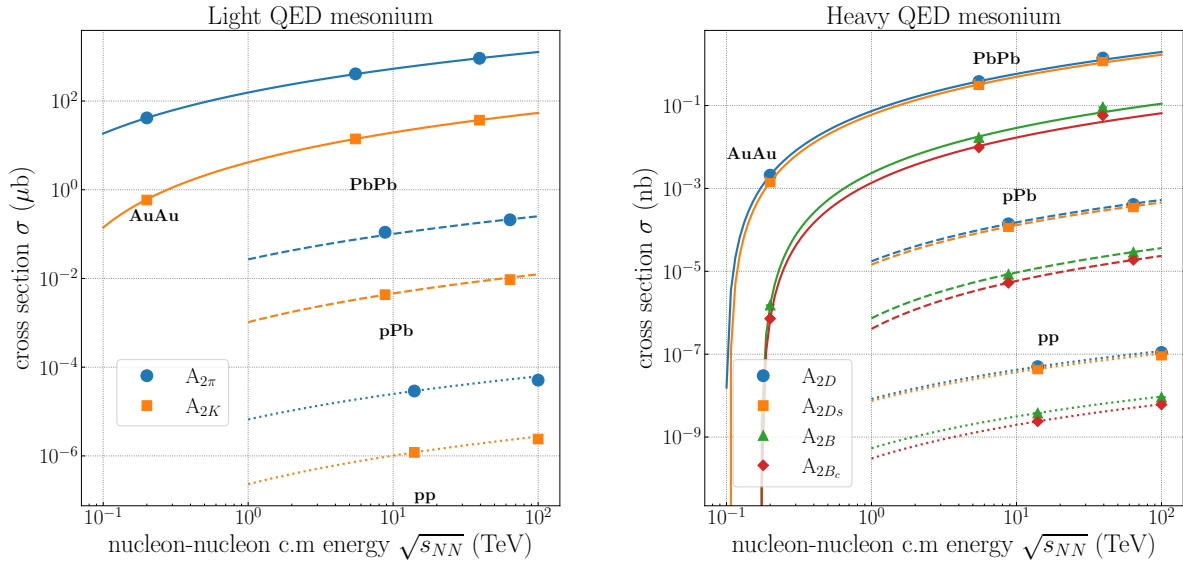


FIG. 11: Cross sections for the $\gamma\gamma$ production of even-spin QED mesonium states as a function of nucleon-nucleon c.m. energy $\sqrt{s_{\text{NN}}}$, in Pb-Pb or Au-Au (solid curves), p-Pb (dashed curves), and p-p (dotted curves) UPCs. The curves are $\ln^3(s_{\text{NN}})$ fits to guide the eye. The left and right panels show the results for light-quark ($A_{2\pi}$, A_{2K}) and heavy-quark (A_{2D} , A_{2D_s} , A_{2B} , A_{2B_c}) states, respectively, whose properties are listed in Table 14.

TABLE 17: Photon-fusion cross sections $\sigma(\gamma\gamma \rightarrow X)$ and total yields $N_{\text{evts}}(\gamma\gamma \rightarrow X)$ for the production of QED baryonium states (Table 15) in UPCs for various colliding systems at RHIC, LHC, and FCC c.m. energies. The last row lists the corresponding cross sections in proton-air collisions at GZK-cutoff energies.

System, $\sqrt{s_{\text{NN}}}$, \mathcal{L}_{int}	Ref.	$(p\bar{p})_0$	$(\Sigma^+\Sigma^-)_0$	$(\Xi^-\Xi^+)_0$	$(\Omega^-\Omega^+)_0$	$(\Lambda_c^+\bar{\Lambda}_c^-)_0$	$(\Xi_c^+\Xi_c^-)_0$	$(\Xi_b^-\Xi_b^+)_0$	$(\Omega_b^-\bar{\Omega}_b^+)_0$
Au-Au, 0.2 TeV, 10 nb ⁻¹ :									
$\sigma(\gamma\gamma \rightarrow X)$	Eq. (7)	0.10 nb	36.3 pb	23.3 pb	7.5 pb	1.4 pb	0.8 pb	2.2 fb	1.8 fb
$N_{\text{evts}}(\gamma\gamma \rightarrow X)$		1	0.4	0.2	0.1	0.01	0.01	–	–
Pb-Pb, 5.5 TeV, 10 nb ⁻¹ :									
$\sigma(\gamma\gamma \rightarrow X)$	Eq. (7)	5.0 nb	2.6 nb	2.0 nb	1.0 nb	0.42 nb	0.34 nb	25 pb	22 pb
$N_{\text{evts}}(\gamma\gamma \rightarrow X)$		50	25	20	10	4	3	0.2	0.2
p-Pb, 8.8 TeV, 1 pb ⁻¹ :									
$\sigma(\gamma\gamma \rightarrow X)$	Eq. (7)	1.63 pb	0.9 pb	0.7 pb	0.37 pb	0.16 pb	0.13 pb	13 fb	12 fb
$N_{\text{evts}}(\gamma\gamma \rightarrow X)$		1.5	1	1	0.5	0.1	0.1	0.01	0.01
p-p, 14 TeV, 1 fb ⁻¹ :									
$\sigma(\gamma\gamma \rightarrow X)$	Eq. (7)	0.53 fb	0.30 fb	0.23 fb	0.13 fb	60 ab	50 ab	6 ab	5.5 ab
$N_{\text{evts}}(\gamma\gamma \rightarrow X)$		0.5	0.3	0.2	0.1	0.05	0.05	–	–
Pb-Pb, 39.4 TeV, 110 nb ⁻¹ :									
$\sigma(\gamma\gamma \rightarrow X)$	Eq. (7)	15.3 nb	8.47 nb	6.51 nb	3.6 nb	1.63 nb	1.34 nb	0.14 nb	0.13 nb
$N_{\text{evts}}(\gamma\gamma \rightarrow X)$		1700	930	720	400	180	150	15	15
p-Pb, 62.8 TeV, 29 pb ⁻¹ :									
$\sigma(\gamma\gamma \rightarrow X)$	Eq. (7)	4.24 pb	2.4 pb	1.9 pb	1.06 pb	0.5 pb	0.4 pb	46 fb	41 fb
$N_{\text{evts}}(\gamma\gamma \rightarrow X)$		120	70	54	30	15	10	1	1
p-p, 100 TeV, 10 fb ⁻¹ :									
$\sigma(\gamma\gamma \rightarrow X)$	Eq. (7)	1.1 fb	0.62 fb	0.48 fb	0.28 fb	0.13 fb	0.12 fb	14.7 ab	13.3 ab
$N_{\text{evts}}(\gamma\gamma \rightarrow X)$		10	5	5	3	1	1	0.1	0.1
p-air, 400 TeV:									
$\sigma(\gamma\gamma \rightarrow X)$	Eq. (7)	66.4 fb	38.6 fb	30.3 fb	17.5 fb	8.5 fb	7.1 fb	0.96 fb	0.87 fb

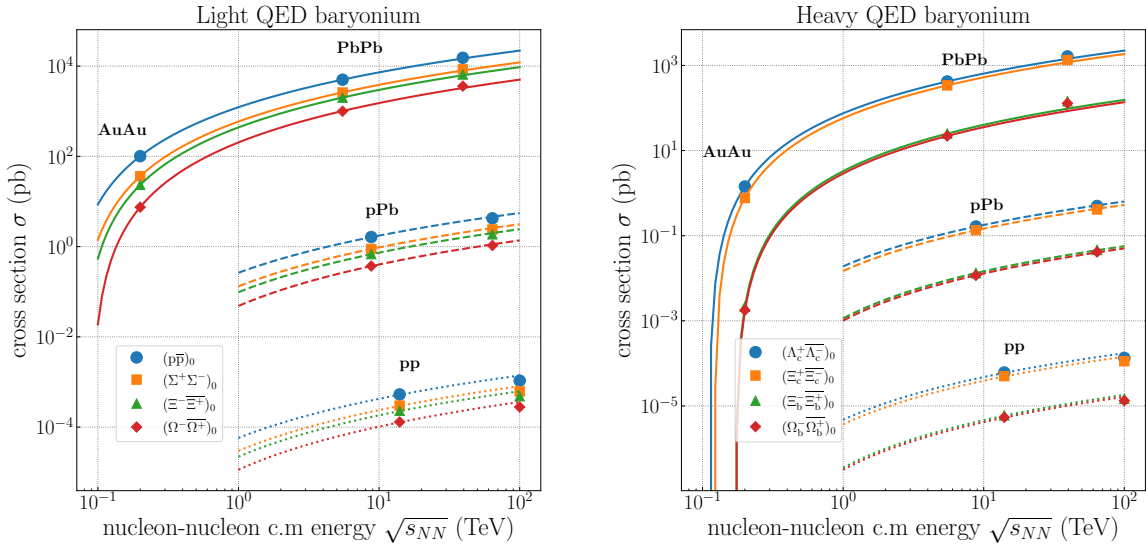


FIG. 12: Cross sections for the $\gamma\gamma$ production of even-spin QED baryonium states as a function of nucleon-nucleon c.m. energy $\sqrt{s_{\text{NN}}}$, in Pb-Pb or Au-Au (solid curves), p-Pb (dashed curves), and p-p (dotted curves) UPCs. The curves are $\ln^3(s_{\text{NN}})$ fits to guide the eye. The left and right panels show the results for light-quark ($(p\bar{p})_0$, $(\Sigma^+\Sigma^-)_0$, $(\Xi^-\Xi^+)_0$, $(\Omega^-\Omega^+)_0$) and heavy-quark ($(\Lambda_c^+\bar{\Lambda}_c^-)_0$, $(\Xi_c^+\Xi_c^-)_0$, $(\Xi_b^-\Xi_b^+)_0$, $(\Omega_b^-\bar{\Omega}_b^+)_0$) baryonium states, respectively, whose properties are listed in Table 15.

part in 10^5) inclusive hadronic cross sections, but the production of even-spin hadron and leptonium systems amount to about 2.5–6% of the Pb-Pb hadronic inelastic cross sections at the LHC and FCC, and are clearly not negligible.

TABLE 18: Sum of all photon-fusion cross sections in UPCs for hadronic resonances, $\sum_i \sigma(\gamma\gamma \rightarrow X_i)$, and leptonium systems $\sum_i \sigma(\gamma\gamma \rightarrow (\ell^+ \ell^-)_0)$, obtained here for all considered colliding systems (Tables 4–17) compared to the total inclusive hadronic cross section, $\sigma(AB)_{\text{had}}$, computed with a Glauber MC model [44] using the $\sigma_{\text{inel,had}}(\text{NN} \rightarrow X)$ vs. $\sqrt{s_{\text{NN}}}$ parametrization of Ref. [46].

colliding system	Au-Au $\sqrt{s_{\text{NN}}}$ 0.2 TeV	Pb-Pb 5.5 TeV	p-Pb 8.8 TeV	p-p 14 TeV	Pb-Pb 39.4 TeV	p-Pb 62.8 TeV	p-p 100 TeV	p-air 400 TeV
$\sum_i \sigma(\gamma\gamma \rightarrow X_i)$ (mb)	13.1 ± 0.56	189 ± 8.8	0.056 ± 0.003	$(1.57 \pm 0.075) \cdot 10^{-5}$	479 ± 23	0.12 ± 0.006	$(2.96 \pm 0.14) \cdot 10^{-5}$	$(1.79 \pm 0.087) \cdot 10^{-3}$
$\sum_i \sigma(\gamma\gamma \rightarrow (\ell^+ \ell^-)_0)$ (mb)	109	328	0.0675	$1.42 \cdot 10^{-5}$	516	0.10	$2.06 \cdot 10^{-5}$	$1.15 \cdot 10^{-3}$
$\sigma_{\text{inel,had}}(AB \rightarrow X)$ (mb)	6840 ± 140	7640 ± 150	2130 ± 30	79.2 ± 1.9	7930 ± 160	2300 ± 50	107.5 ± 6.5	570 ± 20

7. TWO-PHOTON EVEN-SPIN BACKGROUNDS TO LBL SCATTERING IN PB-PB UPCs AT THE LHC

The work of [145] proposed to exploit the very large quasideal photon fluxes available in PbPb UPCs at the LHC to measure and study $\gamma\gamma \rightarrow \gamma\gamma$ scattering, also known as light-by-light (LbL) scattering, a process that had remained experimentally unobserved due to its very small elementary cross section (proportional to the fourth power of the QED coupling, $\alpha^4 \approx 3 \cdot 10^{-9}$). Following the analysis strategy outlined in Ref. [145], both the ATLAS and CMS experiments measured the LbL process at the LHC [146–149] for diphoton masses above $m_{\gamma\gamma} = 5$ GeV, with cross sections consistent (albeit with relatively large experimental uncertainties) with the theoretical prediction at NLO accuracy in QCD and QED [150, 151]. The LbL scattering proceeds via virtual box diagrams containing charged particles, as depicted in the top left diagram of Fig. 13. Whereas the contributions from charged leptons and heavy-quarks boxes are well controlled theoretically, the nonperturbative light-quark hadronic contributions that dominate the cross section at lower diphoton masses are much more uncertain [152]. As a matter of fact, the same hadronic virtual contributions to LbL scattering (also known as HLbL) are among the leading sources of uncertainty in the calculations of QCD corrections to the anomalous magnetic moment of the muon $(g - 2)_\mu$ [57, 153, 154], whose measured value [155] appears in contradiction with standard model predictions based on data-driven dispersive approaches [156]. Measuring LbL scattering at lower diphoton masses in UPCs, in the region $m_{\gamma\gamma} \approx 0.1$ –5 GeV currently unexplored experimentally, would thus provide valuable complementary input on the the HLbL contributions and their interplay with the resonant even-spin hadronic resonances similarly produced via photon fusion (bottom left diagram of Fig. 13). The ALICE and LHCb experiments are well placed to attempt such a measurement, as the ATLAS and CMS experiments have poorer reconstruction capabilities at such low diphoton masses.

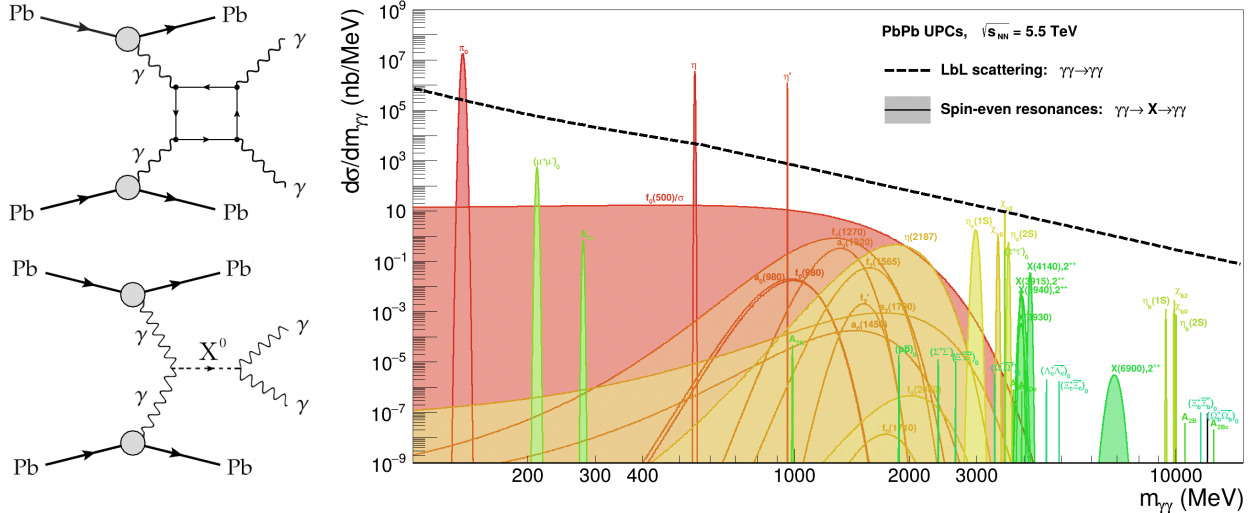


FIG. 13: Left: Diagrams for LbL scattering (top) and exclusive two-photon even-spin particle production decaying into two photons (bottom) in Pb-Pb UPCs. Right: Exclusive diphoton mass distribution over $m_{\gamma\gamma} \approx 0.1$ –15 GeV for Pb-Pb(5.5 TeV) UPCs showing the light-by-light continuum (γ -UPC + @NLO, dashed black curve) and all diphoton even-spin resonances (filled colored areas) over this mass range (the width of the narrowest resonances has been arbitrarily set to 1-MeV for visibility purposes).

Studies of LbL at low masses in UPCs at the LHC have been previously presented in Refs. [157, 158], but only a few

background hadron diphoton states were considered. We include here all diphoton resonances discussed in this paper, and compare their cross sections to the LbL continuum computed with `gamma-UPC + LbL@NLO` [150, 151]. The right panel of Fig. 13 shows the expected diphoton mass distribution in PbPb(5.5 TeV) UPCs from the LbL continuum (dashed black curve) and from all even-spin diphoton resonances (filled colored areas) considered in this work. For visibility purposes, the width of the narrowest resonances has been arbitrarily set to 1-MeV, and the exotic hadron resonances cross sections plotted assume $J^{CP} = 2^{++}$ (which yield larger yields than the scalar case). The LbL curve has been obtained at LO QED and QCD accuracy, including the contributions from light-quarks boxes, which are not well-defined perturbatively, using $m_u = m_d = 0$ (u and d quarks) and $m_s \approx 95$ MeV (strange quark) masses. A full theoretical calculation would require to properly consider also interferences between the two diagrams of Fig. 13 (left) at each relevant mass point, but this goes beyond the scope of this paper where we want to show the relative size of both contributions in different diphoton mass ranges, and emphasize the interest of such an experimental measurement. One can see that, in the absence of any selection cuts, the only even-spin resonances that would stand out clearly above the LbL continuum (provided a good experimental diphoton mass resolution is achieved) are the π^0 , η , η' , and (partially) χ_{c2} mesons. Identifying other diphoton-decaying particles would require applying appropriate event selection criteria through multivariate analysis techniques (e.g., requiring approximate equal energies of the two photons at half the mass of the decaying particle, as well as proper angular distribution cuts to separate scalar/tensor resonances from the box-mediated LbL process), so as to identify any potential resonant excess of events above the (properly controlled and fitted) smooth LbL continuum. Nonetheless, there will remain many resonances with diphoton yields orders-of-magnitude smaller than the LbL background, whose measurement could only be potentially attempted through other more probable decay channels.

8. SUMMARY

The cross sections for the single exclusive production of (pseudo)scalar and (pseudo)tensor hadrons, as well as of even-spin QED bound states formed by pairs of opposite-charge leptons or hadrons, have been estimated for photon-fusion processes in ultraperipheral collisions (UPCs) of proton-proton, proton-nucleus, and nucleus-nucleus at the RHIC, LHC and FCC colliders, as well as in proton-air interactions at the highest energies reached by cosmic-rays impinging on earth. The UPC cross sections have been computed in the equivalent photon approximation with realistic photon fluxes from the charged form factors of proton, lead, gold, and nitrogen ions. The production of four types of even-spin systems have been considered: quarkonium (spin-0, 2, 4 meson bound states, from the lightest π^0 meson up to toponium), exotic mesons (including candidate multi-quark states), leptonium (positronium, dimuonium, and ditauonium), and hadronium QED atoms (including pionium, kaonium, and protonium, plus dimeson/dibaryon onium systems with heavy quarks). The production cross sections for about 50 such even-spin composite particles have been computed. To our knowledge, those are the first calculations of the UPC production cross sections for about half of the particles, including several light-quark resonances, exotic hadronic states, QED-hadronium systems, and para-toponium. Compared to other existing previous works, our study uses improved photon-photon UPC luminosities, properly propagates theoretical uncertainties to the production cross sections, and also includes predictions for future colliders, such as the FCC-hh, as well for cosmic-rays interactions on the earth atmosphere at the highest (GZK cutoff) energies observed.

We find, first, that the number of UPC collisions producing the lightest even-spin light-quark resonances (with masses over the $m_X \approx 0.135$ –2.1 GeV range) reaches the millions to hundred-millions events at the LHC. The ALICE (in particular, the proposed ALICE-3) as well as the LHCb (in particular, the proposed LHCb upgrade II) experiments should be able to reconstruct many of these resonances in their decays into soft hadronic or diphoton final states. Such measurements would allow to shed light on the properties (quantum numbers, diphoton widths, quark/gluon composition,...) of some of the least well-known of such states. Similarly, one expects hundreds to thousands events with even-spin charmonium resonances (with $m_X \approx 2.95$ –3.6 GeV masses) exclusively produced in UPCs at the LHC that decay back into a pair of photons. The measurements of exclusive charmonia in this decay mode (or in their much more abundant hadronic decays) appear also feasible for the ALICE and LHCb detectors, and can help determine their diphoton widths, which are either not known (as is the case for the scalar χ_{c1} and tensor χ_{c2} states) or for which contradictory results exist today (as is the case for the pseudoscalar $\eta_c(1S)$ and $\eta_c(2S)$ states). The number of exclusive bottomonia produced in UPCs at the LHC lies in the hundreds to thousands events (depending on the system and concrete state) and their potential measurement would only be possible in their hadronic decays, as their diphoton partial widths are too small. The heaviest particle known today is the quasibound state formed by a top-antitop quark pair (toponium). An observation of para-toponium could be attempted in p-p UPCs at the HL-LHC (where about 40 events are expected) and at FCC-hh (with about 1300 events expected) by exploiting the whole data set of 6 and 30 ab^{-1} integrated luminosities to be collected under high pileup conditions. Such a measurement would require the search for a back-to-back $t\bar{t}$ pair produced at rest (i.e., with zero pair p_T) in coincidence with two intact

protons reconstructed in very forward proton spectrometers, such as those from the CMS-TOTEM PPS system, whose acceptance for such a heavy system is very large.

We have also studied the production of pure-QED para-leptonium systems formed by a pair of opposite-charged leptons. The UPC cross sections and associated yields are very large for positronium and dimuonium, whereas they are very small for the heaviest (true tauonium) system. The observation of paraleptonium production in UPCs appears, however, unfeasible either because the diphoton final state is ultra soft (positronium), or likely too soft (dimuonium) to be reconstructed, or because it is swamped by the decays of more abundant diphoton resonances in the same mass range (in the ditauonium case). Lastly, we have studied for the first time the two-photon production of even-spin systems formed by two identical hadrons of opposite charge, bound by their Coulomb interaction, which we refer to as QED “hadronium”. We discussed the properties and production cross sections of six QED-mesonium scalar systems: pionium ($A_{2\pi}$), kaonium (A_{2K}), $D_{(s)}^{\pm}$ -onium, and $B_{(s)}^{\pm}$ -onium; as well as eight QED-baryonium para-atoms formed by opposite-charge pairs of p , Σ^{\pm} , $\Xi_{(s)}^{\pm}$, Ω^{\pm} , Λ_c^{\pm} , Ξ_c^{\pm} , Ξ_b^{\pm} , Ω_b^{\pm} . Whereas the cross sections appear too low to be visible above backgrounds in p-p and p-Pb UPCs, they are not that small in Pb-Pb UPCs for the case of light-quark systems, where a few thousands $A_{2\pi}$ and hundreds A_{2K} events, as well as a few tens of protonium ($(p\bar{p})_0$), ($\Sigma^+\Sigma^-$)₀, ($\Xi^-\bar{\Xi}^+$)₀, and ($\Omega^-\bar{\Omega}^+$)₀ events, are expected with the nominal LHC integrated luminosity. At the LHC, the ALICE and LHCb experiments could venture a measurement of the lightest of such exotic QED atoms in their dominant hadronic decay modes. However, the $\gamma\gamma$ production of heavy-quark QED hadronium systems in UPCs features much smaller cross sections, which are only potentially producible at the FCC-hh.

Last but not least, we have computed the differential cross section for light-by-light (LbL) scattering, $\gamma\gamma \rightarrow \gamma\gamma$, in Pb-Pb UPCs at the LHC in the low-mass range, $m_{\gamma\gamma} = 0.1\text{--}15$ GeV, and compared it to the expected contributions from all diphoton resonances discussed in this study. The only even-spin resonances that would stand out clearly above the LbL continuum (provided a good experimental diphoton mass resolution is achieved) are the π^0 , η , η' , and (partially) χ_{c2} mesons. Identifying other diphoton-decaying particles would require applying appropriate event selection criteria through multivariate analyses, or attempting their reconstruction through other more probable decay channels.

We hope that the results reported in this work can help motivate upcoming experimental, and further theoretical, studies of multiple even-spin particles and exotic QED atoms, which either remain unobserved or whose properties are poorly known, as well as of low-mass LbL scattering, in UPCs at the LHC and future hadron colliders.

Acknowledgments.— We want to warmly thank Hua-Sheng Shao and Nicolas Crépet for common work with the gamma-UPC code used to produce many of the results shown in this study. In addition, we are grateful to Hua-Sheng Shao for providing the low-mass light-by-light continuum prediction with the gamma-UPC + LbL@NLO code.

-
- [1] C. F. von Weizsacker, “Radiation emitted in collisions of very fast electrons,” *Z. Phys.* **88** (1934) 612–625.
 - [2] E. J. Williams, “Nature of the high-energy particles of penetrating radiation and status of ionization and radiation formulae,” *Phys. Rev.* **45** (1934) 729–730.
 - [3] S. J. Brodsky, T. Kinoshita, and H. Terazawa, “Two photon mechanism of particle production by high-energy colliding beams,” *Phys. Rev. D* **4** (1971) 1532–1557.
 - [4] V. M. Budnev, I. F. Ginzburg, G. V. Meledin, and V. G. Serbo, “The two photon particle production mechanism. Physical problems. Applications. Equivalent photon approximation,” *Phys. Rept.* **15** (1975) 181–281.
 - [5] D. Morgan, M. R. Pennington, and M. R. Whalley, “A compilation of data on two photon reactions leading to hadron final states,” *J. Phys. G* **20 Suppl.** **8A** (1994) A1–A147.
 - [6] M. R. Whalley, “A Compilation of data on two photon reactions,” *J. Phys. G* **27** (2001) A1–A121.
 - [7] C. A. Bertulani, S. R. Klein, and J. Nystrand, “Physics of ultra-peripheral nuclear collisions,” *Ann. Rev. Nucl. Part. Sci.* **55** (2005) 271–310, [arXiv:nucl-ex/0502005](#).
 - [8] G. Baur *et al.*, “The Physics of Ultraperipheral Collisions at the LHC,” *Phys. Rept.* **458** (2008) 1–171, [arXiv:0706.3356 \[nucl-ex\]](#).
 - [9] J. de Favereau de Jeneret, V. Lemaitre, Y. Liu, S. Olyn, T. Pierzchala, K. Piotrkowski, X. Rouby, N. Schul, and M. Vander Donckt, “High energy photon interactions at the LHC,” [arXiv:0908.2020 \[hep-ph\]](#).
 - [10] C. A. Bertulani and G. Baur, “Electromagnetic Processes in Relativistic Heavy Ion Collisions,” *Phys. Rept.* **163** (1988) 299.
 - [11] G. Baur and C. A. Bertulani, “ $\gamma\gamma$ Physics With Peripheral Relativistic Heavy Ion Collisions,” *Z. Phys. A* **330** (1988) 77–81.
 - [12] R. N. Cahn and J. D. Jackson, “Realistic equivalent photon yields in heavy ion collisions,” *Phys. Rev. D* **42** (1990) 3690–3695.
 - [13] FCC Collaboration, A. Abada *et al.*, “FCC-hh: The Hadron Collider: Future Circular Collider Conceptual Design Report Volume 3,” *Eur. Phys. J. ST* **228** (2019) 755–1107.

- [14] K. Greisen, “End to the cosmic ray spectrum?,” *Phys. Rev. Lett.* **16** (1966) 748–750.
- [15] G. T. Zatsepin and V. A. Kuzmin, “Upper limit of the spectrum of cosmic rays,” *JETP Lett.* **4** (1966) 78–80.
- [16] D. d’Enterria, R. Engel, T. Pierog, S. Ostapchenko, and K. Werner, “Constraints from the first LHC data on hadronic event generators for ultra-high energy cosmic-ray physics,” *Astropart. Phys.* **35** (2011) 98–113, [arXiv:1101.5596 \[astro-ph.HE\]](#).
- [17] R. Bruce *et al.*, “New physics searches with heavy-ion collisions at the CERN Large Hadron Collider,” *J. Phys. G* **47** (2020) 060501, [arXiv:1812.07688 \[hep-ph\]](#).
- [18] D. d’Enterria *et al.*, “Opportunities for new physics searches with heavy ions at colliders,” *J. Phys. G* **50** (2023) 050501, [arXiv:2203.05939 \[hep-ph\]](#).
- [19] A. Dainese *et al.*, “Future heavy-ion facilities: FCC-AA,” *PoS HardProbes2018* (2019) 005, [arXiv:1901.10952 \[hep-ph\]](#).
- [20] L. D. Landau, “On the angular momentum of a system of two photons,” *Dokl. Akad. Nauk SSSR* **60** (1948) 207–209.
- [21] C.-N. Yang, “Selection rules for the dematerialization of a particle into two photons,” *Phys. Rev.* **77** (1950) 242–245.
- [22] F. Krauss, M. Greiner, and G. Soff, “Photon and gluon induced processes in relativistic heavy ion collisions,” *Prog. Part. Nucl. Phys.* **39** (1997) 503–564.
- [23] **Particle Data Group** Collaboration, S. Navas *et al.*, “Review of particle physics,” *Phys. Rev. D* **110** (2024) 030001.
- [24] F. E. Low, “Proposal for measuring the π^0 lifetime by π^- production in electron-electron or electron-positron collisions,” *Phys. Rev.* **120** (1960) 582–583.
- [25] A. A. Natale, “Resonance production in peripheral heavy ion collisions,” *Mod. Phys. Lett. A* **9** (1994) 2075–2081.
- [26] G. Baur, K. Hencken, and D. Trautmann, “Photon-photon physics in very peripheral collisions of relativistic heavy ions,” *J. Phys. G* **24** (1998) 1657–1692, [arXiv:hep-ph/9804348](#).
- [27] G. Baur, K. Hencken, D. Trautmann, S. Sadovsky, and Y. Kharlov, “Coherent $\gamma\gamma$ and γ -A interactions in very peripheral collisions at relativistic ion colliders,” *Phys. Rept.* **364** (2002) 359–450, [arXiv:hep-ph/0112211](#).
- [28] C. A. Bertulani and F. Navarra, “Two photon and three photon fusion in relativistic heavy ion collisions,” *Nucl. Phys. A* **703** (2002) 861–875, [arXiv:nucl-th/0107035](#).
- [29] I. F. Ginzburg, U. D. Jentschura, S. G. Karshenboim, F. Krauss, V. G. Serbo, and G. Soff, “Production of bound $\mu^+\mu^-$ systems in relativistic heavy ion collisions,” *Phys. Rev. C* **58** (1998) 3565–3573, [arXiv:hep-ph/9805375](#).
- [30] G. L. Kotkin, E. A. Kuraev, A. Schiller, and V. G. Serbo, “Production of parapositronium and orthopositronium at relativistic heavy ion colliders,” *Phys. Rev. C* **59** (1999) 2734–2743, [arXiv:hep-ph/9811494](#).
- [31] B. D. Moreira, C. A. Bertulani, V. P. Gonçalves, and F. S. Navarra, “Production of exotic charmonium in $\gamma\gamma$ interactions at hadron colliders,” *Phys. Rev. D* **94** (2016) 094024, [arXiv:1610.06604 \[hep-ph\]](#).
- [32] V. P. Gonçalves and B. D. Moreira, “Probing the $X(4350)$ in $\gamma\gamma$ interactions at the LHC,” *Eur. Phys. J. C* **79** (2019) 7, [arXiv:1809.08125 \[hep-ph\]](#).
- [33] C. Azevedo, V. P. Gonçalves, and B. D. Moreira, “True muonium production in ultraperipheral PbPb collisions,” *Phys. Rev. C* **101** (2020) 024914, [arXiv:1911.10861 \[hep-ph\]](#).
- [34] A. Esposito, C. A. Manzari, A. Pilloni, and A. D. Polosa, “Hunting for tetraquarks in ultraperipheral heavy ion collisions,” *Phys. Rev. D* **104** (2021) 114029, [arXiv:2109.10359 \[hep-ph\]](#).
- [35] V. P. Gonçalves and B. D. Moreira, “Fully - heavy tetraquark production by $\gamma\gamma$ interactions in hadronic collisions at the LHC,” *Phys. Lett. B* **816** (2021) 136249, [arXiv:2101.03798 \[hep-ph\]](#).
- [36] H.-S. Shao and D. d’Enterria, “gamma-UPC: automated generation of exclusive photon-photon processes in ultraperipheral proton and nuclear collisions with varying form factors,” *JHEP* **09** (2022) 248, [arXiv:2207.03012 \[hep-ph\]](#).
- [37] P.-Y. Niu, E. Wang, Q. Wang, and S. Yang, “Determine the quantum numbers of $X(6900)$ from photon-photon fusion in ultra-peripheral heavy ion collisions,” [arXiv:2209.01924 \[hep-ph\]](#).
- [38] V. Biloshytskiy, V. Pascalutsa, L. Harland-Lang, B. Malaescu, K. Schmieden, and M. Schott, “Two-photon decay of $X(6900)$ from light-by-light scattering at the LHC,” *Phys. Rev. D* **106** (2022) L111902, [arXiv:2207.13623 \[hep-ph\]](#).
- [39] D. d’Enterria and H.-S. Shao, “Observing true tauonium via two-photon fusion at e^+e^- and hadron colliders,” *Phys. Rev. D* **105** (2022) 093008, [arXiv:2202.02316 \[hep-ph\]](#).
- [40] R. Francener, V. P. Gonçalves, and B. D. Moreira, “Photoproduction of relativistic QED bound states in hadronic collisions,” *Eur. Phys. J. A* **58** (2022) 35, [arXiv:2110.03466 \[hep-ph\]](#).
- [41] R. Fariello, D. Bhandari, C. A. Bertulani, and F. S. Navarra, “Two- and three-photon fusion into charmonium in ultraperipheral nuclear collisions,” *Phys. Rev. C* **108** (2023) 044901, [arXiv:2306.10642 \[hep-ph\]](#).
- [42] J.-P. Dai and S. Zhao, “Production of true para-muonium in linearly polarized photon fusions,” *Phys. Rev. D* **109** (2024) 054022, [arXiv:2401.04681 \[hep-ph\]](#).
- [43] R. J. Glauber and G. Matthiae, “High-energy scattering of protons by nuclei,” *Nucl. Phys. B* **21** (1970) 135.
- [44] C. Loizides, J. Kamin, and D. d’Enterria, “Improved Monte Carlo Glauber predictions at present and future nuclear colliders,” *Phys. Rev. C* **97** (2018) 054910, [arXiv:1710.07098 \[nucl-ex\]](#). [Erratum: *Phys. Rev. C* **99** (2019) 019901].
- [45] L. Frankfurt, C. E. Hyde, M. Strikman, and C. Weiss, “Generalized parton distributions and rapidity gap survival in exclusive diffractive pp scattering,” *Phys. Rev. D* **75** (2007) 054009, [arXiv:hep-ph/0608271](#).
- [46] D. d’Enterria and C. Loizides, “Progress in the Glauber model at collider energies,” *Ann. Rev. Nucl. Part. Sci.* **71** (2021) 315, [arXiv:2011.14909 \[hep-ph\]](#).
- [47] H.-S. Shao and D. d’Enterria, “Dimuon and ditau production in photon-photon collisions at next-to-leading order in QED,” [arXiv:2407.13610 \[hep-ph\]](#).
- [48] M. I. Eides, H. Grotch, and V. A. Shelyuto, “Theory of light hydrogen - like atoms,” *Phys. Rept.* **342** (2001) 63–261, [arXiv:hep-ph/0002158](#).
- [49] G. V. Efimov, “QED and ortho-para- positronium mass difference,” in *16th International Seminar on High Energy Physics*.

2010. [arXiv:1010.0144](https://arxiv.org/abs/1010.0144) [hep-ph].
- [50] V. B. Berestetskii, E. M. Lifshitz, and L. P. Pitaevskii, *Quantum Electrodynamics*, vol. 4 of *Course of Theoretical Physics*. Pergamon Press, Oxford, 1982.
- [51] J. M. Jauch and F. Rohrlich, *The theory of photons and electrons. The relativistic quantum field theory of charged particles with spin one-half*. Texts and Monographs in Physics. Springer, Berlin, 2nd ed. ed., 1976.
- [52] T. R. Palfrey and J. L. Uretsky, “Photoproduction and detection of the two meson bound state,” *Phys. Rev.* **121** (1961) 1798.
- [53] Particle Data Group, “Scalar Mesons below 1 GeV,” 2024. <https://pdg.lbl.gov/2024/reviews/rpp2024-rev-scalar-mesons.pdf>.
- [54] S. Gardner and U.-G. Meissner, “Rescattering and chiral dynamics in $B \rightarrow \rho\pi$ decay,” *Phys. Rev. D* **65** (2002) 094004, [arXiv:hep-ph/0112281](https://arxiv.org/abs/hep-ph/0112281).
- [55] D. Morgan and M. R. Pennington, “Amplitude analysis of $\gamma\gamma \rightarrow \pi\pi$ from threshold to 1.4-GeV,” *Z. Phys. C* **48** (1990) 623–632.
- [56] J. R. Pelaez, “From controversy to precision on the sigma meson: a review on the status of the non-ordinary $f_0(500)$ resonance,” *Phys. Rept.* **658** (2016) 1, [arXiv:1510.00653](https://arxiv.org/abs/1510.00653) [hep-ph].
- [57] L. Cappiello, O. Catà, and G. D’Ambrosio, “Scalar resonances in the hadronic light-by-light contribution to the muon ($g-2$),” *Phys. Rev. D* **105** (2022) 056020, [arXiv:2110.05962](https://arxiv.org/abs/2110.05962) [hep-ph].
- [58] V. A. Shchegelsky, A. V. Sarantsev, V. A. Nikonov, and A. V. Anisovich, “The $K_S^0 K_S^0$ final state in two-photon collisions and SU(3) tensor nonets,” *Eur. Phys. J. A* **27** (2006) 207–212.
- [59] C. Amsler, “Proton-antiproton annihilation and meson spectroscopy with the Crystal Barrel,” *Rev. Mod. Phys.* **70** (1998) 1293–1340, [arXiv:hep-ex/9708025](https://arxiv.org/abs/hep-ex/9708025).
- [60] Belle Collaboration, S. Uehara *et al.*, “High-statistics study of $\eta\pi^0$ production in two-photon collisions,” *Phys. Rev. D* **80** (2009) 032001, [arXiv:0906.1464](https://arxiv.org/abs/0906.1464) [hep-ex].
- [61] Belle Collaboration, S. Uehara *et al.*, “High-statistics study of K_S^0 pair production in two-photon collisions,” *PTEP* **2013** (2013) 123C01, [arXiv:1307.7457](https://arxiv.org/abs/1307.7457) [hep-ex].
- [62] Crystal Ball Collaboration, K. Karch *et al.*, “Analysis of the $\eta\pi^0\pi^0$ final state in photon-photon collisions,” *Z. Phys. C* **54** (1992) 33–44.
- [63] Belle Collaboration, S. Uehara *et al.*, “High-statistics study of neutral-pion pair production in two-photon collisions,” *Phys. Rev. D* **79** (2009) 052009, [arXiv:0903.3697](https://arxiv.org/abs/0903.3697) [hep-ex].
- [64] L3 Collaboration, P. Achard *et al.*, “Study of resonance formation in the mass region 1400-MeV to 1500-MeV through the reaction $\gamma\gamma \rightarrow K_S^0 K^\pm \pi^\pm$,” *JHEP* **03** (2007) 018.
- [65] Belle Collaboration, K. Abe *et al.*, “Measurement of $K^+ K^-$ production in two photon collisions in the resonant mass region,” *Eur. Phys. J. C* **32** (2003) 323–336, [arXiv:hep-ex/0309077](https://arxiv.org/abs/hep-ex/0309077).
- [66] H. Primakoff, “Photoproduction of neutral mesons in nuclear electric fields and the mean life of the neutral meson,” *Phys. Rev.* **81** (1951) 899.
- [67] ATLAS Collaboration, G. Aad *et al.*, “The ATLAS Experiment at the CERN Large Hadron Collider,” *JINST* **3** (2008) S08003.
- [68] CMS Collaboration, S. Chatrchyan *et al.*, “The CMS Experiment at the CERN LHC,” *JINST* **3** (2008) S08004.
- [69] ALICE Collaboration, K. Aamodt *et al.*, “The ALICE experiment at the CERN LHC,” *JINST* **3** (2008) S08002.
- [70] ALICE Collaboration, “Letter of intent for ALICE 3: A next-generation heavy-ion experiment at the LHC,” [arXiv:2211.02491](https://arxiv.org/abs/2211.02491) [physics.ins-det].
- [71] LHCb Collaboration, A. A. Alves, Jr. *et al.*, “The LHCb Detector at the LHC,” *JINST* **3** (2008) S08005.
- [72] LHCb Collaboration, R. Aaij *et al.*, “Physics case for an LHCb Upgrade II - Opportunities in flavour physics, and beyond, in the HL-LHC era,” [arXiv:1808.08865](https://arxiv.org/abs/1808.08865) [hep-ex].
- [73] LHCb Collaboration, “Heavy ion physics at LHCb Upgrade II.” LHCb-PUB-2025-003, CERN-LHCb-PUB-2025-003, 2025.
- [74] J. H. Kuhn and P. M. Zerwas, “The Toponium Scenario,” *Phys. Rept.* **167** (1988) 321.
- [75] CMS Collaboration, “Search for heavy pseudoscalar and scalar bosons decaying to top quark pairs in proton-proton collisions at 13 TeV,” 2024. CMS-PAS-HIG-22-013.
- [76] BESIII Collaboration, M. Ablikim *et al.*, “Observation of the charmonium decay $\eta_c \rightarrow \gamma\gamma$,” [arXiv:2412.12998](https://arxiv.org/abs/2412.12998) [hep-ex].
- [77] PDG (HPQCD) Collaboration, B. Colquhoun, L. J. Cooper, C. T. H. Davies, and G. P. Lepage, “Precise determination of decay rates for $\eta_c \rightarrow \gamma\gamma$, $J/\psi \rightarrow \eta_c \gamma$, and $J/\psi \rightarrow \eta_c e^+ e^-$ from lattice QCD,” *Phys. Rev. D* **108** (2023) 014513, [arXiv:2305.06231](https://arxiv.org/abs/2305.06231) [hep-lat].
- [78] A. A. Penin, A. Pineda, V. A. Smirnov, and M. Steinhauser, “Spin dependence of heavy quarkonium production and annihilation rates: Complete next-to-next-to-leading logarithmic result,” *Nucl. Phys. B* **699** (2004) 183–206, [arXiv:hep-ph/0406175](https://arxiv.org/abs/hep-ph/0406175). [Erratum: Nucl.Phys.B 829, 398–399 (2010)].
- [79] H. S. Chung, J. Lee, and C. Yu, “NRQCD matrix elements for S-wave bottomonia and $\Gamma[\eta_b(nS) \rightarrow \gamma\gamma]$ with relativistic corrections,” *Phys. Lett. B* **697** (2011) 48–51, [arXiv:1011.1554](https://arxiv.org/abs/1011.1554) [hep-ph].
- [80] B. Colquhoun, C. T. H. Davies, and G. P. Lepage, “Precise prediction of the decay rate for $\eta_b \rightarrow \gamma\gamma$ from lattice QCD,” [arXiv:2410.24041](https://arxiv.org/abs/2410.24041) [hep-lat].
- [81] J.-Z. Wang, Z.-F. Sun, X. Liu, and T. Matsuki, “Higher bottomonium zoo,” *Eur. Phys. J. C* **78** (2018) 915, [arXiv:1802.04938](https://arxiv.org/abs/1802.04938) [hep-ph].
- [82] N. Fabiano, G. Pancheri, and A. Grau, “Toponium from different potential models,” *Nuovo Cim. A* **107** (1994) 2789–2804.
- [83] M. Beneke, Y. Kiyo, and K. Schuller, “Third-order Coulomb corrections to the S-wave Green function, energy levels and wave functions at the origin,” *Nucl. Phys. B* **714** (2005) 67–90, [arXiv:hep-ph/0501289](https://arxiv.org/abs/hep-ph/0501289).

- [84] Y. Kats and M. D. Schwartz, “Annihilation decays of bound states at the LHC,” *JHEP* **04** (2010) 016, arXiv:0912.0526 [hep-ph].
- [85] I. I. Y. Bigi, Y. L. Dokshitzer, V. A. Khoze, J. H. Kuhn, and P. M. Zerwas, “Production and Decay Properties of Ultraheavy Quarks,” *Phys. Lett. B* **181** (1986) 157–163.
- [86] L.-B. Chen, H. T. Li, J. Wang, and Y. Wang, “Analytic result for the top-quark width at next-to-next-to-leading order in QCD,” *Phys. Rev. D* **108** (2023) 054003, arXiv:2212.06341 [hep-ph].
- [87] W. Kwong, P. B. Mackenzie, R. Rosenfeld, and J. L. Rosner, “Quarkonium Annihilation Rates,” *Phys. Rev. D* **37** (1988) 3210.
- [88] CMS, TOTEM Collaboration, A. Tumasyan *et al.*, “Proton reconstruction with the CMS-TOTEM Precision Proton Spectrometer,” *JINST* **18** (2023) P09009, arXiv:2210.05854 [hep-ex].
- [89] CMS, TOTEM Collaboration, A. M. Sirunyan *et al.*, “Observation of proton-tagged, central (semi)exclusive production of high-mass lepton pairs in pp collisions at 13 TeV with the CMS-TOTEM precision proton spectrometer,” *JHEP* **07** (2018) 153, arXiv:1803.04496 [hep-ex].
- [90] ATLAS Collaboration, G. Aad *et al.*, “Observation and Measurement of Forward Proton Scattering in Association with Lepton Pairs Produced via the Photon Fusion Mechanism at ATLAS,” *Phys. Rev. Lett.* **125** (2020) 261801, arXiv:2009.14537 [hep-ex].
- [91] CMS, TOTEM Collaboration, A. Tumasyan *et al.*, “Search for central exclusive production of top quark pairs in proton-proton collisions at $\sqrt{s} = 13$ TeV with tagged protons,” *JHEP* **06** (2024) 187, arXiv:2310.11231 [hep-ex].
- [92] D. d’Enterria and J.-P. Lansberg, “Study of Higgs boson production and its b anti-b decay in gamma-gamma processes in proton-nucleus collisions at the LHC,” *Phys. Rev. D* **81** (2010) 014004, arXiv:0909.3047 [hep-ph].
- [93] C. Amsler and N. A. Tornqvist, “Mesons beyond the naive quark model,” *Phys. Rept.* **389** (2004) 61–117.
- [94] E. Klempt and A. Zaitsev, “Glueballs, Hybrids, Multiquarks. Experimental facts versus QCD inspired concepts,” *Phys. Rept.* **454** (2007) 1–202, arXiv:0708.4016 [hep-ph].
- [95] Belle Collaboration, S. K. Choi *et al.*, “Observation of a narrow charmonium-like state in exclusive $B^{\pm} \rightarrow K^{\pm}\pi^{\pm}J/\psi$ decays,” *Phys. Rev. Lett.* **91** (2003) 262001, arXiv:hep-ex/0309032.
- [96] N. Brambilla, S. Eidelman, C. Hanhart, A. Nefediev, C.-P. Shen, C. E. Thomas, A. Vairo, and C.-Z. Yuan, “The XYZ states: experimental and theoretical status and perspectives,” *Phys. Rept.* **873** (2020) 1–154, arXiv:1907.07583 [hep-ex].
- [97] D. Johnson, I. Polyakov, T. Skwarnicki, and M. Wang, “Exotic Hadrons at LHCb,” arXiv:2403.04051 [hep-ex].
- [98] N. Hüsken, E. S. Norella, and I. Polyakov, “A Brief Guide to Exotic Hadrons,” arXiv:2410.06923 [hep-ph].
- [99] BESIII Collaboration, M. Ablikim *et al.*, “Determination of Spin-Parity Quantum Numbers of X(2370) as 0^{++} from $J/\psi \rightarrow \gamma K_s^0 K_s^0 \eta'$,” *Phys. Rev. Lett.* **132** (2024) 181901, arXiv:2312.05324 [hep-ex].
- [100] LHCb Collaboration, R. Aaij *et al.*, “A model-independent study of resonant structure in $B^+ \rightarrow D^+ D^- K^+$ decays,” *Phys. Rev. Lett.* **125** (2020) 242001, arXiv:2009.00025 [hep-ex].
- [101] LHCb Collaboration, R. Aaij *et al.*, “Amplitude analysis of the $B^+ \rightarrow D^+ D^- K^+$ decay,” *Phys. Rev. D* **102** (2020) 112003, arXiv:2009.00026 [hep-ex].
- [102] M. Deutsch, “Evidence for the Formation of Positronium in Gases,” *Phys. Rev.* **82** (1951) 455–456.
- [103] A. Czarnecki and S. G. Karshenboim, “Decays of positronium,” in *14th International Workshop on High-Energy Physics and Quantum Field Theory (QFTHEP 99)*, pp. 538–544. 1999. arXiv:hep-ph/9911410.
- [104] A. Czarnecki, “Positronium properties,” *Acta Phys. Polon. B* **30** (1999) 3837–3847, arXiv:hep-ph/9911455.
- [105] B. A. Kniehl and A. A. Penin, “Order $\alpha^3 \ln(1/\alpha)$ corrections to positronium decays,” *Phys. Rev. Lett.* **85** (2000) 1210, arXiv:hep-ph/0004267. [Erratum: Phys.Rev.Lett. 85, 3065 (2000)].
- [106] K. Melnikov and A. Yelkhovsky, “ $O(\alpha^3 \ln \alpha)$ corrections to positronium decay rates,” *Phys. Rev. D* **62** (2000) 116003, arXiv:hep-ph/0008099.
- [107] U. D. Jentschura, V. G. Ivanov, G. Soff, and S. G. Karshenboim, “Next-to-leading and higher order corrections to the decay rate of dimuonium,” *Phys. Lett. B* **424** (1998) 397–404, arXiv:hep-ph/9706401.
- [108] S. J. Brodsky and R. F. Lebed, “Production of the smallest QED atom: True muonium ($\mu^+ \mu^-$),” *Phys. Rev. Lett.* **102** (2009) 213401, arXiv:0904.2225 [hep-ph].
- [109] D. d’Enterria, R. Perez-Ramos, and H.-S. Shao, “Ditauonium spectroscopy,” *Eur. Phys. J. C* **82** (2022) 923, arXiv:2204.07269 [hep-ph].
- [110] D. d’Enterria and H.-S. Shao, “Prospects for ditauonium discovery at colliders,” *Phys. Lett. B* **842** (2023) 137960, arXiv:2302.07365 [hep-ph].
- [111] C. J. Batty, “Anti-protonic hydrogen atoms,” *Rept. Prog. Phys.* **52** (1989) 1165–1216.
- [112] J. Carbonell, G. Ihle, and J. M. Richard, “Protonium annihilation in optical models,” *Z. Phys. A* **334** (1989) 329–341.
- [113] M. Augsburg *et al.*, “Measurement of the strong interaction parameters in anti-protonic hydrogen and probable evidence for an interference with inner bremsstrahlung,” *Nucl. Phys. A* **658** (1999) 149–162.
- [114] E. Klempt, F. Bradamante, A. Martin, and J. M. Richard, “Antinucleon nucleon interaction at low energy: Scattering and protonium,” *Phys. Rept.* **368** (2002) 119–316.
- [115] M. Doser, “Antiprotonic bound systems,” *Prog. Part. Nucl. Phys.* **125** (2022) 103964.
- [116] H. Jallouli and H. Sazdjian, “Relativistic effects in the pionium lifetime,” *Phys. Rev. D* **58** (1998) 014011, arXiv:hep-ph/9706450. [Erratum: Phys.Rev.D 58, 099901 (1998)].
- [117] P. Labelle and K. Buckley, “A New $O(\alpha)$ correction to the decay rate of pionium,” arXiv:hep-ph/9804201.
- [118] H. W. Hammer and J. N. Ng, “Rare pionium decays and pion polarizability,” *Eur. Phys. J. A* **6** (1999) 115–118, arXiv:hep-ph/9902284.
- [119] P. Suebka and Y. Yan, “Accurate evaluation of pionium wave functions,” *Phys. Rev. C* **70** (2004) 034006.
- [120] Y. Yan, R. Tegen, T. Gutsche, and A. Faessler, “Sturmian function approach and anti-N N bound states,” *Phys. Rev. C* **56**

- (1997) 1596–1604.
- [121] C. Hanhart, Y. S. Kalashnikova, A. E. Kudryavtsev, and A. V. Nefediev, “Two-photon decays of hadronic molecules,” *Phys. Rev. D* **75** (2007) 074015, [arXiv:hep-ph/0701214](#).
- [122] J. Gasser, V. E. Lyubovitskij, and A. Rusetsky, “Hadronic atoms in QCD + QED,” *Phys. Rept.* **456** (2008) 167–251, [arXiv:0711.3522 \[hep-ph\]](#).
- [123] J. Gasser, V. E. Lyubovitskij, and A. Rusetsky, “Hadronic Atoms,” *Ann. Rev. Nucl. Part. Sci.* **59** (2009) 169–190, [arXiv:0903.0257 \[hep-ph\]](#).
- [124] Z.-H. Zhang and F.-K. Guo, “ $D^+D^{*\mp}$ Hadronic Atom as a Key to Revealing the X(3872) Mystery,” *Phys. Rev. Lett.* **127** (2021) 012002, [arXiv:2012.08281 \[hep-ph\]](#).
- [125] O. Dumbrajs, “The $(\pi^+\pi^-)$, (π^+K^-) , $(\pi^-\Sigma^+)$, (K^+K^-) , and $(\bar{\Sigma}^+\Sigma^+)$ atomic states,” *Z. Phys. A* **321** (1985) 297–299.
- [126] S. Wycech and A. M. Green, “Production of the exotic atoms $\pi^+\pi^-$, $K^+\pi^-$ and K^+K^- ,” *Nucl. Phys. A* **562** (1993) 446–460, [arXiv:hep-ph/9302293](#).
- [127] B. Kerbikov, “The Interplay of the K^+K^- atom and the $f_0(975)$ resonance,” *Z. Phys. A* **353** (1995) 113–115, [arXiv:hep-ph/9503385](#).
- [128] L. Afanasyev, S. Gevorkyan, and O. Voskresenskaya, “Production of dimeson atoms in high-energy collisions,” *Eur. Phys. J. A* **53** (2017) 78.
- [129] **DIRAC** Collaboration, B. Adeva *et al.*, “DIRAC: A High resolution spectrometer for pionium detection,” *Nucl. Instrum. Meth. A* **515** (2003) 467–496, [arXiv:hep-ex/0305022](#).
- [130] T. L. Trueman, “Energy level shifts in atomic states of strongly-interacting particles,” *Nucl. Phys.* **26** (1961) 57–67.
- [131] S. Krewald, R. H. Lemmer, and F. P. Sassen, “Lifetime of kaonium,” *Phys. Rev. D* **69** (2004) 016003, [arXiv:hep-ph/0307288](#).
- [132] Y. Yan, C. Nualchimplee, P. Suebka, C. Kobdaj, and K. Khosonthogkee, “Accurate evaluation of wave functions of pionium and kaonium,” *Mod. Phys. Lett. A* **24** (2009) 901–906.
- [133] P.-P. Shi, Z.-H. Zhang, F.-K. Guo, and Z. Yang, “ D^+D^- hadronic atom and its production in pp and $p\bar{p}$ collisions,” *Phys. Rev. D* **105** (2022) 034024, [arXiv:2111.13496 \[hep-ph\]](#).
- [134] L. G. Afanasev *et al.*, “Observation of atoms consisting of π^+ and π^- mesons,” *Phys. Lett. B* **308** (1993) 200–206.
- [135] **DIRAC** Collaboration, B. Adeva *et al.*, “First measurement of the $\pi^+\pi^-$ atom lifetime,” *Phys. Lett. B* **619** (2005) 50–60, [arXiv:hep-ex/0504044](#).
- [136] **DIRAC** Collaboration, B. Adeva *et al.*, “First measurement of a long-lived $\pi^+\pi^-$ atom lifetime,” *Phys. Rev. Lett.* **122** (2019) 082003, [arXiv:1811.08659 \[hep-ex\]](#).
- [137] G. Colangelo, J. Gasser, and H. Leutwyler, “ $\pi\pi$ scattering,” *Nucl. Phys. B* **603** (2001) 125–179, [arXiv:hep-ph/0103088](#).
- [138] M. A. Ivanov, V. E. Lyubovitskij, E. Z. Lipartia, and A. G. Rusetsky, “ $\pi^+\pi^-$ atom in chiral perturbation theory,” *Phys. Rev. D* **58** (1998) 094024, [arXiv:hep-ph/9805356](#).
- [139] J. Gasser, V. E. Lyubovitskij, A. Rusetsky, and A. Gall, “Decays of the $\pi^+\pi^-$ atom,” *Phys. Rev. D* **64** (2001) 016008, [arXiv:hep-ph/0103157](#).
- [140] Y.-J. Zhang, H.-C. Chiang, P.-N. Shen, and B.-S. Zou, “Possible S-wave bound-states of two pseudoscalar mesons,” *Phys. Rev. D* **74** (2006) 014013, [arXiv:hep-ph/0604271](#).
- [141] S. P. Klevansky and R. H. Lemmer, “Decay of kaonium in a chiral approach,” *Phys. Lett. B* **702** (2011) 235–241, [arXiv:1102.1391 \[hep-ph\]](#).
- [142] S. Prelovsek, S. Collins, D. Mohler, M. Padmanath, and S. Piemonte, “Charmonium-like resonances with $J^{PC} = 0^{++}, 2^{++}$ in coupled $D\bar{D}, D_s\bar{D}_s$ scattering on the lattice,” *JHEP* **06** (2021) 035, [arXiv:2011.02542 \[hep-lat\]](#).
- [143] **BESIII** Collaboration, M. Ablikim *et al.*, “Observation of the anomalous shape of X(1840) in $J/\psi \rightarrow \gamma 3(\pi^+\pi^-)$ indicating a second resonance near $p\bar{p}$ threshold,” *Phys. Rev. Lett.* **132** (2024) 151901, [arXiv:2310.17937 \[hep-ex\]](#).
- [144] **ATHENA** Collaboration, N. Zurlo *et al.*, “Evidence For The Production Of Slow Antiprotonic Hydrogen In Vacuum,” *Phys. Rev. Lett.* **97** (2006) 153401, [arXiv:0708.3717 \[hep-ex\]](#).
- [145] D. d’Enterria and G. G. da Silveira, “Observing light-by-light scattering at the Large Hadron Collider,” *Phys. Rev. Lett.* **111** (2013) 080405, [arXiv:1305.7142 \[hep-ph\]](#). [Erratum: *Phys.Rev.Lett.* 116, 129901 (2016)].
- [146] **ATLAS** Collaboration, M. Aaboud *et al.*, “Evidence for light-by-light scattering in heavy-ion collisions with the ATLAS detector at the LHC,” *Nature Phys.* **13** (2017) 852–858, [arXiv:1702.01625 \[hep-ex\]](#).
- [147] **CMS** Collaboration, A. M. Sirunyan *et al.*, “Evidence for light-by-light scattering and searches for axion-like particles in ultraperipheral PbPb collisions at $\sqrt{s_{NN}} = 5.02$ TeV,” *Phys. Lett. B* **797** (2019) 134826, [arXiv:1810.04602 \[hep-ex\]](#).
- [148] **ATLAS** Collaboration, G. Aad *et al.*, “Observation of light-by-light scattering in ultraperipheral Pb+Pb collisions with the ATLAS detector,” *Phys. Rev. Lett.* **123** (2019) 052001, [arXiv:1904.03536 \[hep-ex\]](#).
- [149] **CMS** Collaboration, A. Hayrapetyan *et al.*, “Measurement of light-by-light scattering and the Breit-Wheeler process, and search for axion-like particles in ultraperipheral PbPb collisions at $\sqrt{s_{NN}} = 5.02$ TeV,” [arXiv:2412.15413 \[nucl-ex\]](#).
- [150] A. A. H. E. Chaubey, and H.-S. Shao, “Two-loop massive QCD and QED helicity amplitudes for light-by-light scattering,” *JHEP* **03** (2024) 121, [arXiv:2312.16966 \[hep-ph\]](#).
- [151] A. A. H. E. Chaubey, M. Fraaije, V. Hirschi, and H.-S. Shao, “Light-by-light scattering at next-to-leading order in QCD and QED,” *Phys. Lett. B* **851** (2024) 138555, [arXiv:2312.16956 \[hep-ph\]](#).
- [152] Z. Bern, A. De Freitas, L. J. Dixon, A. Ghinculov, and H. L. Wong, “QCD and QED corrections to light by light scattering,” *JHEP* **11** (2001) 031, [arXiv:hep-ph/0109079](#).
- [153] G. Colangelo, M. Hoferichter, M. Procura, and P. Stoffer, “Dispersion relation for hadronic light-by-light scattering: theoretical foundations,” *JHEP* **09** (2015) 074, [arXiv:1506.01386 \[hep-ph\]](#).
- [154] M. Hoferichter, P. Stoffer, and M. Zillinger, “Complete Dispersive Evaluation of the Hadronic Light-by-Light Contribution to Muon $g - 2$,” *Phys. Rev. Lett.* **134** (2025) 061902, [arXiv:2412.00190 \[hep-ph\]](#).

- [155] **Muon g-2** Collaboration, B. Abi *et al.*, “Measurement of the Positive Muon Anomalous Magnetic Moment to 0.46 ppm,” *Phys. Rev. Lett.* **126** (2021) 141801, [arXiv:2104.03281 \[hep-ex\]](#).
- [156] T. Aoyama *et al.*, “The anomalous magnetic moment of the muon in the Standard Model,” *Phys. Rept.* **887** (2020) 1–166, [arXiv:2006.04822 \[hep-ph\]](#).
- [157] M. Klusek-Gawenda, R. McNulty, R. Schicker, and A. Szczurek, “Light-by-light scattering in ultraperipheral heavy-ion collisions at low diphoton masses,” *Phys. Rev. D* **99** (2019) 093013, [arXiv:1904.01243 \[hep-ph\]](#).
- [158] P. Jucha, M. Klusek-Gawenda, and A. Szczurek, “Light-by-light scattering in ultraperipheral collisions of heavy ions at two future detectors,” *Phys. Rev. D* **109** (2024) 014004, [arXiv:2308.01550 \[hep-ph\]](#).